LOCALIZED HYPERTHERMIA FOR ENHANCED TARGETED DELIVERY OF POLYMER THERAPEUTICS

by

Nicholas Frazier

A dissertation submitted to the faculty of
The University of Utah
in partial fulfillment of the requirements for the degree of

Doctor of Philosophy

Department of Bioengineering

The University of Utah

May 2017

The University of Utah Graduate School

STATEMENT OF DISSERTATION APPROVAL

The dissertation of **Nicholas Frazier**

has been approved by the following supervisory committee members:

Hamidreza Ghandehari	, Chair	**06.30.16** Date Approved
David Grainger	, Member	**06.30.16** Date Approved
Jindrich Kopecek	, Member	**06.30.16** Date Approved
Allison Payne	, Member	**06.30.16** Date Approved
Sunil Sharma	, Member	**07.14.16** Date Approved

and by **Patrick Tresco** , Chair/Dean of

the Department/College/School of **Bioengineering**

and by David B. Kieda, Dean of The Graduate School.

ABSTRACT

It is estimated that in 2016, more than 848,000 new cases of cancer will be diagnosed in men with more than a quarter being prostate cancer and more than 26,000 deaths attributed to this disease. Prostate cancer poses a limited risk when detected at an early stage and treatment of stages II-III has a 5-year survival rate of almost 100%. However, these early-stage cancers can eventually progress and develop into stage IV, dramatically dropping the 5-year survival rate to 28%. Thus, development of a new therapy is needed to fully eliminate these tumors. Combination of heat and chemotherapy improves therapeutic efficacy while allowing for reduced dosing of drugs and limiting side effects. Localized hyperthermia has been used to enhance the delivery of polymer therapeutics to prostate tumors through increased blood flow, vascular permeability, and incorporation of heat shock targeting. This strategy has been shown to increase the delivery and retention of polymer-drug conjugates leading to enhanced efficacy. Although much work has been done using this strategy, the effects of different thermal dosing on polymer accumulation are unknown. The first aim of this research is to examine how altering heating parameters influences polymer tumor accumulation. The hypothesis for this aim is that there is an optimal thermal treatment that leads to the maximal amount of polymer accumulation in the tumors. Additionally, the previously used heating method of plasmonic photothermal therapy (PPTT) can result in long-term accumulation of gold nanoparticles in healthy organs, potentially limiting clinical applicability. The second aim of this proposal will be

focused on investigating the alternative method of high intensity focused ultrasound (HIFU) for selective heating of tumors and enhancing macromolecular delivery. HIFU has shown the capability for precise, noninvasive heating of specific regions within the prostate through magnetic resonance imaging (MRI) guidance. The hypothesis to be tested in this aim is that mild hyperthermia produced with HIFU will have the same effect as that produced by PPTT in improving the delivery of macromolecular systems to solid tumors. Finally, in the third aim, the enhanced delivery of targeted polymer therapeutics to prostate tumors in mice models will be investigated using mild hyperthermia produced with HIFU. In the long term, it is anticipated that HIFU can be used in conjunction with delivery of polymer-drug conjugates for enhanced efficacy and reduced toxicity of chemotherapy to produce a clinically relevant treatment of advanced prostate cancer.

TABLE OF CONTENTS

LIST OF FIGURES

LIST OF TABLES

ABBREVIATIONS

AC	Alternating current
ACN	Acetonitrile
AIBN	Azobisisobutyronitrile
ANOVA	Analysis of variance
APMA-DOTA	Aminopropylmethacrylamide-1,4,7,10-tetraazacyclododecane-1,4,7,10-tetraacetic acid
AUC	Area under the curve
CTA	Chain transfer agent
CTAB	Hexadecyltrimethylammonium bromide
DCE	Dynamic contrast-enhanced
DI	Deionized
DMSO	Dimethyl sulfoxide
DNA	Deoxyribonucleic acid
DOC	Docetaxel
DOX	Doxorubicin
DPPC	Dipalmitoylphosphatidylcholine
EBD	Evans blue dye
EDTA	Ethylenediaminetetraacetic acid
ELP	Elastin-like protein

EM	Electromagnetic
EPR	Enhanced permeability and retention
ESI/MS	Electrospray ionization mass spectroscopy
ETL	Echo-train length
EtOH	Ethanol
FBS	Fetal bovine serum
FDA	Food and Drug Administration
Gd	Gadolinium
GNC	Gold nanocage
GNR	Gold nanorod
GNP	Gold nanoparticle
GRP78	Glucose-regulated protein 78 kDa
H&E	Hematoxylin/eosin
HIFU	High intensity focused ultrasound
HPMA	*N*-(2-hydroxypropyl)methacrylamide
HPLC	High performance liquid chromatography
HS	Heat shock
HSP	Heat shock protein
IACUC	Institutional Animal Care and Use Committee
IC_{50}	Inhibitory concentration 50%
ICP-MS	Inductively coupled plasma mass spectrometry
ID	Injected dose
IONP	Iron oxide nanoparticle

IV	Intravenous
LCST	Lower critical solution temperature
MA-GFLG-DOC	*N*-methacryloyl-glycylphenylalanylleucylglycine-docetaxel
MA-GG-TT	*N*-methacryloylglycylglycyl-2-thiazolidine-2-thione
MA-Tyr	*N*-methacryloyl-tyrosinamide
MFH	Magnetic fluid hyperthermia
MNP	Magnetic nanoparticle
MR	Magnetic resonance
MRgHIFU	Magnetic resonance image guided HIFU
MRI	Magnetic resonance imaging
MTD	Maximum tolerated dose
M_n	Number average molecular weight
M_w	Weight average molecular weight
M_w/M_n	Polydispersity index
MOLLI	Modified look locker inversion recovery imaging
MW	Molecular weight
MWCO	Molecular weight cutoff
NIPPAAm	N-isopropyl acrylamide
NIR	Near-infrared
OD	Optical density
OS	Overall survival
PBS	Phosphate buffered saline
PDI	Polydispersity index

PEG	Poly(ethylene glycol)
PPSu	Poly(propylene succinate)
PPTT	Plasmonic photothermal therapy
PR	Partial response
PRF	Proton resonance frequency
R1	Relaxation rate
RAFT	Reversible addition-fragmentation chain-transfer
RBC	Red blood cell
RES	Reticuloendothelial system
RFA	Radiofrequency ablation
ROI	Region of interest
SD	Stable disease
SEC	Size-exclusion chromatography
Seg-EPI	Segmented-echo planar imaging
SPR	Surface plasmon resonance
STD	Standard deviation
T1	Longitudinal relaxivity
TE	Echo time
TEM	Transmission electron microscopy
TER	Thermal enhancement ratio
TR	Repetition time
TSL	Thermosensitive liposome
TSP	Thermosensitive polymer

UV	Ultraviolet
VA-044	2,2'-Azobis[2-(2-imidazolin-2-yl)propane] dihydrochloride

ACKNOWLEDGMENTS

From start to finish, the last five years working on my Ph.D. has been an incredible journey. I would never have in my wildest dreams expected to have so many great experiences and meet so many wonderful people. I thought I knew what hard work really meant but realized how naïve I was.

I truly want to thank all of my committee members for their help and guidance along the way. Thank you to Dr. Ghandehari for giving me the opportunity to work in his lab and a chance to prove myself and for continually challenging me to do more. Thank you to Dr. Payne for all of her hard work and late nights at the MRI. I would not have been able to get this work done without her sacrifices. Thank you to Dr. Grainger for being a true role model for all young scientists and students. Thank you to Dr. Kopecek for teaching me to be very meticulous with my chemistry and research in general. Finally, thank you to Dr. Sharma for helping to bring clinical knowledge to this project.

I would also like to acknowledge all of my friends and family. My mother has always been someone I could confide in when I needed consoling even when we were on opposite sides of the country. My late father passed away during the end of my second year. He always showed enthusiasm for what I did even if he had no idea what I was talking about. My grandparents loved to brag to their friends about their favorite grandson. Azadeh and her family looked out for me during my whole stay in Utah. Adam Gormley, Nate Larson, and Brandon Buckway were great mentors. Thanks to all of those who

helped with sample prep and analyses (Krishna, Jack, Blake, Sheryl, Linda, Diego, James).

All the experiences I've had in Utah and abroad in Paris, France have given me new perspectives on life. I am extremely grateful to have been so lucky to have seen different parts of the world and been able to enjoy life in each of these places.

CHAPTER 1

INTRODUCTION

1.1 Introduction

Prostate cancer is the most common type of cancer among men in the United States [1]. Many of these tumors can be treated surgically, but only if detected at an early stage [2]. In advanced stages of the disease (stage II-III) the ability to remove the tumor may not be available. Alternative methods including radiotherapy, hormone therapy, and ablative therapies are used to shrink or eliminate the tumor but have the risk of complications. While the 5-year survival rate for stage II-III is close to 100%, the chance for disease progression and metastasis is 50% [3]. Once the cancer reaches stage IV, the 5-year survival rate dramatically drops to 28% [1]. Current treatments do not adequately eliminate late-stage prostate cancers and leave the patient at high risk. Due to the inherent genetic instability of cancers, insufficient disease elimination can lead to the development of treatment resistance [4]. This potential issue highlights the need to develop a new therapy that fully eradicates late-stage prostate cancer before the risk of developing metastases.

Combination therapy can be a more effective treatment while reducing side effects. One such therapy that shows potential is a combination of chemotherapy and hyperthermia. Synergistic effects of heat and certain chemotherapeutics, including docetaxel, have shown enhanced efficacy [5-7]. In this therapy, the effects of a single dose of the drug can be

mediated by a fraction of the typical dose in combination with localized hyperthermia. To create this effect, localized heating of the tumor should be achieved in conjunction with the delivery of chemotherapeutics.

Localized delivery of hyperthermia also initiates vascular effects that enhance accumulation of macromolecular drug conjugates. Mild hyperthermia within the tumor increases blood flow and vascular permeability as blood vessels expand to dissipate excess heat [8-10] allowing accumulation of macromolecular drug conjugates to a greater degree. The macromolecular drug carriers *N*-(2-hydroxypropyl)methacrylamide (HPMA) copolymers improve solubility of hydrophobic drugs by increasing their size to prolong blood circulation half-life by evasion of renal filtration, and taking advantage of the enhanced permeability and retention (EPR) effect to improve tumor accumulation. These polymeric carriers also change the mode of entry into cancer cells from diffusion to endocytosis allowing for better treatment of drug-resistant cancers [11]. HPMA copolymers are further advantageous in their multifunctionality for attachment of imaging agents and targeting moieties.

Mild hyperthermia induces effects at the cellular level including up-regulation of cell surface heat shock protein (HSP) receptor glucose regulated protein 78 (GRP78) which can be targeted [12]. The heat shock (HS)-targeting strategy relies on the induction of these receptors following hyperthermia and allows for site-specific targeting within the heated tumor. Targeting these receptors in combination with hyperthermia leads to enhanced uptake by receptor-mediated endocytosis. When HPMA copolymer-drug conjugates are targeted towards GRP78, retention is prolonged within heated tumor tissue *in vivo* [12]. Comparison of accumulation over time shows that targeted and untargeted systems had

significantly more tumor accumulation when using hyperthermia. At later times, the untargeted copolymers diffused back out of the tumor returning to the same level as tumors left untreated, whereas HS-targeted copolymers retained a larger portion of the copolymers. These results demonstrate that the HSP targeting strategy combined with hyperthermia increases the delivery and retention of HPMA copolymers. With this combination therapy, we can minimize drug dose, reduce systemic side effects, increase and prolong accumulation, and eliminate the advanced localized disease.

Over the past few years, the Ghandehari lab has demonstrated that gold nanorod (GNR)-mediated plasmonic photothermal therapy (PPTT) can be utilized to deliver localized hyperthermia, increase delivery of HPMA copolymers, and utilize HS-targeting to result in synergistic effects in prostate cancer models [13]. This strategy increases the overall accumulation of Evans blue dye (EBD), HPMA copolymer conjugates [12,14], tumor penetration [15], and improves the therapeutic efficacy of prostate cancer treatment [13,16]. GNR-mediated PPTT is a method of heating tumors selectively through absorption of near-infrared (NIR) laser light by the GNRs previously accumulated in the tumor tissue. In these previous studies, tumors were treated with mild hyperthermia (43°C for 10 min determined as a single point measurement via needle thermocouple) which was first shown to maintain the temperature within the tumor at 42-43°C and enhance macromolecular delivery through increased accumulation of EBD at 5 h post treatment [14]. PPTT was additionally shown to improve delivery of untargeted and HS-targeted HPMA copolymers [12]. In these studies, it was shown that untargeted polymer accumulation after PPTT leads to a transient increase in accumulation peaking at 4 h and returning to baseline at 8 h post treatment [12]. With the incorporation of HS-targeting, the enhanced accumulation was

retained over longer periods of time [12]. The enhanced accumulation was additionally visualized by magnetic resonance imaging (MRI). These experiments showed that PPTT could also increase the penetration of HPMA copolymers within the tumor tissue [15]. Finally, the enhanced accumulation and penetration was examined with chemo- and radio-therapeutic copolymer conjugates. Efficacies of HS-targeted and untargeted HPMA copolymer-docetaxel conjugates were shown to be significantly improved over free drug alone with improvements in synergy as well [13]. Additionally, ^{90}Yttrium was chelated to HPMA copolymers and used in conjunction with PPTT [16]. The efficacy of these conjugates was also greatly improved.

In each of these experiments, the same heat treatment was used to improve the delivery and enhance treatment in preclinical prostate cancer models. Limited information is available on the role of varying heating parameters (temperature and duration) of PPTT and the effects on HPMA copolymer accumulation, retention, and consequently efficacy. The thermal dose used may not, in fact, be the optimal treatment for delivering maximal amounts of polymer conjugates to the tumor site. It is unknown how altering the heating regimen will, in turn, alter the polymer accumulation profile. Therefore, it is of interest to investigate if conjugate accumulation could be further optimized for maximal enhancement with the use of different heating parameters.

Although much promising work has been done using PPTT, it is still in the early developmental phase toward clinical applicability. PPTT utilizes passive accumulation of GNRs to the tumor by the EPR effect to then absorb NIR laser light and generate localized heat. The systemic delivery of these GNRs leads to nonspecific accumulation in healthy, vital organs [17]. Chronic accumulation in these organs may potentially cause adverse

effects which are not fully understood. Accumulation in these organs also limits the possibility of additionally applying this strategy for selective treatment of liver cancers. Since the GNRs will accumulate throughout the liver, this treatment strategy would not be able to distinguish healthy liver from cancerous liver tissues. PPTT also only has a depth penetration of approximately 1-2 cm further limiting the application of this heating method to superficial tumors or otherwise requires the use of a fiber optic probe to reach deep-seeded tumors. Finally, there will be absorption of laser light in the surrounding healthy tissues. This absorption has the potential to cause collateral damage leading to severe side-effects such as incontinence in prostate cancer treatments. Therefore, it would then be advantageous to deliver heat specifically to the tumor tissue by a noninvasive technique which also has a larger depth penetration and greater precision of treatment.

Therapeutic high intensity focused ultrasound (HIFU) can be used to noninvasively heat tissues, causing hyperthermia and guide polymer delivery [18]. Currently, clinical trials are being performed using transrectal HIFU to ablate prostate cancer tumors [19]. This noninvasive ablative therapy could potentially be altered for use in our combination therapy. The noninvasive delivery of hyperthermia specifically to the tumor site will minimize the risk of complications and the combination therapy will eliminate the risk of inadequate tumor treatment, which can lead to possible resistant cancers and risk of recurrence.

1.2 Aims and scope of this dissertation

In prostate cancer, once the tumor has spread and metastasized, the 5-year survival rate dramatically drops. To alleviate this problem, a treatment needs to be available to not

only slow progression of the late-staged disease but completely eliminate the tumor before metastasis. Targeted drug delivery specifically to the tumor using polymeric carriers shows promise. A challenge is limited accumulation in solid tumors. Recent studies in the Ghandehari lab, using heat specifically delivered to the tumor site, have shown increased accumulation of a potent chemotherapy in the form of HS-targeted *N*-(2-hydroxypropyl)methacrylamide (HPMA) copolymer-drug conjugates within prostate tumors. In this previous work, heating was achieved through gold nanorod (GNR)-mediated plasmonic photothermal therapy (PPTT) at mild hyperthermic conditions (43°C for 10 min) to enhance the delivery of HPMA copolymer conjugates. Currently, there is a lack of understanding on how altering heating parameters (temperature and duration) will affect HPMA copolymer accumulation and retention. Additionally, systemic delivery of GNRs in PPTT results in significant accumulation in the liver and spleen leading to questions about long-term effects potentially limiting clinical translation and use for selective heating of liver cancers. Finally, PPTT can lead to collateral tissue damage from laser light alone and has limited depth penetration requiring the use of a fiber optic cable to reach deep-seeded tumors. Therefore, other noninvasive, more precise, and clinically acceptable heating methods need to be investigated to avoid problems and improve the applicability of this combination therapy. One such method is high intensity focused ultrasound (HIFU). Advantages of using HIFU instead of PPTT include noninvasive application and improved precision and depth penetration. In addition, HIFU is currently FDA approved to be used in several clinical applications. The goal of this project is first to examine the effects of altering PPTT heat dosing on polymer accumulation and second investigate the utility of HIFU to induce mild hyperthermia and enhance delivery of

targeted polymer-drug conjugates to prostate tumors. The hypotheses to be tested are that altering the thermal dose of PPTT can lead to optimized polymer tumor accumulation, HIFU can be used to selectively heat tumors at mild hyperthermic conditions and enhance macromolecular delivery, and combination with targeted polymer-drug conjugates will lead to an improved therapeutic outcome. To test this hypothesis, three Specific Aims were pursued as outlined in Sections 1.2.1, 1.2.2, and 1.2.3.

1.2.1 Examine the effects of heating temperature and duration by GNR-mediated PPTT on copolymer accumulation in tumor tissue

This study elucidated the conditions for the maximal accumulation of polymer-drug conjugates using PPTT. Four different temperatures (40, 43, 46, or 49°C) and two different durations (10 or 30 min) were examined and accumulation of untargeted HPMA copolymers in a mouse sarcoma model was initially observed at 4 h post treatment. Additionally, the polymer accumulation profile was observed over 8 h for select groups that had unexpected accumulation at 4 h. Finally, histological analyses were used to examine changes within the tumor tissue due to heating with different thermal doses. Untargeted radiolabeled HPMA copolymers were used to track polymer accumulation *in vivo.* The polymers remained untargeted for these experiments since the goal was to examine the thermal effects and HS-targeting would further complicate the system. Accumulation studies were performed in CD1 mice bearing S-180 sarcoma tumors as they are known to exhibit the EPR effect for passive accumulation of GNRs and observe augmentation of this effect with hyperthermia without the need of an immune compromised mouse strain. The temperatures were chosen in increments of 3°C starting

from 43°C as this was used in prior experiments and initially chosen to be consistent with other literature methods [12-16]. It is widely considered that temperatures above 46°C are thermoablative [20], but also depends on time spent at the given temperature. Therefore, one temperature at 46°C and one above (49°C) was selected. Finally, one temperature lower than 43°C was selected to observe how longer durations could affect treatments with lower temperatures (40°C).

1.2.2 Investigate HIFU as an alternative heating method for inducing mild hyperthermia and enhancing macromolecular delivery to tumors

HIFU parameters (focal spot pattern, speed, and power) were optimized with the development of a feedback controller to achieve mild hyperthermia using a tumor phantom and then translated to an *in vivo* tumor model. Temperature distribution was imaged by MRI. The capability for HIFU to enhance macromolecular delivery was determined by Evans blue dye (EBD) and Gadolinium-labeled HPMA copolymer tumor accumulation. To evaluate the controller performance, the parameters of HIFU were first tested *ex vivo* using a tumor phantom model. For these experiments, chicken breast was used in preliminary studies as its acoustic and thermal properties are well known [21,22] and can be translated to an *in vivo* tumor model. In order to account for the variabilities seen *in vivo*, a feedback controller was developed to use MR thermometry data to automatically adjust the HIFU parameters to heat and maintain the tumor at 43°C. Once this set of experiments was completed, accumulation studies using HIFU as the heating method was performed with EBD and gadolinium (Gd)-labeled copolymers for visualization of tumor accumulation by MRI. These studies were performed in the CD1 mouse S-180 tumor

model to observe an enhancement of macromolecular delivery and allow for comparison to previous experiments that were done with PPTT [14].

1.2.3 Determine the capability for HIFU to improve efficacy of HS-targeted polymer-drug conjugates

The ability for HIFU to induce up-regulation of HSPs was determined by histology, and enhanced *in vivo* efficacy of targeted polymer-drug conjugates was determined by tumor regression and immunohistochemical analyses for molecular characterization of efficacy. In these experiments, the animal model used was nu/nu mice bearing DU145 prostate tumors to compare to previous efficacy experiments done with PPTT [12,13,16]. Untargeted and targeted copolymer-docetaxel conjugates were used in combination with and without HIFU to observe changes in the efficacy of treatment, as well as cytotoxic effects. Copolymer-docetaxel-drug conjugates that showed synergism with HS-targeting using PPTT [13] were used in these studies.

The following chapters of this dissertation describe the experimental work used to complete the presented aims. A comprehensive literature review of hyperthermia approaches to enhance delivery of nanomedicines to solid tumors is presented in Chapter 2 and reviewed elsewhere [23]. Chapters 3 [24], 4 [25], and 5 [26] present the methods, results, and discussions addressing Specific Aims 1-3. Chapter 6 outlines the conclusions from this dissertation and future directions.

1.3 References

1. ACS. Cancer Facts and Figures 2016, American Cancer Society, Atlanta, GA, 2016.

2. A. Bill-Axelson, L. Holmberg, M. Ruutu, M. Häggman, S.O. Andersson, S. Bratell, A. Spångberg, C. Busch, S. Nordling, H. Garmo, Radical prostatectomy versus watchful waiting in early prostate cancer, New England Journal of Medicine 352(19) (2005) 1977-1984.

3. J.E. Damberand G. Aus, Prostate cancer, The Lancet 371(9625) (2008) 1710-1721.

4. V. Ling, Multidrug resistance: Molecular mechanisms and clinical relevance. Cancer Chemotherapy and Pharmacology 40 (1997) S3-S8.

5. F. Mohamed, O.A. Stuart, O. Glehen, M. Urano, P.H. Sugarbaker, Docetaxel and hyperthermia: Factors that modify thermal enhancement, Journal of Surgical Oncology 88(1) (2004) 14-20.

6. R. Issels, Hyperthermia combined with chemotherapy–biological rationale, clinical application, and treatment results, Onkologie 22 (2000) 374-381.

7. J.M.C. Bull, An update on the anticancer effects of a combination of chemotherapy and hyperthermia, Cancer Research 44(10 Supplement) (1984) 4853s-4856s.

8. G. Kong, R.D. Braun, M.W. Dewhirst, Characterization of the effect of hyperthermia on nanoparticle extravasation from tumor vasculature, Cancer Research 61(7) (2001) 3027-3032.

9. G. Kong, M.W. Dewhirst, Hyperthermia and liposomes, International Journal of Hyperthermia 15 (1999) 345-370.

10. G. Kong, R.D. Braun, M.W. Dewhirst, Hyperthermia enables tumor-specific nanoparticle delivery: Effect of particle size, Cancer Research 60 (2000) 4440-4445.

11. T. Minko, P. Kopečková, J. Kopeček, Efficacy of the chemotherapeutic action of HPMA copolymer-bound doxorubicin in a solid tumor model of ovarian carcinoma, International Journal of Cancer 86(1) (2000) 108–117.

12. A.J. Gormley, N. Larson, S. Sadekar, R. Robinson, A. Ray, H. Ghandehari, Guided delivery of polymer therapeutics using plasmonic photothermal therapy, Nano Today 7 (2012) 158-167.

13. N. Larson, A. Gormley, N. Frazier, H. Ghandehari, Synergistic enhancement of cancer therapy using a combination of heat shock protein targeted HPMA copolymer–drug conjugates and gold nanorod induced hyperthermia, Journal of Controlled Release 170(1) (2013) 41-50.

14. A.J. Gormley, K. Greish, A. Ray, R. Robinson, J.A. Gustafson, H. Ghandehari, Gold nanorod mediated plasmonic photothermal therapy: A tool to enhance macromolecular delivery, International Journal of Pharmaceutics 415 (2011) 315-318.

15. A.J. Gormley, N. Larson, A. Banisadr, R. Robinson, N. Frazier, A. Ray, H. Ghandehari, Plasmonic photothermal therapy increases the tumor mass penetration of HPMA copolymers, Journal of Controlled Release 166 (2013) 130-138.

16. B. Buckway, N. Frazier, A. Ray, H. Ghandehari, Gold nanorod-mediated hyperthermia enhances the efficacy of HPMA copolymer - 90Y conjugates in treatment of prostate tumors, Nuclear Medicine and Biology 41(3) (2014) 282-289.

17. A.J. Gormley, A. Malugin, A. Ray, R. Robinson, H. Ghandehari, Biological evaluation of RGDfK gold nanorod conjugates for prostate cancer treatment, Journal of Drug Targeting 19 (2011) 915-924.

18. J. Kennedy, High intensity focused ultrasound in the treatment of solid tumors, Nature Reviews Cancer 5 (2005) 321-327.

19. L. Poissonnier, J. Chapelon, O. Rouviere, L. Curiel, R. Bouvier, X. Martin, J.M. Dubernard, A. Gelet, Control of prostate cancer by transrectal HIFU in 227 patients, European Urology 51 (2007) 381-387.

20. C.S.S.R. Kumar, F. Mohammad, Magnetic nanomaterials for hyperthermia-based therapy and controlled drug delivery, Advanced Drug Delivery Reviews 63(9) (2011) 789-808.

21. A. Alassaf, A. Aleid, and V. Frenkel, In vitro methods for evaluating therapeutic ultrasound exposures: Present-day models and future innovations, Journal of Therapeutic Ultrasound 1(21) (2013).

22. D. Kruse, C.Y. Lai, D.N. Stephens, P. Sutcliffe, E.E. Paoli, S.H. Barnes, and K.W. Ferrara, Spatial and temporal controlled tissue heating on a modified clinical ultrasound scanner for generating mild hyperthermia in tumors, IEEE Transactions on Biomedical Engineering 57(1) (2011) 155-166.

23. N. Frazier, H. Ghandehari, Hyperthermia approaches for enhanced delivery of nanomedicines to solid tumors, Biotechnology and Bioengineering 112(10) (2015) 1967-1983.

24. N. Frazier, R. Robinson, A. Ray, H. Ghandehari, Effects of heating temperature and duration by gold nanorod-mediated plasmonic photothermal therapy on copolymer accumulation in tumor tissue, Molecular Pharmaceutics 12(5) (2015) 1605-1614.

25. N. Frazier, A. Payne, J. de Bever, C. Dillon, A. Panda, N. Subrahmanyam, H. Ghandehari, High intensity focused ultrasound for enhanced macromolecular delivery, Journal of Controlled Release 241 (2016) 186-193.

26. N. Frazier, A. Payne, C. Dillon, N. Subrahmanyam, H. Ghandehari, Enhanced efficacy of combination heat shock targeted polymer therapeutics with high intensity focused ultrasound, Nanomedicine: Nanotechnology, Biology, and Medicine, In Press (2016).

CHAPTER 2

LITERATURE BACKGROUND

2.1 Introduction

Despite the latest technological advances in cancer therapies, a significant impact on survival rates has not been observed from improved treatments alone [1]. Changes in survival can largely be argued to be based on biases created from early detection through increased lead-time bias, length bias, and overdiagnosis. There are still many challenges to developing treatments that fully eradicate this complex disease. One such challenge is to overcome barriers to the delivery of drugs or other therapeutic agents to the tumor site. Many conventional chemotherapeutic drugs lack significant accumulation at the tumor site where only less than 1% of the injected dose (ID) is localized [2]. This phenomenon can be broken down into a few different aspects including poor water solubility of drugs, short circulation half-life (on the scale of only a couple hours), and the physiological barriers that exist within the tumor limiting extravasation and penetration into the tissue [3]. These barriers include growth induced solid stresses, dense interstitial structure, elevated interstitial fluid pressures, and abnormal blood vessel networks [3]. Accumulation can be improved through the use of nanomedicine formulations, but the amount delivered to the

---

Reprinted *in part* with permission of Wiley. N. Frazier, H. Ghandehari. Hyperthermia approaches for enhanced delivery of nanomedicines to solid tumors. Biotechnology and Bioengineering. 112(10):1967-1983. (2015).

tumor still remains low at <5% ID [2]. Additionally, the administration of drugs systemically through intravenous (IV) injection can result in an undesirable biodistribution leading to accumulation within healthy vital organs causing harmful side-effects and toxicity. These adverse effects can limit dosing of chemotherapy due to concerns for patient safety and leads to the patient potentially going untreated allowing the cancer to continue to grow. To help resolve the problems of low tumor accumulation and systemic toxicity, many nanoparticle systems have been developed to enhance the delivery of chemotherapeutic drugs to the tumor site as well as target the tumor specifically to avoid or limit off-target accumulation and dose-limiting toxicity.

A variety of nanoparticles have been developed for targeted drug delivery to solid tumors. These can broadly be categorized as inorganic [4] and organic [5] nanoparticles. Inorganic nanoparticles investigated for drug delivery to solid tumors include, but are not limited to, gold [6-8], magnetic [9-11], and silica-based nanoparticles [12]. Organic nanoparticles include, but are not limited to, synthetic polymeric systems such as linear water soluble polymers [13-17], branched macromolecules such as dendrimers [18], amphiphilic micellar structures [19-22], lipid-based particles such as liposomes [23], and natural carriers such as albumin [24, 25]. Figure 2.1 represents a few examples of some of the nanoparticles used for drug delivery.

Associating drugs with any type of nanoparticle formulation alters the pharmacokinetic properties of the drug. For example, accumulation in the tumor of drug containing liposomal, micellar, and polymeric delivery systems is generally higher compared to free drugs [19, 20, 26-28]. This is largely due to extravasation through the highly permeable vasculature of tumors in combination with the poorly operating

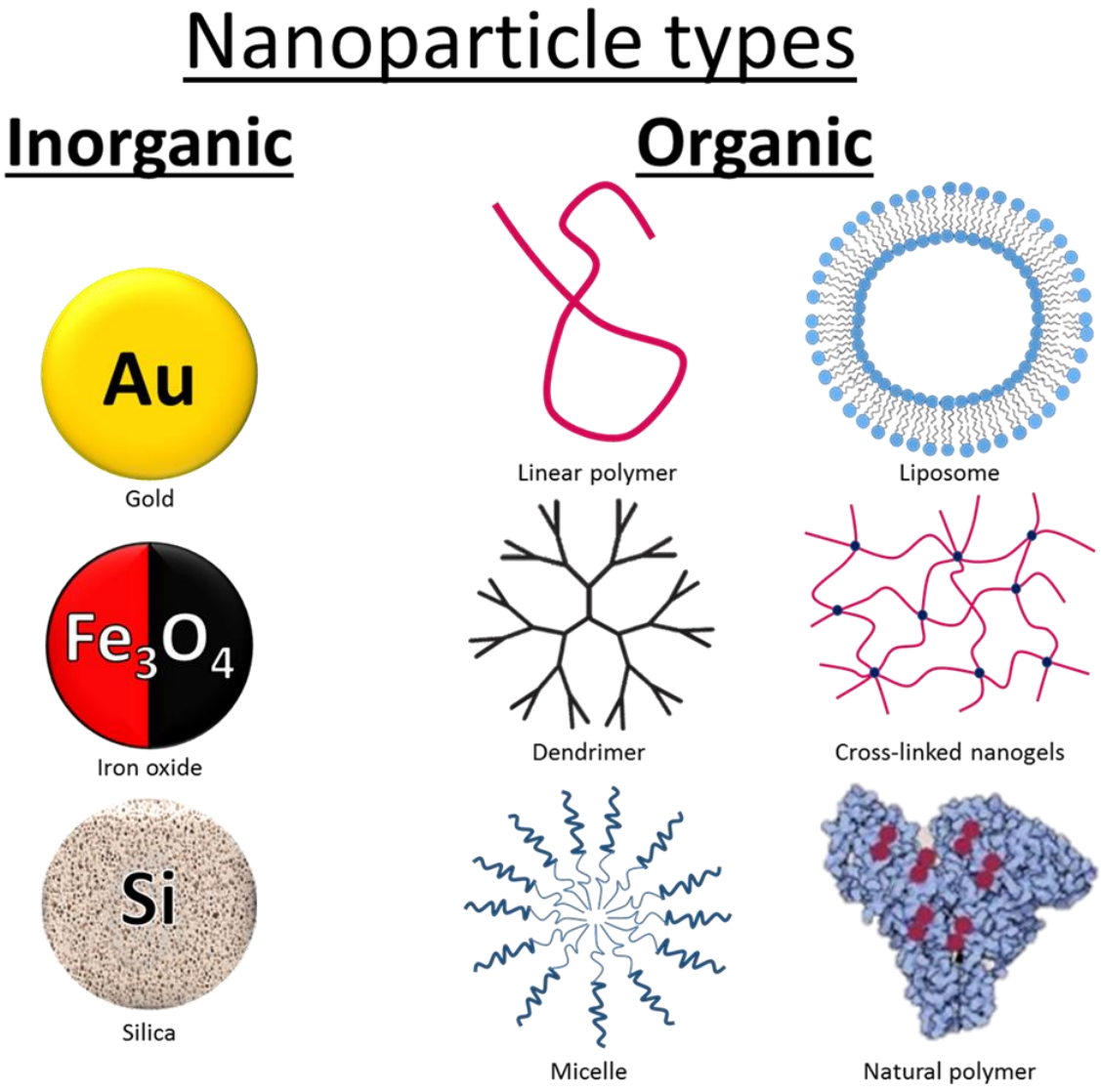

Figure 2.1: Examples of different nanoparticle types used for drug delivery. Inorganic nanoparticles include gold, magnetic, and silica-based systems. Organic nanoparticles include linear polymers, hyperbranched dendrimers, micelles, liposomes, cross-linked nanogels, and natural polymers.

lymphatic system exploiting the enhanced permeability and retention (EPR) effect, as well as lowering systemic toxicity [29, 30].

The majority of nanoparticles investigated for cancer treatment exploit the EPR effect [29-33]. The EPR effect arises within many solid tumors due to the unique structural features during vascular formation. Blood vessels are irregularly shaped and undergo sprouting, proliferation, remodeling, and regression [31]. The tumor vascular network lacks normal hierarchical arrangement and includes hyper-vasculature, defective vascular architecture, and impaired lymphatic drainage [30, 31, 34]. The resulting blood vessels can have large pore sizes that allow for the passive accumulation of nanoparticles leading to extravasation from the blood supply while being retained from the lack of functional lymphatics [32, 35]. In contrast to low molecular weight molecules (i.e., free drug), nanoparticles large enough to avoid renal filtration circulate throughout the body (circulation half-life) on the scale of several hours up to one day rather than a period of only a few minutes for commonly used chemotherapeutics [36]. This prolonged circulation leads to more accumulation in the tumor by the EPR effect [33]. However, there is significant heterogeneity within and between tumor types [37]. Heterogeneity of tumors can lead to differences in vascular pore dimensions and EPR based on tumor size, type, location, and extent of macrophage infiltration and activity of the mononuclear phagocytic system [37]. The heterogeneity of the EPR effect in solid tumors may contribute to the limited impact of nanoparticle conjugated drugs [37]. Additionally, the impact of nanomedicines has been limited by clearance and sequestration by the mononuclear phagocyte system (MPS) and kidneys eliminating >90% of administered nanoparticles from the blood supply [38].

Despite a large investment over the last 30 years toward the development of nanomedicines to selectively treat cancer, significant clinical translation has not been observed [38]. Passive targeting by the EPR effect has been the foundation of many nanomedicines designed to increased anticancer activity and lower toxicity [39]. However, only very few nanosystems based on this principle have had success in the clinic [39]. This may be due to several key differences between human and murine tumors accounting for the disparity between preclinical and clinical trial results of most drug carriers [40]. Human tumors can have numerous causes, where the right set of mutations are required to initiate uncontrolled proliferation undergoing a process of elimination, equilibrium, and escape that can often take years [40]. Murine tumors are more apt to be subject to research constraints and generally developing tumors within a few weeks instead of years. During this growth process, angiogenesis must occur at a rapid pace making the blood vessel structure particularly disorganized, hyperpermeable, and exhibit EPR [40]. Lastly, the large tumor-to-body weight ratio in mice as compared to human patients may also significantly alter the pharmacokinetics of drug carriers. Human tumors tend to be no more than a few grams in weight, giving it an insignificant share of the total body weight of the patient, whereas murine tumors are often grown to be as much as 10% of the mouse's body weight. Such large tumors filter a significant portion of the injected dose of the nanomedicine, effectively improving the accumulation and efficacy while mitigating the toxicity. Therefore, with these revelations, it seems that targeting tumor tissue by EPR alone likely will not achieve improved efficacy in humans and other strategies besides passive targeting must be considered to enhance delivery.

Alternative strategies to enhance delivery include augmentation of the EPR effect

with the use of vascular mediators as well as heat treatment with mild hyperthermia to increase blood flow and vascular permeability in the heated tumor tissue [41]. Vascular mediators can be used to increase the blood pressure during infusion of the nanomedicine with certain mediators [37]. However, hyperthermia has the capability to be controlled over time and can additionally create other beneficial effects for the treatment of cancer. The focus of this chapter is on the use of hyperthermia to enhance the delivery of nanomedicines to solid tumors.

2.2 Hyperthermia to enhance delivery

The EPR effect can be augmented in a number of ways to enhance the delivery of nanomedicines to solid tumors. One such method that has shown great promise for improving localization, penetration, and targeting effects of nanomedicines to solid tumors is through the generation of heat within the tumor. Hyperthermia can be applied in a variety of ways for cancer treatment, each with their own advantages and disadvantages.

Hyperthermia in cancer treatment is defined as the generation of heat generally between temperatures of 41°C and 46°C [42]. Mild or moderate hyperthermia is considered to be 41-43°C, whereas severe hyperthermia is at 44-46°C [42]. When the tumor is subjected to temperatures > 46°C, this is considered to be thermoablation, causing cells to undergo direct tissue necrosis, coagulation, or carbonization [43]. Hyperthermia can be applied to either heating the entire body, a region of the body, or selectively heating of a solid tumor only [44]. Of these, local hyperthermia is gaining much more attention than whole body or regional hyperthermia where various techniques are being developed to deliver heat to the tumor specifically [42, 43]. In this review, we will focus our discussion

on modalities used for local therapies. The challenge for these treatments is to noninvasively heat only the tumor cells without damaging the healthy tissues where complications can occur.

Localized hyperthermia has particularly been used as an adjuvant with chemo- or radio-therapy for the treatment of primary tumors and early stage cancers as these tumor cells are considered to be more susceptible to hyperthermic effects [45]. Biological tissues exposed to higher than normal temperatures promote the selective destruction of these abnormal cells [45]. Hyperthermia leads to several physiological changes within the heated tumor tissue (Figure 2.2). At the vascular level, these include increased blood flow, vasodilation, and enhanced permeability [41]. This can, in turn, alter pH and oxygenation of the tumor microenvironment. Hyperthermia also affects cellular processes through protein denaturation, protein folding, aggregation, and deoxyribonucleic acid (DNA) cross-linking leading to disruption of biomolecular assemblies, induction of heat-shock proteins, and also disruption of cellular mechanisms promoting the onset of acidosis or apoptosis [43, 45].

2.3 Combination effects of hyperthermia

Hyperthermia can be used in cancer therapies both to enhance the delivery of specific carriers, or nanomedicines, as well as enhance the efficacy of therapeutic agents. These heat treatments complement currently available therapies such as chemotherapy, radiation therapy, gene therapy, immunotherapy, and surgery [44]. Oncologists have often used the heat treatment in combination with radiotherapy and/or chemotherapy [46, 47]. hyperthermia is known to cause major increases in tumor perfusion, this being one of the

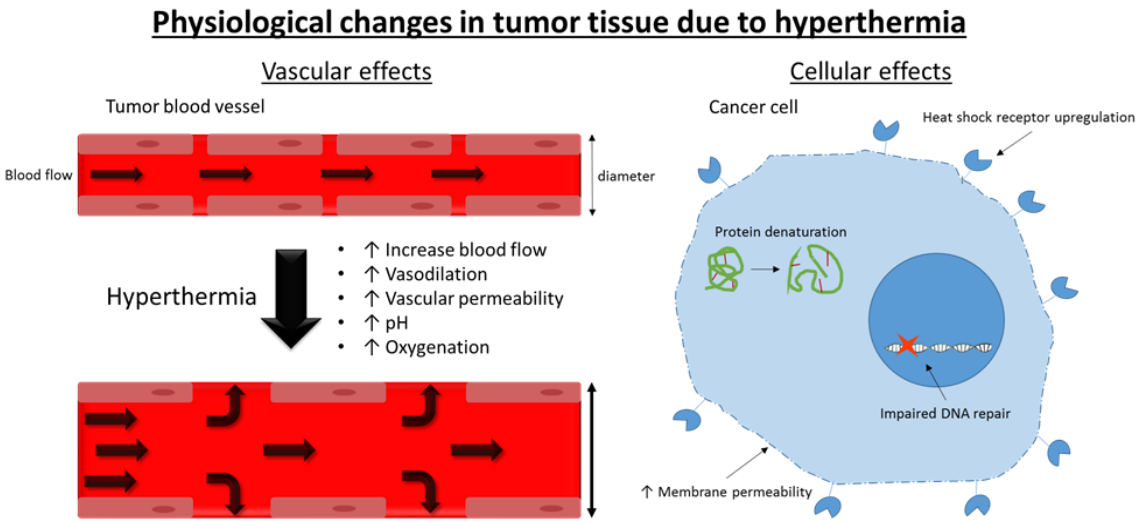

Figure 2.2: Vascular and cellular effects of hyperthermia on heated tumor tissue. Vascular effects include increased blood flow, vascular permeability, and vasodilation. Cellular effects include DNA repair inhibition, protein denaturation, and upregulation of heat shock proteins.

main effects leading to synergistic effects with chemotherapy and radiation treatments [48]. Blood flow within the tumor is highly irregular and poses several challenges as we discussed earlier. However, evidence suggests that hyperthermia can be effective in improving flow throughout these tumors that can overcome some of the biological barriers to delivery when significant localized heating is achieved. Increases in blood flow and accumulation have been observed both during and after hyperthermia [49, 50].

Combined approaches with hyperthermia result in a more effective elimination of many cancer cells in addition to making resistant cells more vulnerable to these treatments [51]. Moderate increases in temperature sensitize cancer cells to cytotoxic agents by increasing the permeability of tumor vasculature and cell membranes and lowering hydrostatic pressure. In addition, hyperthermia can render tumor cells temporarily more sensitive to the damaging effects of radiation or chemotherapeutics through cellular mechanisms. An important effect of hyperthermia is the inhibition of DNA repair [48]. Hyperthermia results in protein unfolding that, if not chaperoned properly by heat shock proteins (HSPs), can lead to irreversible toxic protein aggregates and ultimately leading to apoptosis [52]. It has been shown though that different cell lines exhibit different sensitivities to hyperthermia as this aspect is mostly due to differences in recovery from heat shock [51]. Inducing hyperthermia above a certain threshold temperature (>46°C) is more likely to induce necrosis than apoptosis [51].

Hyperthermia is a promising mode of adjuvant cancer therapy intended to enhance the efficacy of traditional therapies of chemo- and radio-therapy [50]. The synergistic effects of hyperthermia have been studied in cell cultures, animal models, and clinical trials [47]. However, clinical adoption of hyperthermia faces limitations such as the challenge of

localizing heat only to the tumor site and the reduced effectiveness of heating in cancer cells that have developed thermotolerance from up-regulated HSP expression. Modern clinical hyperthermia trials focus mainly on optimizing of thermal homogeneity with moderate temperatures in the target volume using noninvasive methods, a problem which requires extensive technical efforts for development of advanced treatment and thermometry systems [42].

In the continuous search for cancer therapies with a high therapeutic index (ratio of the amount of a therapeutic agent that causes the therapeutic effect to the amount that causes toxicity), localized temperature-induced drug delivery may offer a breakthrough solution in minimally- or noninvasive treatments of cancer. This multidisciplinary approach has evolved from recent advances in pharmaceutical chemistry, nanoscience, hyperthermia technologies, and clinical research with the potential to provide an efficient and patient-friendly treatment option under image guidance.

Several different methods for producing heat in cancer treatments have been developed using alternative energy sources to induce heating. Currently, available techniques to produce heat use external devices such as laser irradiation and electromagnetic currents aided with or without nanoparticles aimed to improve localized heating. Additionally, radiowaves and ultrasound have been used to generate heat but without nanoparticle transducers. Still, limitations exist where incidental heating of healthy tissue can result in burns and discomfort, limited depth of penetration, and insufficient heating of the target region yielding incomplete treatment and recurrent tumor growth [43]. To solve problems of limited penetration depth, one approach has been to insert minimally invasive devices such as antennas or optic fibers directly within or near the tumor, but this

approach is restricted only to locations that are readily feasible for insertion (e.g., head and neck, prostate, liver, and renal) [53].

In the following section, the methods of heating are further detailed and their advantages and disadvantages for the treatment of cancers with localized heating are highlighted. All of these methods have the ability to be used for any type of localized heating mentioned above (hyperthermia or thermoablation) depending on the intensity at which they are applied and the desired outcome.

2.4 Methods of local heat generation for treatment of cancer

2.4.1 Photothermal therapy

Laser light alone can be used to treat cancer by creating heat energy leading to the destruction of the cancer tissue [54-56]. One of the limitations of using laser alone, however, is the nonspecific absorption in surrounding tissues requiring more energy to adequately treat the tumor site and subsequently causes burning, blistering, and pain. Improvements to heat delivery are required to reduce these effects and create specificity of heat generation, homogeneous heat distribution, and therapeutic temperatures in the deep regions of tumors [57]. A common method that has been practiced to improve the depth of penetration and improve selective heating is to use gold nanoparticles (GNPs) specifically synthesized to exhibit plasmonic properties and absorb near-infrared (NIR) wavelengths [45]. Laser irradiation at NIR frequencies can penetrate tissues with sufficient intensity and higher spatial precision for inducing localized hyperthermia [45]. NIR light has the largest depth penetration through most human tissues as blood and soft tissues are relatively transparent allowing light to pass while being weakly absorbed [58, 59]. This region of

light can penetrate several centimeters through tissue and greatly depends on the tissue it travels through [59, 60]. While the light propagation occurs in the tissues, effective mechanisms are then needed to transform the light energy into heat and discriminate unhealthy from healthy cells.

Over the last decade, many research groups have focused on developing novel gold nanostructures to achieve surface plasmon resonance (SPR) in the NIR region. GNPs exhibit SPR at certain wavelengths and when the light is directed to the particles, the SPR causes oscillations of the particles' electron cloud which converts the absorbed light into heat energy [61, 62]. This mechanism can be used to sensitize the tumor tissue for light absorption where it would not have occurred otherwise. In particular, GNP optical properties and flexible surface chemistry permit their use in plasmonic photothermal therapy (PPTT) treatments. Plasmonic gold nanostructures thus show great promise for the selective PPTT of cancer as well as other diseases [63]. The different gold nanostructures that have shown this property include nanoshells [64-68], nanorods [45, 57, 62, 69, 70], and nanocages [58, 71-73].

Delivery of the nanoparticles specifically to the tumor tissue becomes important for successful treatment. The efficiency of delivering GNPs can be enhanced by exploiting EPR effect to concentrate particles in solid tumors. However, as discussed above, this may not be applicable to all tumors as there can be heterogeneity in vascularity in these tissues [37]. The addition of active targeting strategies has been utilized to potentially increase the delivery of GNPs to the tumor tissue in order to reduce the required laser power for PPTT and minimize collateral damage to surrounding healthy tissues [58]. Still, these strategies have not achieved this desired effect and the opposite effect was observed by reduced

accumulation due to faster elimination from the blood [61, 74]. Further work on methods to evade the immune system with these targeted carriers needs to be considered. Targeting to particular tissues can be complicated by possibly inducing interactions with immune cells leading to off-target accumulation in filtration organs such as the liver and spleen [61]. The long-term accumulation in these organs is observed even without conjugation of targeting moieties and the side effects over time are still not fully understood limiting their application in the clinic.

Gold nanoshells can be tailored to absorb NIR light and serve as a photothermal therapeutic strategy [69]. Halas et al. have developed 10 nm thick gold nanoshells supported on 110 nm diameter silica cores with a NIR absorption peak and demonstrated their use in photothermal ablation of cancer cells and tissues [75]. By adjusting the relative core and shell thickness, nanoshells can be synthesized to absorb or scatter light at a desired wavelength. This optical tunability permits fabrication of nanoshells with a peak optical absorbance in the NIR region [76]. These nanoshells were studied for application in producing laser-induced thermal effects in tumors delivered through systemic administration [65]. Studies have shown that nanoshells absorb NIR light and generate increased temperatures sufficient to produce irreversible photothermal damage to subcutaneous tumors [64, 65, 68]. Gold nanoshell applications for tumor photothermal ablation have advanced considerably in the past few years making their way to clinical trials where a single dose pilot study of AuroShell® particles (Nanospectra Biosciences, Inc., Houston, TX) was given intravenously to patients with recurrent or refractory head and neck cancer for treatment with PPTT [67, 77, 78].

Gold nanorods (GNRs) are another type of nanostructure for the application of

PPTT-induced hyperthermia. By synthetically varying the aspect ratio of the nanorods, longitudinal plasmon absorption can be shifted throughout the visible, NIR, and IR regions [79]. The aspect ratio (length: width) that correlates with absorption in this region is approximately 4:1. GNRs exhibit significantly narrower line widths than spherical nanoparticles and are also highly efficient at converting light energy into heat, with a higher absorption cross-section at NIR frequencies per unit volume than most other nanoparticles [57]. The absorption cross-section of nanorod structures is shown to be nominally larger than that of nanocages and more than twice that of nanoshells at their NIR SPR [80]. GNRs perform well as a photothermal device responding to light irradiation because of their strong extinction band corresponding to the longitudinal surface plasmon band [62]. The region of heat generation in photothermal therapy using GNRs can be confined to tumor tissues with high spatial precision because significant heat is generated upon light illumination only at the sites where the GNRs are located [57].

PPTT studies have additionally been performed using gold nanocages (GNCs). GNCs are particularly attractive for additional therapeutic applications from their unique hollow structure allowing for drug encapsulation and controlled release [73, 81]. By controlling the titrated amount of $HAuCl_4$ in the reaction, the SPR peak position of GNCs can be precisely tuned to any wavelength of interest in the range of 600–1200 nm. These GNCs strongly absorb at their SPR peak wavelength which can also be tuned to be in the NIR region [58]. Studies using GNCs for PPTT have been shown to serve as effective transducers converting light energy to heat and effectively treating cancer [73]. These particles have been validated *in vivo* showing photothermal effects were able to decrease tumor metabolic activity only observed in tumors treated with the combination of GNCs

and laser exposure [73].

GNPs of different shapes and structures can be synthesized readily and in a tunable manner to absorb in the NIR region. The advantages and disadvantages of each structure are summarized in Figure 2.3. The NIR light is optimal for penetration through tissues to then be absorbed by GNPs previously accumulated in the tumor. With the application of these two components in conjunction, they can be used to create tumor-specific heating for hyperthermia applications.

Besides the use of GNPs, other types of nanoparticles have recently been developed and used for photothermal therapies. These include Prussian blue nanoparticles [82, 83], carbon nanotubes [84, 85], copper sulfides [86-88], and polypyrrole nanoparticles [89]. These alternatives to GNPs have also been able to show strong absorption in the NIR region. For Prussian blue nanoparticles, an ancient dye made of mixed-valence transition metal hexacyanoferrates with the general formula of $FeIII4[FeII(CN)_6]_3 \cdot nH_2O$, the argument has been made that they are advantageous in their ease and low cost of synthesis and have FDA approval for treatment of radioactive exposure [82, 90]. Comparison to GNRs was performed but required larger amounts of Prussian blue nanoparticles in parts per million and had a much broader absorption peak [83]. Carbon nanotubes have been shown to achieve sufficient heating *in vivo* [84, 85] and exhibit extraordinary photon-to-thermal energy conversion efficiency with a high absorption cross-section of NIR light [91] but are severely limited by their toxicity and difficulties in synthesis [92]. Copper sulfide nanocrystals show high photothermal conversion efficiency similar to that of gold nanostructures but exhibit peak absorbance at 900–980 nm rather than 808 nm, the wavelength commonly used for *in vivo* photothermal ablation [93]. Copper sulfide

	Advantages	Disadvantages
Gold nanoshells 	• Easy tunablility • Good biocompatibility of all components • Progressed to clinical trials for thermoablation	• Absorption cross-section not as high as other structures
Gold nanrods 	• Superior absorption cross-section in the NIR region compared to other structures	• Use of cytotoxic CTAB requires sufficient removal through washing and dialysis
Gold nanocages 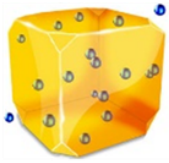	• Hollow interior for drug loading and triggered release	• Additional synthesis steps and difficulty tuning the SPR to the NIR region
Magnetic nanoparticles 	• Ability to simultaneously deliver drugs, induce heating, and serve as an imaging agent	• Corrosion of iron-oxide core can release toxic compounds and cellular damage

Figure 2.3: Nanoparticles for inducing hyperthermia. Advantages and disadvantages of gold nanoshells, nanorods, nanocages, and magnetic nanoparticles.

nanoparticles for photothermal therapies have not been extensively studied but face a few major limitations including very high laser power for nanoparticle activation, not optimized synthesis methods for precise control over size and shape as well as surface modification, and lack of understanding of *in vivo* interactions influencing pharmacokinetics, reticuloendothelial system (RES) sequestration, and renal clearance [93]. Finally, unlike the previously described nanostructures, polypyrrole nanoparticles, formed from a conductive organic polymer, show potential as a biodegradable photothermal agent. These nanoparticles present a new type of low-cost, biocompatible photothermal agent, with high photothermal conversion efficiency and good photostability [89, 94-96].

2.4.2 Magnetic fluid hyperthermia

Magnetic nanoparticles (MNPs) are also used for selective induction of heat specifically within tumor tissues. This method is called magnetic fluid hyperthermia (MFH) and uses MNPs heated by an externally applied alternating current (AC) magnetic field [42, 97]. MFH is a minimally invasive method to treat cancer cells through heat and offers great promise as an approach for localized hyperthermia [98]. MFH creates an increase in temperature from oscillations in the magnetic field which is “absorbed” by the MNPs in the tissue. It requires efficient delivery of the MNPs to the tumor site and subsequently applying a well-defined AC magnetic field [50]. Similar to PPTT, this method leads to heat generation only where the particles reside and requires nanoparticles to be previously dispersed throughout the target tissue to produce sufficient, homogeneous heating when the AC magnetic field is applied.

The amount of heat generated depends on several factors including the strength and

frequency of the applied magnetic field, particle size and composition, and concentration within the tissue [99-101]. Strategies for delivering the particles to the tumor are similar to those above for GNPs. To induce hyperthermic temperatures, the strength of the magnetic field must be sufficient (3.8 to 13.5 kA/m) [102].

MFH may offer several advantages over conventional heating techniques especially since this method has superior selectivity for heat generation where MNPs reside. The magnetic field is not absorbed by surrounding tissues as can be observed with PPTT or other energy sources that are absorbed by conductive tissues. In this case, the tissues do not interfere with power absorption and only the MNPs absorb the oscillating magnetic energy. This therapy has been used in clinical trials and has potential for treatment of a variety of cancers including those of the prostate and brain [102]. MFH has also been clinically evaluated in patients suffering from pretreated recurrent tumors, where hyperthermia in conjunction with irradiation and/or chemotherapy was an option [103]. MFH has shown great capabilities for hyperthermia and thermoablative therapies and should be considered for treatment of various cancers.

The use of MNPs to deliver thermal energy by MFH has been under development for almost six decades but has still not been able to reach significant clinical application. The commercial development of this technology as Nanotherm® has additionally seen limited use in the clinic. Much of this has to do with the significant limitations of this method attributed to dispersion of MNPs throughout the body from systemic administration, lack of homogenous distribution through the tissue for even heating, and insufficient delivery of adequate amounts of MNPs to the tumor site [104]. The long-term impacts of acute exposures are not well understood and it is plausible that internalized

MNPs may corrode over a long period of time releasing metallic ions that can lead to DNA damage [105]. Accumulation in these organs can also lead to heating within undesired tissues when the AC field is applied if the field is not focused to the tumor region. Aggregation of the particles can affect the heat response leading to ineffective treatment. The required amount of MNP tumor accumulation has previously been calculated showing that even for optimized systems, a 5 mm diameter tumor would need a concentration of approximately 650μg/cm^3 [104]. These large amounts of MNPs are needed to accumulate locally and uniformly within the tumor tissue to achieve sufficient heating. In order to achieve such large amounts of localization, the MNPs must be injected intratumorally and which cannot likely be accomplished through IV injection. If this is the case, then the tumor location would need to be determined prior and can potentially miss metastatic regions that could be located with systemic administration. Finally, for patients that have magnetic implants or other implantable devices, this treatment may not be safe for exposure to these large magnetic forces. Although the concept of MFH is very intriguing, its limitations are largely too great to compete with other methods of hyperthermia.

2.4.3 High intensity focused ultrasound

High intensity focused ultrasound (HIFU; frequencies greater than 20 kHz) has been developed into a technology for local hyperthermia and ablation of pathological and cancerous tissues [106, 107]. HIFU is a noninvasive method for producing heat within the body through focusing ultrasound beams into a single focal spot. This can be achieved with single or multiple element transducers. This phenomenon can then create heating by the propagation of ultrasound waves through any type of tissue including bone. When using

multiple-element transducers, the focusing of the beams can take into account the refraction and absorption of heterogenous tissues to focus many beams into a single point [108]. However, because ultrasound waves cannot propagate through air, it is difficult to apply HIFU in regions containing air such as lung or bowel. In addition to being completely noninvasive (not requiring a previous injection of nanoparticles), HIFU has a very large depth of penetration throughout the body with the possibility of treating most any part of the body based on transducer dimensions. HIFU additionally allows for heating with a high degree of temporal control, as the rate of heating depends on the magnitude and duration of the ultrasound exposure, which can be readily controlled [109]. When performed under magnetic resonance imaging (MRI) guidance, the treatment can be enhanced through treatment planning and real time monitoring of the tumor temperature. This simultaneous imaging guides the treatment and can provide real time feedback [110, 111].

One drawback in comparison to the previous methods of heating is that focal zone does not preferentially heat the tumor tissue as we have seen with the other nanoparticle methods. HIFU has a relatively small, cigar-shaped, focal zone, on the scale of a few millimeters (e.g., 1-3 x 3-8 mm), and needs to be moved throughout a larger tumor to achieve uniform heating if hyperthermia is the ultimate goal. Electronic beam steering can be used in this case using a phased array ultrasound transducer in combination with real time temperature mapping by MR thermometry to heat the pathological tissues at a predefined temperature over a certain length of time [112]. This MR-guided HIFU (MRgHIFU) technology platform is currently being clinically evaluated for thermal ablation of uterine fibroids but has also potential applications in temperature-induced local drug delivery with mild hyperthermia [113] and other ablative therapies in oncology (i.e.,

breast, prostate, liver, brain) [114]. Because of these attributes, HIFU has emerged as a leading modality for heat-triggered drug delivery applications. As discussed below, for combination therapies with nanomedicines, HIFU has been extensively used for targeted release of therapeutic payloads from temperature-sensitive liposomes.

2.4.4 Microwaves, radiowaves, other electromagnetic radiation

Electromagnetic (EM) energies such as microwaves and radiowaves have been used to generate heat within tissues including tumors [47]. These types of energy are forms of EM waves and fall within the spectrum of ranging wavelengths and frequencies. Microwaves include EM waves ranging from one meter to a millimeter with frequencies between 300 MHz and 300 GHz while radiowaves are considered to be wavelengths ranging from 1 millimeter to 100 kilometers and frequencies from 300 GHz to 3 kHz. These types of energy interact with the tissue through charged particle oscillations which gain energy within the molecular structure [115]. The energy can be ultimately scattered, reflected, or absorbed by heating the material. Superficial tumors can be locally heated by means of external antennas or applicators that emit microwaves or radiowaves [53]. Several types of applicators exist (e.g., ring, horn, spiral, and current sheet) and have been used in preclinical models [46, 116]. Intratumoral temperature is controlled by both the output of the power generator and also by the positioning of the applicator [53]. In order to ensure sufficiently high temperatures are produced evenly throughout the tumor, multiple applicators can be used. This practice can then become very invasive as multiple needles are required to be inserted around the tumor. All methods previously described for inducing localized hyperthermia are summarized in Figure 2.4. The methods on the right (MFH and

PPTT) require a previous injection of nanoparticles whereas those on the left do not (Figure 2.4). For microwave/radiofrequency application, invasive applicators are required (Figure 2.4). Lastly, HIFU does not require either to heat tumor tissue shown as the red circle in the human outline (Figure 2.4).

2.5 Applications with nanomedicines

It has been shown that nanoparticles alone have added benefits of reducing toxicity while maintaining longer blood circulation and exhibiting controlled release as discussed previously. Targeting of different receptors and pathways can be used with these nanomedicines to improve selectivity, accumulation, retention, and ultimately efficacy [117, 118]. However, the targeting of nanoparticles in many cases does not substantially improve localization or targeted release and still has the potential for further improvements [119, 120]. Localized hyperthermia is one such strategy that possesses this potential and can be applied in combination with any of these nanomedicines to enhance delivery. Also further improving the therapy by reducing general toxicity, triggered release through thermoresponsive nanomedicines can localize the therapeutic payload in the heated region or heated tumor. The latest research using the combination of hyperthermia and nanomedicines has demonstrated that this strategy can be used for better treatment of localized solid tumors which will be discussed further. Hyperthermia has the ability to enhance delivery through increased blood flow and vascular permeability and these mechanisms are the main factors exploited.

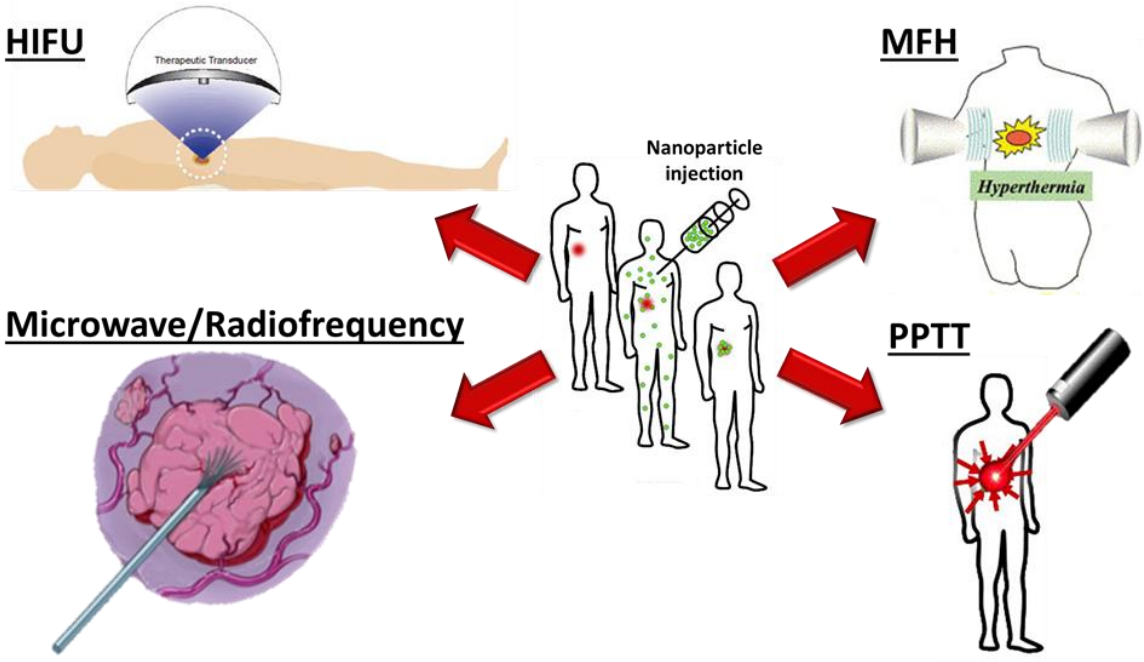

Figure 2.4: Various methods for inducing hyperthermia. High Intensity Focused Ultrasound (HIFU), Magnetic Fluid Hyperthermia (MFH), Microwave/Radiofrequency, and Plasmonic Photothermal Therapy (PPTT).

2.5.1 Enhanced delivery by exploiting vascular effects

As mentioned earlier, applying hyperthermia immediately before or during the administration of nanomedicines can lead to increased accumulation in solid tumors [121]. This approach aims to increase perfusion and vascular permeability leading to favorable effects on extravasation in treated tumor areas. To achieve increased perfusion for enhancing drug delivery, gold nanoshells have been used to mediate the thermal effects [66]. Gold nanoshells were delivered to the tumor site by passive extravasation and retention of the circulating nanoshells from the tumor vasculature into the tumor interstitium. The temperature rise was monitored in real time using MR thermometry and increases in perfusion were measured by MR dynamic contrast-enhanced (DCE) imaging to observe changes in perfusion before and after each hyperthermia treatment. These results indicate that this nanoshell-mediated heating can be used to improve perfusion and subsequently enhance drug delivery [66].

Recently it was shown that these events can also be induced from GNR-mediated PPTT to enhance macromolecular delivery [122]. This method of hyperthermia produced the same effects on tumor vasculature and improves extravasation of nanomedicines into the tumor tissue. To produce the PPTT hyperthermia, the GNRs were also passively delivered to the tumor site through systemic administration and extravasation by the EPR effect. The accumulation was allowed to take place over 48 h when maximal concentration occurs [122]. Immediately before laser therapy to induce hyperthermia, Evans blue dye was injected IV and used to track macromolecular accumulation in the tumor site [122]. With the use of PPTT, the enhanced accumulation was improved up to 80% 5 h post treatment as compared to untreated tumors (Figure 2.5A).

Further, GNR-PPTT hyperthermia was shown to cause up-regulation of cell surface expression of HSPs that can be targeted with specific targeting peptides [123]. Also, this method of hyperthermia was used to enhance the delivery of water-soluble copolymers of *N*-(2-hydroxypropyl)methacrylamide (HPMA) both *in vitro* and *in vivo* [123]. In these studies, DU145 prostate cancer cells were used and showed *in vitro* that combination of hyperthermia and heat shock targeting significantly enhanced the cellular uptake of targeted copolymers [123]. When examined with *in vivo* mouse models using nu/nu mice and the same prostate cancer cell line, PPTT was applied in the same fashion to produce hyperthermia. HPMA copolymer delivery was tracked using ^{125}Iodine radiolabeling and was able to show the effects of HSP targeted and untargeted copolymers with and without hyperthermia [123]. The results indicated that hyperthermia significantly improved untargeted copolymer accumulation over the first 4 h but then returned to baseline accumulation of untargeted copolymers without hyperthermia (Figure 2.5B) [123]. Heat shock targeting alone slightly improved tumor accumulation but when combined with hyperthermia the effects were much greater than any other group improving accumulation and retention. It is suggested that hyperthermia can transiently enhance the delivery to the heated tumor site and that the use of heat shock targeting increases the interactions with cellular receptors resulting in greater uptake and retention within the cells [123].

The effects of hyperthermia were visualized by MRI to examine the delivery and tumor distribution of untargeted HPMA copolymers labeled with gadolinium (Gd) as an MR contrast agent [124]. Using the same *in vivo* animal model, hyperthermia was applied whole tumor tissue including the tumor core [124]. This indicates that PPTT has the ability to one of two tumors and imaged over 5 h [124]. It was observed that during this time

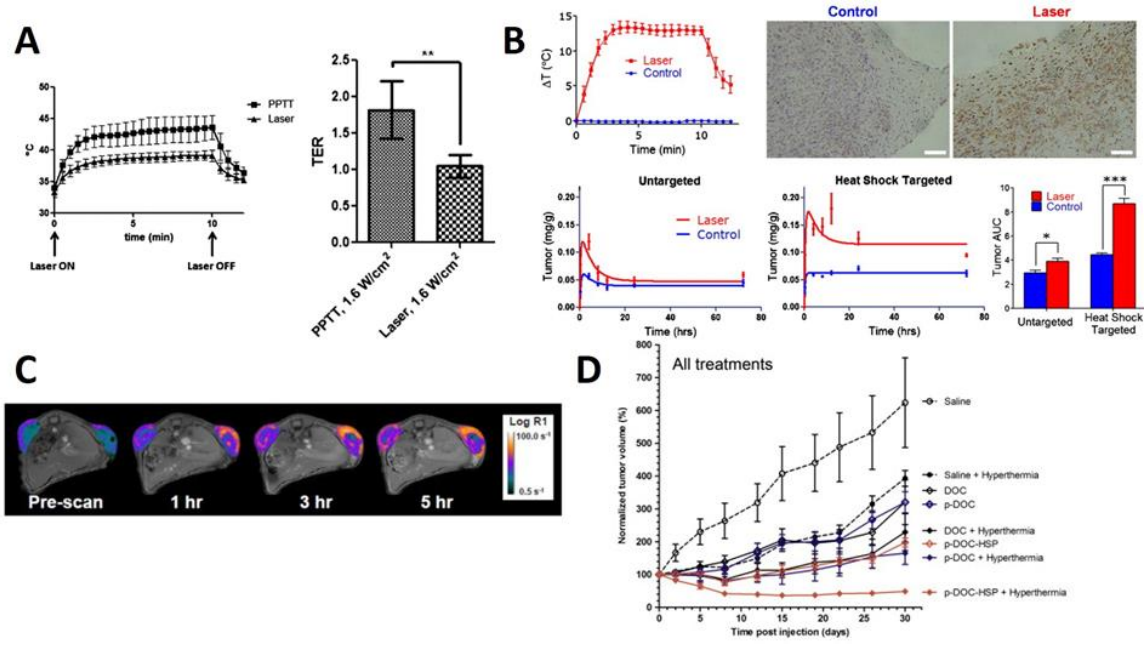

Figure 2.5: A) PPTT heating control for hyperthermia and enhanced accumulation of Evans blue dye (EBD) at 5 h post treatment compared to laser control. B) Plasmonic photothermal therapy (PPTT) temperature control, induction of heat shock proteins *in vivo*, polymer accumulation profile, and area under the curve (AUC) of the different polymer +/- hyperthermia groups. C) Enhanced Gd-labeled polymer accumulation over time as visualized by MRI. D) Enhanced efficacy of combination therapy. Results indicate that gold nanorod (GNR) mediated PPTT is able to selectively heat tumors while increasing the delivery and penetration of nanomedicines and ultimately improving treatment in combination therapy. These data were used with permission [122-125].

period, after PPTT hyperthermia and simultaneous injection of Gd-labeled copolymers, the polymers accumulated to a greater extent within the heat treated tumors (Figure 2.5C) [124]. Furthermore, the accumulation of the copolymers was improved throughout the to partially overcome the high interstitial pressures within the tumor to improve spatial distribution in regions of the tumor that are difficult to penetrate. This can potentially be explained by the importance of nanocarrier size on interstitial diffusion and the use of hyperthermia to enhance convective and diffusive transport [124].

The improved accumulation, retention, and penetration of HPMA copolymers was correlated with enhanced efficacy showing that targeted polymer-drug conjugates improved tumor size reduction as compared to control groups without hyperthermia or HSP targeting (Figure 2.5D) [125]. In this study, synergistic effects of different copolymer-drug conjugates were examined with hyperthermia showing that the targeted HPMA copolymer-docetaxel conjugates had the largest synergistic effect. It is interesting to note that *in vivo* hyperthermia alone also contributed to a reduction in tumor growth in the control group. However, this is expected as we have discussed hyperthermia alone influences cellular processes. Along with improving the effectiveness of chemotherapy, this strategy was used to show the added benefits for improved efficacy of combination treatment using radiotherapy [126].

Another study focused on evaluating the use of GNR-mediated PPTT to increase delivery of somewhat larger dextran nanoparticles into the tumor [127]. This study used larger particles of dextran (54 nm in diameter) [127] as compared to the HPMA copolymers (~6 nm hydrodynamic radius) [123]. Nonetheless, this strategy for enhancing delivery has shown to be useful by applying heat selectively to the tumor site and improving transport

of nanomedicines. Finally, hyperthermia effects of GNP mediated PPTT were shown to produce small disruptions in the cell membrane providing enhanced uptake of drug molecules [128]. This enhancement of intracellular delivery was also observed using FeCo/graphitic carbon shell (FeCo/GC) nanocrystals (~4-5 nm) [129]. It was demonstrated that enhanced intracellular drug delivery was achieved when FeCo/GC conjugated with doxorubicin (DOX) was exposed to 20 min of NIR laser irradiation to induce hyperthermia [129]. The ultimate result was a significant increase in toxicity toward breast cancer cells due to the PPTT heat treatment leading to an approximate two-fold enhancement of cancer cell uptake of the FeCo/GC-DOX complexes as well as synergistic effects of heat and DOX [129].

HIFU hyperthermia has also been shown to improve transport across the blood–brain and tumor barriers [130]. HIFU-induced hyperthermia was able to increase delivery and therapeutic efficacy of polyethylene glycol-coated (PEGylated) liposomal DOX to brain metastasis of breast cancer [130]. Murine breast cancer 4T1 cells were injected into BALB/c mice striatum tissues and used as a brain metastasis model. The mice were injected IV with the liposomal formulation and treated with or without 10 min of transcranial HIFU hyperthermia [130]. This HIFU hyperthermia was able to significantly enhance the delivery of liposomal DOX into brain tumors and effectively inhibit tumor growth with a single combination treatment as compared to controls. Again, this further demonstrates that the application of hyperthermia after nanomedicine injection is an effective approach to enhance delivery and improve the treatment of cancers [130].

Hyperthermia effects on the tumor tissues (increased blood flow and vascular permeability) are largely responsible for enhanced delivery of nanomedicines.

Nonetheless, this can be additionally improved upon with stimuli-responsive systems.

2.5.2 Thermoresponsive triggered release systems

For hyperthermia triggered drug delivery, a majority of current research uses triggered temperature-sensitive delivery systems for targeted release. Much of these applications have been developed to target or preferentially accumulate at the tumor site and then selectively release their entire payload in the presence of heat or hyperthermia. Others have had additional success with intravascular triggered release during simultaneous delivery of a nanoparticle injection and localized hyperthermia.

2.5.2.1 Inorganic systems

Similar to previous PPTT methods discussed in drug delivery, GNCs have been used to induce hyperthermia through PPTT and create a novel drug delivery system when heat triggers the release of preloaded drugs from the cages' hollow interior. GNCs were synthesized to absorb NIR laser light, loaded with a PEGylated alizarin dye, and coated with thermoresponsive poly(N-isopropyl acrylamide)-co-poly(acrylamide) (pNIPAAm-co-pAAm) copolymers as proof of concept [81]. When irradiated with NIR laser light, most of the dye molecules were released within 16 min [81]. Furthermore, the GNCs were loaded with doxorubicin (DOX) and showed the same triggered release in the presence of laser irradiation *in vitro* for eliminating breast cancer cells. As the irradiation time increased, more cancer cells were killed as more DOX was released. In comparison, laser alone had no effect on cell death and laser with GNCs exhibited slight cell death due to photothermal effects [81].

MNPs have also been used to form thermoresponsive systems where the particles were coated with temperature-sensitive polymers and encapsulated drugs forming a hyperthermia-based drug delivery system. These systems have been developed and recently dubbed as magnetothermally triggered drug delivery systems, where MFH triggers thermally activated materials [131]. By combining IONPs with lower critical solution temperature (LCST) polymers, an AC magnetic field can be used to initiate localized heating and trigger a phase change in the polymer coating to release drugs [131]. One such study has used an A-B-A triblock copolymer coating of A) PEG and B) poly(propylene succinate) (PPSu) [132]. This copolymer coating was shown to be biocompatible, biodegradable, and thermosensitive for the release of encapsulated paclitaxel when exposed to an AC magnetic field [132]. When the temperature was raised from 37 to 42°C, the polymer coating became softer as the crystalline structure was destroyed and became an amorphous melt structure. The loaded drug molecules were then released at a faster rate through the amorphous matrix as diffusion became easier through the flexible amorphous polymer chains [132]. Magneto-thermally triggered systems have also been used by coated IONPs with N-isopropyl acrylamide as a thermosensitive monomer and N,N-methylene bisacrylamide as the crosslinker. These particles were shown to generate sufficient heat for hyperthermia application and controlled release experiments demonstrated excellent drug loading and temperature-triggered release of 5-fluorouracil [133].

2.5.2.2 Organic systems

Release from liposomal drug delivery systems in the absence of external stimuli can be very slow [134]. The entrapped drugs need to be released from the liposomes in

order to reach tumor cells for a therapeutic effect. Thus, to create a system that can protect the drug from rapid excretion and have a targeted release, thermosensitive liposomes (TSLs) have been developed in conjunction with local hyperthermia [135]. Many strategies have been employed to create a rapid release and much of this research has focused around liposomal nanomedicines that have temperature sensitive groups (i.e., specific lipids, polymers, or other modifiers) incorporated within the liposomal formulation to trigger the release of their payload in the presence of heat above a certain threshold [136-140]. Yatvin et al. has pioneered this area, developing TSLs composed of phospholipids having transition temperatures slightly above normal physiological temperature to rapidly release pharmaceuticals under heating conditions [135]. For applications in oncology, TSLs can be used in combination with localized hyperthermia to create a new effective drug delivery system. *In vivo*, the liposomal formulation is injected just prior to or during hyperthermia treatment and immediate release of their contents is initiated upon arrival to the heated tumor area. Local hyperthermia causes the lipid structures in the liposomes to ‘‘melt’’, and the liposomes flowing through the vascular bed of a heat treated area rapidly release the entrapped drug into the surrounding tissues [135].

The use of TSLs with hyperthermia has been studied extensively with heating modalities such as MFH and HIFU. MNPs have been used successfully in cancer therapy for MFH as described earlier. In combination with TSLs, magnetic formulations have been developed for drug targeting and eventual triggered release by MFH [141, 142]. These liposomes have been additionally directed to the tumor site by a permanent gradient magnetic field [143]. Once at the tumor site, magnetic liposomes are then triggered to create heating and quickly release the therapeutic payload under an AC magnetic field

[141]. This fast release is due to the particles being embedded within the lipid bilayer and produces direct lipid phase transition [142]. Taken together, these multifunctional targeted magnetic TSLs enable improved tumor cell killing in comparison to nonmagnetic targeted liposomes [141, 144].

Many additional strategies have been used to improve the combination of TSLs with hyperthermia. On the chemistry and synthesis side, this includes creating liposomes that have optimized heat sensitivity. TSLs are comprised of lipids and some combination of cholesterol and/or PEG-conjugated lipid for prolonged blood circulation [53]. Release properties of these TSLs have been extensively studied and lead to an optimized molar percentage of lysolipids in dipalmitoylphosphatidylcholine (DPPC) bilayers to form stabilized defects in the membrane during the phase transition and enhanced release within tens of seconds [53]. Alternatives to lysolipids, which may desorb from liposomal shells and thus compromise the stability and/or thermosensitivity of the liposome, have also been studied such as the use of synthetic temperature-sensitive polymers to improve the responsiveness [145]. Liposomes modified with thermosensitive polymers (TSPs), for example, poly(N-isopropyl acrylamide) (NIPAAm), aggregate at temperatures above this LCST [146]. Anchored to lipid membranes via hydrophobic interactions, they dehydrate and collapse at the LCST, disrupting the TSL membrane inducing drug release. Additionally, the LCST of these TSPs can be tuned through copolymerization with a variety of monomers, which also affects the extent of drug release [53].

Strategies have focused on making these liposomes more sensitive to hyperthermia while others have taken the approach of additionally targeting the system towards receptors or ligands. One such method was developed encapsulating drugs within targeted cationic

TSLs [147]. The cationic charged lipids improve specificity to tumor vasculature and tumor cells along with a thermosensitive liposomal bilayer for heat-triggered drug release [147]. The cationic TSLs selectively target angiogenic endothelial cells and tumor cells based on electrostatic interactions between their cationic surface and overexpressed anionic molecules on angiogenic endothelial and tumor cell membranes [148, 149]. Combining the targeting functionality and internalization properties of cationic liposomes with a heat-triggered release function can ensure controlled release of drug contents at the tumor site while also improving the permeability of these liposomes throughout the tumor tissue [147]. Several investigators have studied TSLs that were modified with targeting ligands such as peptides, aptamers, and folate [150]. These targeting ligands exhibit binding affinity for cancer cells and triggered drug release when exposed to hyperthermia [151, 152].

The method of hyperthermia which has received the most attention in combination with nanomedicines such as TSLs has been HIFU. This method has several advantages mentioned previously. Other heating modalities for triggering drug release from these TSLs have generally suffered from limited penetration depth, invasiveness, insufficient spatial and temporal control of heating, and insufficient and invasive monitoring of heating. For localized heat-triggered drug release from TSLs, several groups have demonstrated the potential of HIFU-TSL systems [48, 153-158]. In particular, Dromi et al. demonstrated in a preclinical model that TSL combined with hyperthermia from HIFU enhances drug deposition at the tumor and delays tumor growth relative to treatment without HIFU [153].

Combinations of HIFU hyperthermia can be used to enhance the delivery of TSLs and show increased levels of extravasation of liposomes with increasing temperatures from

39 to 42°C applied for 60 min [159]. It was also demonstrated that the increased vascular permeability in this tumor model lasted up to 4 h after treatment. In more recent work with the combination of TSLs and MRgHIFU, Ranjan et al. were able to demonstrate enhanced drug accumulation within the tumor site [160]. Manzoor et al. have also shown that the use of TSLs in combination with hyperthermia is able to increase the amount of drug accumulation in heated tumors versus nonheated and nonencapsulated drug controls [161]. The combination of TSL encapsulated administration of DOX and hyperthermia leads to the intravascular release of drug and higher amounts of tumor accumulation than with either alone [161]. The absence of heat leaves the drug within the liposomes and confined within the vessels whereas free drug and heat only create a transient increase in drug accumulation for 1-5 min [161]. Interestingly, both groups have shown that tumors heated with TSL and hyperthermia showed a greater amount of drug was able to penetrate to the tumor core [160, 161]. This effect was additionally observed using PPTT and HPMA copolymers and is again important to note since delivery of drugs to this region has been difficult. This phenomenon is likely due to the hyperthermia effects reducing the interstitial pressure while improving tumor perfusion but may also be attributed to vibrational forces from ultrasound creating better penetration [160]. Nevertheless, this combination therapy was shown to enhance the delivery of therapeutics by Rajan et al. resulting in a 3.5- and 7.6-fold more tumor accumulation in TSL and DOX control groups, respectively, and Manzoor et al. were able to show a nine-fold increase in DOX accumulation over 20 min as compared to control groups of free drug [160, 161].

The sequence at which HIFU-induced hyperthermia is applied has been studied by a few different groups. Grüll et al. applied hyperthermia either directly after or 24 h after

injection with the drug formulation [157]. HIFU hyperthermia directly after the injection of TSLs resulted in the greatest increase in drug concentration in the tumor in their studies. HIFU hyperthermia performed 24 h after the injection of the TSLs showed no further increase in drug accumulation likely due to clearance of the TSLs from the blood within that time frame. As expected, the increased drug concentrations within the tumor lead to reductions in tumor growth compared to controls [157]. This type of study was also performed by Li et al. but in the opposite sequence meaning HIFU hyperthermia was applied first and then TSLs were injected [121]. Hyperthermia induced hyperpermeability within the tumor vasculature which remained for approximately 8 h and was used to enhance the delivery of TSLs [162]. After maximal accumulation and penetration, a second dose of hyperthermia was used to trigger release from the TSLs. This two-step approach lead to greater accumulation as compared to if there was no first step hyperthermia [121]. Therefore, taken altogether, it is likely best to start hyperthermia before injection of TSLs in order to predispose the tumor tissue for enhanced accumulation by vascular mechanisms and continue heating for some time after injection for complete intravascular release of the therapeutic payload of all TSLs in the heated area during peak plasma concentration of the liposomal drug. Finally, mathematical models have been used to compare the administration of free DOX, liposomal encapsulation (stealth and TSL) and the optimal regimen for inducing hyperthermia for triggered release, be it intra- or extra-vascular [163]. In these studies, the amounts of intracellular drug concentrations were compared showing that intravascular release had the highest accumulation with a concentration of 100.6 μg/g versus 15.9 μg/g for extravascular release, 3.4 μg/g for free DOX, and 0.4 μg/g for stealth liposomal DOX [163]. As liposomal formulations of DOX are known to reduce cardiac

toxicity [164], the accumulation of the drug in cardiac tissues was also examined. The ratio of drug exposure between tumor and cardiac tissue for each DOX formulation was determined that extravascular released TSLs were best followed by fast-release intravascular TSLs, slow-release intravascular TSLs, stealth liposomal DOX, and free DOX in that order [163].

In summary, several groups have shown that this combination results in a greater amount of drug accumulation at the tumor in response to heating and triggered release, reducing the required drug dose and more importantly enhancing the efficacy of treatment leading to better tumor reduction having the potential to effectively eliminate cancers. As a source of hyperthermia to trigger drug release from TSLs, several have employed HIFU as it is more advantageous in terms of its noninvasiveness as compared with other methods such as microwave, radio frequency, and NIR laser heating that require an interstitial needle or insertion of an antenna or fiber optic probe.

It is noteworthy for possible translation of this method that the lysolipid TSL formulation developed by Needham and Dewhirst's groups at Duke University has undergone further pharmaceutical development by the biopharmaceutical company Celsion, marketed as ThermoDox®. This system has previously gone through Phase I/II clinical trials for the treatment of hepatocellular carcinoma and has now reached Phase III clinical trials in combination with radiofrequency ablation (RFA). In Phase I trials patients were given a 30-min infusion, 15 min prior to RFA. The study was able to determine the peak plasma concentration to be at 30 min (coincident with the end of infusion), an initial half-life of approximately 1 h, and maximum tolerated dose (MTD) of 50/mg/m^2 [165]. A statistically significant difference in the time to treatment failure was observed between the

patients receiving at least the MTD and patients receiving less than the MTD (374 vs. 80 days, respectively). The study concluded that the combination of RFA and ThermoDox® was safe and likely more efficacious than RFA alone. These results formed the rationale for a multinational phase III trial for the treatment of hepatocellular carcinoma. The latest results have shown that as of January 15, 2015, the latest quarterly overall survival (OS) analysis at the time of this writing, in a large subgroup of patients with single HCC lesions (n=285, 41% of the study patients), the combination of ThermoDox® and optimized RFA provided a 59% improvement in OS compared to optimized RFA alone [166]. A phase I trial has been completed and a phase II trial has been initiated for the treatment of recurrent chest wall disease in breast cancer patients with the combination of ThermoDox® and hyperthermia [167]. The interim results have been posted on Celsion's website and based on the data available to date (4/2015), 67% of patients experienced a clinical benefit of their highly refractory disease with a local response rate of 58% observed in the 12 evaluable patients, notably 5 complete responses (CR), 2 partial responses (PR) and 1 patient with stable disease (SD) [168]. Because of the broad range of doxorubicin antitumor efficacy, ThermoDox® has the potential to be used to treat multiple other cancer types. Celsion is also interested in initiating clinical trials to assess the use of HIFU in combination with ThermoDox® for the treatment of metastatic bone cancer. Additionally, Celsion is looking into the treatment of pancreatic cancer with ThermoDox® [169].

Similarly, thermosensitive micelles have been studied with hyperthermia for enhanced delivery to solid tumors. Over the past decade, considerable efforts have been devoted to design and prepare NIPAAm-based thermosensitive polymeric micelles as delivery vehicles for controlled drug release [170]. Biodegradability can also be

incorporated using poly(D,L-lactide), poly(ε-caprolactone), or poly(D,L-lactide-co-ε-caprolactone) as the hydrophobic block of the amphiphilic block copolymers [171]. These micelles exhibit rapid and thermoresponsive drug release for combination with thermal therapy [171].

In vitro release behavior showed a dramatic thermoresponsive fast/slow switching behavior according to the temperature responsive structural changes of a micellar structure [172]. *In vivo* with radiofrequency heating, smaller thermosensitive micelles resulted in superior tumor penetration and more effective local molecular modulation whereas larger long-circulating liposomal carriers resulted in greater intratumoral drug accumulation over time and reduced tumor growth. Accordingly, different carriers provide specific advantages, which should be considered when formulating optimal combination therapies [173].

It has been shown that thermally responsive elastin-like polymers (ELPs) can be used as triggered delivery release system to enhance targeted delivery to solid tumors. ELPs are genetically engineered, thermally responsive polypeptides that can be guided to accumulate in solid tumors treated with mild hyperthermia [174]. Thermoresponsive ELPs accumulated in solid tumors at a significantly greater level than in unheated tumors or with a thermally insensitive ELP in heated tumors [174]. It was additionally shown that the thermos-cycling (repeated heating with hyperthermia) of the tumor region would form micron-sized aggregates from circulating ELPs that would adhere to the tumor vasculature thus enhancing the delivery to the tumor site [158]. This effect was shown to be repeatable as the formation of adherent microparticles of ELP were produced in the heated tumor vasculature in each thermal cycle [158]. This leads to a highly specific thermally targeted

system to improve delivery to heated tumors as the thermosensitive ELPs will only aggregate in the heated tumor.

2.6 Conclusion

Much work has been accomplished to create a combination therapy for hyperthermia with nanomedicines. Several types of nanoparticles have been developed including those with thermosensitivity as well as different methods for inducing localized heating with solid tumors. Clinical challenges of hyperthermia methods include improved selectivity to the tumor site as well as reducing invasiveness. The use of either GNPs or MNPs for PPTT or MFH respectively requires injection of particles systemically or directly into the tumor site. The accumulation in healthy filtration organs, when delivered systemically, causes concern for long-term exposures and largely prevents further development in the clinic. Additionally, if the particles are injected directly into the tumor, this requires that the tumor be superficial (i.e., head and neck cancer) or otherwise easily accessible. EM radiation of microwaves and radiowaves has been used in clinical applications, but the use of minimally invasive needles or antennas can cause damage to surrounding tissues and may require several probes to effectively heat the entire tumor.

Of the methods that were described above, the heating method that has shown the most promise for localized hyperthermia of solid tumors has been HIFU. This method is noninvasive and can be used to treat tumors with the exception of those in air-filled cavities such as the lungs. It may be possible though that PPTT or MFH can be used in those instances. Nonetheless, HIFU has undergone recent advances for selectively heating tumors with MRI guidance. For hyperthermia treatment, however, there is a need for a

computational feedback system with MR thermometry that can determine the thermal dosing and other parameters such as raster pattern and speed to reproducibly heat different tumor sizes and types with hyperthermia. Robust temperature controlling, including algorithms for motion compensation during the procedure, are essential for such a system. Uniform heating of specific temperatures within the tumor tissue and reproducibility from tumor to tumor is very important for improved drug delivery. Improved modeling software and computer algorithms are required to create this system. The clinical relevance of HIFU provides hope that there will be a clinically approved hyperthermia system for combination therapy with nanomedicines.

Novel nanoparticle formulations have been created for combination with hyperthermia, through heat shock targeting and temperature sensitive delivery systems. Additionally, other methods have been developed to deliver both heat from PPTT or MFH with triggered drug release. It is important to note that several of these nanoparticles are going through or have been through clinical trials such as Thermodox and other carriers including HPMA copolymers. Several nanoparticle types have been studied in their combination with hyperthermia, both thermo- and nonresponsive. These systems in combination with hyperthermia have been shown to greatly enhance tumor localization and accumulation as well as efficacy. Despite the challenges described above, substantial progress has been made in using hyperthermia for enhancing the delivery of nanomedicines for the treatment of solid tumors. Such a strategy holds promise for future of local cancer therapy.

2.7 References

[1] H. Cho, A.B. Mariotto, L.M. Schwartz, J. Luo, S. Woloshin, When do changes in cancer survival mean progress? The insight from population incidence and mortality, JNCI Monographs 2014(49) (2014) 187-197.

[2] Y.H. Bae, R.J. Mrsny, K. Park, Cancer targeted drug delivery: An elusive dream, Springer Science & Business Media, 2013.

[3] V.P. Chauhan, T. Stylianopoulos, Y. Boucher, R.K. Jain, Delivery of molecular and nanoscale medicine to tumors: Transport barriers and strategies, Annual Review of Chemical and Biomolecular Engineering 2(1) (2011) 281-298.

[4] I. Ojea-Jimenez, J. Comenge, L. Garcia-Fernandez, Z.A. Megson, E. Casals, V.F. Puntes, Engineered inorganic nanoparticles for drug delivery applications, Current Drug Metabolism 14(5) (2013) 518-530.

[5] S. Mitragotri, P. Stayton, Organic nanoparticles for drug delivery and imaging, MRS Bulletin 39(03) (2014) 219-223.

[6] P. Ghosh, G. Han, M. De, C.K. Kim, V.M. Rotello, Gold nanoparticles in delivery applications, Advanced Drug Delivery Reviews 60(11) (2008) 1307-1315.

[7] B. Duncan, C. Kim, V.M. Rotello, Gold nanoparticle platforms as drug and biomacromolecule delivery systems, Journal of Controlled Release 148(1) (2010) 122-127.

[8] D. Pissuwan, T. Niidome, M.B. Cortie, The forthcoming applications of gold nanoparticles in drug and gene delivery systems, Journal of Controlled Release 149(1) (2011) 65-71.

[9] C. Sun, J.S.H. Lee, M. Zhang, Magnetic nanoparticles in MR imaging and drug delivery, Advanced Drug Delivery Reviews 60(11) (2008) 1252-1265.

[10] V.I. Shubayev, T.R. Pisanic Ii, S. Jin, Magnetic nanoparticles for theragnostics, Advanced Drug Delivery Reviews 61(6) (2009) 467-477.

[11] O. Veiseh, J.W. Gunn, M. Zhang, Design and fabrication of magnetic nanoparticles for targeted drug delivery and imaging, Advanced Drug Delivery Reviews 62(3) (2010) 284-304.

[12] V. Mamaeva, C. Sahlgren, M. Lindén, Mesoporous silica nanoparticles in medicine—Recent advances, Advanced Drug Delivery Reviews 65(5) (2013) 689-702.

[13] R. Duncan, The dawning era of polymer therapeutics, Nature Reviews Drug Discovery 2(5) (2003) 347-360.

[14] R. Haag, F. Kratz, Polymer therapeutics: Concepts and applications, Angewandte Chemie International Edition 45(8) (2006) 1198-1215.

[15] R. Duncan, Polymer therapeutics as nanomedicines: New perspectives, Current Opinion in Biotechnology 22(4) (2011) 492-501.

[16] F. Canal, J. Sanchis, M.J. Vicent, Polymer–drug conjugates as nano-sized medicines, Current Opinion in Biotechnology 22(6) (2011) 894-900.

[17] J. Kopeček, Polymer–drug conjugates: Origins, progress to date and future directions, Advanced Drug Delivery Reviews 65(1) (2013) 49-59.

[18] S. Svenson, D.A. Tomalia, Dendrimers in biomedical applications—reflections on the field, Advanced Drug Delivery Reviews 64, Supplement(0) (2012) 102-115.

[19] V.P. Torchilin, Micellar nanocarriers: Pharmaceutical perspectives, Pharmaceutical Research 24(1) (2007) 1-16.

[20] E. Blanco, C.W. Kessinger, B.D. Sumer, J. Gao, Multifunctional micellar nanomedicine for cancer therapy, Experimental Biology and Medicine 234(2) (2009) 123-131.

[21] M. Yokoyama, Clinical applications of polymeric micelle carrier systems in chemotherapy and image diagnosis of solid tumors, Journal of Experimental & Clinical Medicine 3(4) (2011) 151-158.

[22] K. Miyata, R.J. Christie, K. Kataoka, Polymeric micelles for nano-scale drug delivery, Reactive and Functional Polymers 71(3) (2011) 227-234.

[23] T.M. Allen, P.R. Cullis, Liposomal drug delivery systems: From concept to clinical applications, Advanced Drug Delivery Reviews 65(1) (2013) 36-48.

[24] F. Kratz, Albumin as a drug carrier: Design of prodrugs, drug conjugates and nanoparticles, Journal of Controlled Release 132(3) (2008) 171-183.

[25] B. Elsadek, F. Kratz, Impact of albumin on drug delivery — New applications on the horizon, Journal of Controlled Release 157(1) (2012) 4-28.

[26] D.B. Fenske, A. Chonn, P.R. Cullis, Liposomal nanomedicines: An emerging field, Toxicologic Pathology 36(1) (2008) 21-29.

[27] D.B. Fenske, P.R. Cullis, Liposomal nanomedicines, Expert Opinion on Drug Delivery 5(1) (2007) 25-44.

[28] K.S. Soppimath, T.M. Aminabhavi, A.R. Kulkarni, W.E. Rudzinski, Biodegradable polymeric nanoparticles as drug delivery devices, Journal of Controlled Release 70(1–2) (2001) 1-20.

[29] H. Maeda, J. Wu, T. Sawa, Y. Matsumura, K. Hori, Tumor vascular permeability and the EPR effect in macromolecular therapeutics: A review, Journal of Controlled Release 65(1–2) (2000) 271-284.

[30] H. Maeda, The enhanced permeability and retention (EPR) effect in tumor vasculature: The key role of tumor-selective macromolecular drug targeting, Advances in Enzyme Regulation 41 (2001) 189-207.

[31] P. Baluk, H. Hashizume, D.M. McDonald, Cellular abnormalities of blood vessels as targets in cancer, Current Opinion in Genetics & Development 15(1) (2005) 102-111.

[32] H. Hashizume, P. Baluk, S. Morikawa, J.W. McLean, G. Thurston, S. Roberge, R.K. Jain, D.M. McDonald, Openings between defective endothelial cells explain tumor vessel leakiness, The American Journal of Pathology 156(4) (2000) 1363-1380.

[33] H. Maeda, H. Nakamura, J. Fang, The EPR effect for macromolecular drug delivery to solid tumors: Improvement of tumor uptake, lowering of systemic toxicity, and distinct tumor imaging in vivo, Advanced Drug Delivery Reviews 65(1) (2013) 71-79.

[34] D. Ribatti, B. Nico, E. Crivellato, A. Vacca, The structure of the vascular network of tumors, Cancer Letters 248(1) (2007) 18-23.

[35] Y. Matsumura, H. Maeda, A new concept for macromolecular therapeutics in cancer chemotherapy: Mechanism of tumoritropic accumulation of proteins and the antitumor agent smancs, Cancer Research 46(12 Part 1) (1986) 6387-6392.

[36] A. Gabizon, R. Catane, B. Uziely, B. Kaufman, T. Safra, R. Cohen, F. Martin, A. Huang, Y. Barenholz, Prolonged circulation time and enhanced accumulation in malignant exudates of doxorubicin encapsulated in polyethylene-glycol coated liposomes, Cancer Research 54(4) 1994 987-992.

[37] U. Prabhakar, H. Maeda, R.K. Jain, E.M. Sevick-Muraca, W. Zamboni, O.C. Farokhzad, S.T. Barry, A. Gabizon, P. Grodzinski, D.C. Blakey, Challenges and key considerations of the enhanced permeability and retention effect for nanomedicine drug delivery in oncology, Cancer Research 73(8) (2013) 2412-2417.

[38] S. Wilhelm, A.J. Tavares, Q. Dai, S. Ohta, J. Audet, H.F. Dvorak, W.C.W. Chan, Analysis of nanoparticle delivery to tumours, Nature Reviews 1 (2016) 16014.

[39] S. Taurin, H. Nehoff, K. Greish, Anticancer nanomedicine and tumor vascular permeability; Where is the missing link?, Journal of Controlled Release 164(3) (2012) 265-275.

[40] J.W. Nichols, Y.H. Bae, EPR: Evidence and fallacy, Journal of Controlled Release 190 (2014) 451-464.

[41] C.W. Song, Effect of local hyperthermia on blood flow and microenvironment: a review, Cancer Research 44(10 Supplement) (1984) 4721s-4730s.

[42] A. Jordan, R. Scholz, P. Wust, H. Fähling, F. Roland, Magnetic fluid hyperthermia (MFH): Cancer treatment with AC magnetic field induced excitation of biocompatible superparamagnetic nanoparticles, Journal of Magnetism and Magnetic Materials 201(1–3)

(1999) 413-419.

[43] C.S.S.R. Kumar, F. Mohammad, Magnetic nanomaterials for hyperthermia-based therapy and controlled drug delivery, Advanced Drug Delivery Reviews 63(9) (2011) 789-808.

[44] A. Chicheł, J. Skowronek, M. Kubaszewska, M. Kanikowski, Hyperthermia – description of a method and a review of clinical applications, Reports of Practical Oncology & Radiotherapy 12(5) (2007) 267-275.

[45] T.B. Huff, L. Tong, Y. Zhao, M.N. Hansen, J.-X. Cheng, A. Wei, Hyperthermic effects of gold nanorods on tumor cells, Nanomedicine 2(1) (2007) 125-132.

[46] P. Wust, B. Hildebrandt, G. Sreenivasa, B. Rau, J. Gellermann, H. Riess, R. Felix, P.M. Schlag, Hyperthermia in combined treatment of cancer, The Lancet Oncology 3(8) (2002) 487-497.

[47] M.H.I.R.D. Falk, Hyperthermia in oncology, International Journal of Hyperthermia 17(1) (2001) 1-18.

[48] G.A. Koning, A.M. Eggermont, L.H. Lindner, T.L. ten Hagen, Hyperthermia and thermosensitive liposomes for improved delivery of chemotherapeutic drugs to solid tumors, Pharmaceutical Research 27(8) (2010) 1750-1754.

[49] A.A. Petryk, R.V. Stigliano, A.J. Giustini, R.E. Gottesman, B.S. Trembly, P.A. Kaufman, P.J. Hoopes, Comparison of iron oxide nanoparticle and microwave hyperthermia alone or combined with cisplatinum in murine breast tumors, 2011, pp. 790119-790119-7.

[50] A.P. Khandhar, R.M. Ferguson, J.A. Simon, K.M. Krishnan, Enhancing cancer therapeutics using size-optimized magnetic fluid hyperthermia, Journal of Applied Physics 111(7) (2012) -.

[51] B. Hildebrandt, P. Wust, O. Ahlers, A. Dieing, G. Sreenivasa, T. Kerner, R. Felix, H. Riess, The cellular and molecular basis of hyperthermia, Critical Reviews in Oncology/Hematology 43(1) (2002) 33-56.

[52] H.H. Kampinga, Cell biological effects of hyperthermia alone or combined with radiation or drugs: A short introduction to newcomers in the field, International Journal of Hyperthermia 22(3) (2006) 191-196.

[53] T. Ta, T.M. Porter, Thermosensitive liposomes for localized delivery and triggered release of chemotherapy, Journal of Controlled Release 169(1–2) (2013) 112-125.

[54] L. Gossner, A. May, M. Stolte, G. Seitz, E.G. Hahn, C. Ell, KTP laser destruction of dysplasia and early cancer in columnar-lined Barrett's esophagus, Gastrointestinal Endoscopy 49(1) (1999) 8-12.

[55] U. Lindner, N. Lawrentschuk, R.A. Weersink, S.R.H. Davidson, O. Raz, E. Hlasny, D.L. Langer, M.R. Gertner, T. Van der Kwast, M.A. Haider, Focal laser ablation for prostate cancer followed by radical prostatectomy: validation of focal therapy and imaging accuracy, European Urology 57(6) (2010) 1111-1114.

[56] R. Puls, S. Langner, C. Rosenberg, K. Hegenscheid, J.P. Kuehn, K. Noeckler, N. Hosten, Laser ablation of liver metastases from colorectal cancer with MR thermometry: 5-year survival, Journal of Vascular and Interventional Radiology 20(2) (2009) 225-234.

[57] B. Jang, Y.S. Kim, Y. Choi, Effects of gold nanorod concentration on the depth-related temperature increase during hyperthermic ablation, Small 7(2) (2011) 265-270.

[58] J. Chen, D. Wang, J. Xi, L. Au, A. Siekkinen, A. Warsen, Z.-Y. Li, H. Zhang, Y. Xia, X. Li, Immuno gold nanocages with tailored optical properties for targeted photothermal destruction of cancer cells, Nano Letters 7(5) (2007) 1318-1322.

[59] G. Strangman, D.A. Boas, J.P. Sutton, Noninvasive neuroimaging using near-infrared light, Biological Psychiatry 52(7) (2002) 679-693.

[60] S. Stolik, J.A. Delgado, A. Pérez, L. Anasagasti, Measurement of the penetration depths of red and near infrared light in human “ex vivo” tissues, Journal of Photochemistry and Photobiology B: Biology 57(2–3) (2000) 90-93.

[61] D. Pissuwan, S.M. Valenzuela, M.B. Cortie, Therapeutic possibilities of plasmonically heated gold nanoparticles, Trends in Biotechnology 24(2) (2006) 62-67.

[62] T. Niidome, Y. Akiyama, M. Yamagata, T. Kawano, T. Mori, Y. Niidome, Y. Katayama, Poly (ethylene glycol)-modified gold nanorods as a photothermal nanodevice for hyperthermia, Journal of Biomaterials Science, Polymer Edition 20(9) (2009) 1203-1215.

[63] X. Huang, P.K. Jain, I.H. El-Sayed, M.A. El-Sayed, Plasmonic photothermal therapy (PPTT) using gold nanoparticles, Lasers in Medical Science 23 (2008) 217-228.

[64] L.R. Hirsch, R.J. Stafford, J.A. Bankson, S.R. Sershen, B. Rivera, R.E. Price, J.D. Hazle, N.J. Halas, J.L. West, Nanoshell-mediated near-infrared thermal therapy of tumors under magnetic resonance guidance, Proceedings of the National Academy of Sciences 100(23) (2003) 13549-13554.

[65] D.P. O'Neal, L.R. Hirsch, N.J. Halas, J.D. Payne, J.L. West, Photo-thermal tumor ablation in mice using near infrared-absorbing nanoparticles, Cancer Letters 209(2) (2004) 171-176.

[66] A. Shetty, A.M. Elliott, J.A. Schwartz, J. Wang, E. Esparza-Coss, S. Klumpp, B. Taylor, J.D. Hazle, R.J. Stafford, Use of gold nanoshells to mediate heating induced perfusion changes in prostate tumors, 2008, pp. 68420S-68420S-9.

[67] S. Lal, S.E. Clare, N.J. Halas, Nanoshell-enabled photothermal cancer therapy:

Impending clinical impact, Accounts of Chemical Research 41(12) (2008) 1842-1851.

[68] A.M. Gobin, M.H. Lee, N.J. Halas, W.D. James, R.A. Drezek, J.L. West, Near-infrared resonant nanoshells for combined optical imaging and photothermal cancer therapy, Nano Letters 7(7) (2007) 1929-1934.

[69] X. Huang, I.H. El-Sayed, W. Qian, M.A. El-Sayed, Cancer cell imaging and photothermal therapy in the near-infrared region by using gold nanorods, Journal of the American Chemical Society 128(6) (2006) 2115-2120.

[70] T.S. Hauck, T.L. Jennings, T. Yatsenko, J.C. Kumaradas, W.C.W. Chan, Enhancing the toxicity of cancer chemotherapeutics with gold nanorod hyperthermia, Advanced Materials 20(20) (2008) 3832-3838.

[71] J. Chen, B. Wiley, Z.Y. Li, D. Campbell, F. Saeki, H. Cang, L. Au, J. Lee, X. Li, Y. Xia, Gold nanocages: engineering their structure for biomedical applications, Advanced Materials 17(18) (2005) 2255-2261.

[72] M. Hu, H. Petrova, J. Chen, J.M. McLellan, A.R. Siekkinen, M. Marquez, X. Li, Y. Xia, G.V. Hartland, Ultrafast laser studies of the photothermal properties of gold nanocages, The Journal of Physical Chemistry B 110(4) (2006) 1520-1524.

[73] J. Chen, C. Glaus, R. Laforest, Q. Zhang, M. Yang, M. Gidding, M.J. Welch, Y. Xia, Gold nanocages as photothermal transducers for cancer treatment, Small 6(7) (2010) 811-817.

[74] A.J. Gormley, A. Malugin, A. Ray, R. Robinson, H. Ghandehari, Biological evaluation of RGDfK-gold nanorod conjugates for prostate cancer treatment, Journal of Drug Targeting 19(10) (2011) 915-924.

[75] C. Loo, A. Lowery, N. Halas, J. West, R. Drezek, Immunotargeted nanoshells for integrated cancer imaging and therapy, Nano Letters 5(4) (2005) 709-711.

[76] R. Weissleder, A clearer vision for in vivo imaging, Nature Biotechnology 19(4) (2001) 316-317.

[77] S. Jain, D.G. Hirst, J.M. O'Sullivan, Gold nanoparticles as novel agents for cancer therapy, The British Journal of Radiology 85(1010) (2012) 101-113.

[78] B. Staves, Pilot study of Aurolase™ therapy in refractory and/or recurrent tumors of the head and neck.
<http://clinicaltrials.gov/ct2/show/related/NCT00848042?term=auroshells&rank=1.>, 2010).

[79] E.B. Dickerson, E.C. Dreaden, X. Huang, I.H. El-Sayed, H. Chu, S. Pushpanketh, J.F. McDonald, M.A. El-Sayed, Gold nanorod assisted near-infrared plasmonic photothermal therapy (PPTT) of squamous cell carcinoma in mice, Cancer Letters 269(1) (2008) 57-66.

[80] M. Hu, J. Chen, Z.-Y. Li, L. Au, G.V. Hartland, X. Li, M. Marquez, Y. Xia, Gold nanostructures: engineering their plasmonic properties for biomedical applications, Chemical Society Reviews 35(11) (2006) 1084-1094.

[81] M.S. Yavuz, Y. Cheng, J. Chen, C.M. Cobley, Q. Zhang, M. Rycenga, J. Xie, C. Kim, K.H. Song, A.G. Schwartz, L.V. Wang, Y. Xia, Gold nanocages covered by smart polymers for controlled release with near-infrared light, Nature Materials 8(12) (2009) 935-939.

[82] H.A. Hoffman, L. Chakrabarti, M.F. Dumont, A.D. Sandler, R. Fernandes, Prussian blue nanoparticles for laser-induced photothermal therapy of tumors, RSC Advances 4(56) (2014) 29729-29734.

[83] G. Fu, W. Liu, S. Feng, X. Yue, Prussian blue nanoparticles operate as a new generation of photothermal ablation agents for cancer therapy, Chemical Communications 48(94) (2012) 11567-11569.

[84] A.R. Burke, R.N. Singh, D.L. Carroll, J.C.S. Wood, R.B. D'Agostino Jr, P.M. Ajayan, F.M. Torti, S.V. Torti, The resistance of breast cancer stem cells to conventional hyperthermia and their sensitivity to nanoparticle-mediated photothermal therapy, Biomaterials 33(10) (2012) 2961-2970.

[85] H.K. Moon, S.H. Lee, H.C. Choi, In vivo near-infrared mediated tumor destruction by photothermal effect of carbon nanotubes, ACS Nano 3(11) (2009) 3707-3713.

[86] B. Li, Q. Wang, R. Zou, X. Liu, K. Xu, W. Li, J. Hu, Cu7.2S4 nanocrystals: a novel photothermal agent with a 56.7% photothermal conversion efficiency for photothermal therapy of cancer cells, Nanoscale 6(6) (2014) 3274-3282.

[87] Q. Tian, F. Jiang, R. Zou, Q. Liu, Z. Chen, M. Zhu, S. Yang, J. Wang, J. Wang, J. Hu, Hydrophilic Cu9S5 nanocrystals: A photothermal agent with a 25.7% heat conversion efficiency for photothermal ablation of cancer cells in vivo, ACS Nano 5(12) (2011) 9761-9771.

[88] L. Guo, D.D. Yan, D. Yang, Y. Li, X. Wang, O. Zalewski, B. Yan, W. Lu, Combinatorial photothermal and immuno cancer therapy using chitosan-coated hollow copper sulfide nanoparticles, ACS Nano 8(6) (2014) 5670-5681.

[89] K. Yang, H. Xu, L. Cheng, C.Y. Sun, J. Wang, Z. Liu, In vitro and in vivo near-infrared photothermal therapy of cancer using polypyrrole organic nanoparticles, Advanced Materials 24(41) (2012) 5586-5592.

[90] M. Shokouhimehr, E.S. Soehnlen, J. Hao, M. Griswold, C. Flask, X. Fan, J.P. Basilion, S. Basu, S.D. Huang, Dual purpose Prussian blue nanoparticles for cellular imaging and drug delivery: a new generation of T1-weighted MRI contrast and small molecule delivery agents, Journal of Materials Chemistry 20(25) (2010) 5251-5259.

[91] M.J. O'Connell, S.M. Bachilo, C.B. Huffman, V.C. Moore, M.S. Strano, E.H. Haroz,

K.L. Rialon, P.J. Boul, W.H. Noon, C. Kittrell, J. Ma, R.H. Hauge, R.B. Weisman, R.E. Smalley, Band gap fluorescence from individual single-walled carbon nanotubes, Science 297(5581) (2002) 593-596.

[92] S. Wei, A. Paul, Y. Mai, R. Laetitia, P. Satya, Carbon nanotubes for use in medicine: Potentials and limitations, 2013.

[93] S. Goel, F. Chen, W. Cai, Synthesis and biomedical applications of copper sulfide nanoparticles: From sensors to theranostics, Small 10(4) (2014) 631-645.

[94] Z. Zha, X. Yue, Q. Ren, Z. Dai, Uniform polypyrrole nanoparticles with high photothermal conversion efficiency for photothermal ablation of cancer cells, Advanced Materials 25(5) (2013) 777-782.

[95] Q. Tian, Q. Wang, K.X. Yao, B. Teng, J. Zhang, S. Yang, Y. Han, Multifunctional polypyrrole@Fe3O4 nanoparticles for dual-modal imaging and in vivo photothermal cancer therapy, Small 10(6) (2014) 1063-1068.

[96] X. Song, H. Gong, S. Yin, L. Cheng, C. Wang, Z. Li, Y. Li, X. Wang, G. Liu, Z. Liu, Ultra-small iron oxide doped polypyrrole nanoparticles for in vivo multimodal imaging guided photothermal therapy, Advanced Functional Materials 24(9) (2014) 1194-1201.

[97] S. Laurent, S. Dutz, U.O. Häfeli, M. Mahmoudi, Magnetic fluid hyperthermia: Focus on superparamagnetic iron oxide nanoparticles, Advances in Colloid and Interface Science 166(1–2) (2011) 8-23.

[98] R. Kappiyoor, M. Liangruksa, R. Ganguly, I.K. Puri, The effects of magnetic nanoparticle properties on magnetic fluid hyperthermia, Journal of Applied Physics 108(9) (2010) -.

[99] R. Hergt, W. Andra, C.G. d'Ambly, I. Hilger, W.A. Kaiser, U. Richter, H.G. Schmidt, Physical limits of hyperthermia using magnetite fine particles, Magnetics, IEEE Transactions on 34(5) (1998) 3745-3754.

[100] Z. Chuanqian, D.T. Johnson, C.S. Brazel, Numerical study on the multi-region bio-heat equation to model magnetic fluid hyperthermia (MFH) using low curie temperature nanoparticles, NanoBioscience, IEEE Transactions on 7(4) (2008) 267-275.

[101] R.E. Rosensweig, Heating magnetic fluid with alternating magnetic field, Journal of Magnetism and Magnetic Materials 252(0) (2002) 370-374.

[102] B.A. Thiesen, Clinical applications of magnetic nanoparticles for hyperthermia, International Journal of Hyperthermia 24(6) (2008) 467-474.

[103] P. Wust, U. Gneveckow, M. Johannsen, D. Böhmer, T. Henkel, F. Kahmann, J. Sehouli, R. Felix, J. Ricke, A. Jordan, Magnetic nanoparticles for interstitial thermotherapy – feasibility, tolerance and achieved temperatures, International Journal of Hyperthermia 22(8) (2006) 673-685.

[104] B. Kozissnik, A.C. Bohorquez, J. Dobson, C. Rinaldi, Magnetic fluid hyperthermia: Advances, challenges, and opportunity, International Journal of Hyperthermia 29(8) (2013) 706-714.

[105] N. Singh, G.J.S. Jenkins, R. Asadi, S.H. Doak, Potential toxicity of superparamagnetic iron oxide nanoparticles (SPION), Nano Reviews 1 (2010) 10.3402/nano.v1i0.5358.

[106] J.G. Lynn, R.L. Zwemer, A.J. Chick, A.E. Miller, A new method for the generation and use of focused ultrasound in experimental biology, The Journal of General Physiology 26(2) (1942) 179-193.

[107] G.R. Ter Haar, High intensity focused ultrasound for the treatment of tumors, Echocardiography 18(4) (2001) 317-322.

[108] J.-L. Thomas, M.A. Fink, Ultrasonic beam focusing through tissue inhomogeneities with a time reversal mirror: application to transskull therapy, Ultrasonics, Ferroelectrics, and Frequency Control, IEEE Transactions on 43(6) (1996) 1122-1129.

[109] F.J. Fry, Precision high intensity focusing ultrasonic machines for surgery, American Journal of Physical Medicine & Rehabilitation 37(3) (1958).

[110] K. Hynynen, MRIgHIFU: A tool for image-guided therapeutics, Journal of Magnetic Resonance Imaging 34(3) (2011) 482-493.

[111] K. Hynynen, W.R. Freund, H.E. Cline, A.H. Chung, R.D. Watkins, J.P. Vetro, F.A. Jolesz, A clinical, noninvasive, MR imaging-monitored ultrasound surgery method, RadioGraphics 16(1) (1996) 185-195.

[112] M. Pernot, J.F. Aubry, M. Tanter, J.L. Thomas, M. Fink, High power transcranial beam steering for ultrasonic brain therapy, Physics in Medicine and Biology 48(16) (2003) 2577-2589.

[113] M. de Smet, E. Heijman, S. Langereis, N.M. Hijnen, H. Grüll, Magnetic resonance imaging of high intensity focused ultrasound mediated drug delivery from temperature-sensitive liposomes: An in vivo proof-of-concept study, Journal of Controlled Release 150(1) (2011) 102-110.

[114] Y.-F. Zhou, High intensity focused ultrasound in clinical tumor ablation, World Journal of Clinical Oncology 2(1) (2011) 8-27.

[115] A.D. Liehr, Interaction of electromagnetic radiation with matter. I. Theory of optical rotatory power: Topic A. Trigonal dihedral compounds 1a, The Journal of Physical Chemistry 68(4) (1964) 665-722.

[116] S. Shrivastav, W.G. Kaelin, W.T. Joines, R.L. Jirtle, Microwave hyperthermia and its effect on tumor blood flow in rats, Cancer Research 43(10) (1983) 4665-4669.

[117] J.D. Byrne, T. Betancourt, L. BrannonPeppas, Active targeting schemes for nanoparticle systems in cancer therapeutics, Advanced Drug Delivery Reviews 60(15) (2008) 1615-1626.

[118] S. Xu, B.Z. Olenyuk, C.T. Okamoto, S.F. Hamm-Alvarez, Targeting receptor-mediated endocytotic pathways with nanoparticles: Rationale and advances, Advanced Drug Delivery Reviews 65(1) (2013) 121-138.

[119] Y.H. Bae, K. Park, Targeted drug delivery to tumors: myths, reality and possibility, Journal of Controlled Release 153(3) (2011) 198.

[120] T. Lammers, F. Kiessling, W.E. Hennink, G. Storm, Drug targeting to tumors: Principles, pitfalls and (pre-) clinical progress, Journal of Controlled Release 161(2) (2012) 175-187.

[121] L. Li, T.L.M. ten Hagen, A. Haeri, T. Soullié, C. Scholten, A.L.B. Seynhaeve, A.M.M. Eggermont, G.A. Koning, A novel two-step mild hyperthermia for advanced liposomal chemotherapy, Journal of Controlled Release 174(0) (2014) 202-208.

[122] A.J. Gormley, K. Greish, A. Ray, R. Robinson, J.A. Gustafson, H. Ghandehari, Gold nanorod mediated plasmonic photothermal therapy: A tool to enhance macromolecular delivery, International Journal of Pharmaceutics 415(1–2) (2011) 315-318.

[123] A.J. Gormley, N. Larson, S. Sadekar, R. Robinson, A. Ray, H. Ghandehari, Guided delivery of polymer therapeutics using plasmonic photothermal therapy, Nano Today 7(3) (2012) 158-167.

[124] A.J. Gormley, N. Larson, A. Banisadr, R. Robinson, N. Frazier, A. Ray, H. Ghandehari, Plasmonic photothermal therapy increases the tumor mass penetration of HPMA copolymers, Journal of Controlled Release 166(2) (2013) 130-138.

[125] N. Larson, A. Gormley, N. Frazier, H. Ghandehari, Synergistic enhancement of cancer therapy using a combination of heat shock protein targeted HPMA copolymer–drug conjugates and gold nanorod induced hyperthermia, Journal of Controlled Release 170(1) (2013) 41-50.

[126] B. Buckway, N. Frazier, A.J. Gormley, A. Ray, H. Ghandehari, Gold nanorod-mediated hyperthermia enhances the efficacy of HPMA copolymer-90Y conjugates in treatment of prostate tumors, Nuclear Medicine and Biology 41(3) (2014) 282-289.

[127] D.K. Kirui, E.J. Koay, X. Guo, V. Cristini, H. Shen, M. Ferrari, Tumor vascular permeabilization using localized mild hyperthermia to improve macromolecule transport, Nanomedicine: Nanotechnology, Biology and Medicine 10(7) (2014) 1487-1496.

[128] X. Sun, G. Zhang, R.S. Keynton, M.G. O'Toole, D. Patel, A.M. Gobin, Enhanced drug delivery via hyperthermal membrane disruption using targeted gold nanoparticles with PEGylated Protein-G as a cofactor, Nanomedicine: Nanotechnology, Biology and Medicine 9(8) (2013) 1214-1222.

[129] S.P. Sherlock, S.M. Tabakman, L. Xie, H. Dai, Photothermally enhanced drug delivery by ultrasmall multifunctional FeCo/Graphitic shell nanocrystals, ACS Nano 5(2) (2011) 1505-1512.

[130] S.-K. Wu, C.-F. Chiang, Y.-H. Hsu, T.-H. Lin, H.-C. Liou, W.-M. Fu, W.-L. Lin, Short-time focused ultrasound hyperthermia enhances liposomal doxorubicin delivery and antitumor efficacy for brain metastasis of breast cancer, International Journal of Nanomedicine 9 (2014) 4485-4494.

[131] C.S. Brazel, Magnetothermally-responsive nanomaterials: Combining magnetic nanostructures and thermally-sensitive polymers for triggered drug release, Pharmaceutical Research 26(3) (2009) 644-656.

[132] M. Filippousi, T. Altantzis, G. Stefanou, M. Betsiou, D.N. Bikiaris, M. Angelakeris, E. Pavlidou, D. Zamboulis, G. Van Tendeloo, Polyhedral iron oxide core-shell nanoparticles in a biodegradable polymeric matrix: preparation, characterization and application in magnetic particle hyperthermia and drug delivery, RSC Advances 3(46) (2013) 24367-24377.

[133] L. Chen, L. Li, H. Zhang, W. Liu, Y. Yang, X. Liu, B. Xu, Magnetic thermosensitive core/shell microspheres: synthesis, characterization and performance in hyperthermia and drug delivery, RSC Advances 4(87) (2014) 46806-46812.

[134] L. Li, T.L.M. ten Hagen, D. Schipper, T.M. Wijnberg, G.C. van Rhoon, A.M.M. Eggermont, L.H. Lindner, G.A. Koning, Triggered content release from optimized stealth thermosensitive liposomes using mild hyperthermia, Journal of Controlled Release 143(2) (2010) 274-279.

[135] M.B. Yatvin, J.N. Weinstein, W.H. Dennis, R. Blumenthal, Design of liposomes for enhanced local release of drugs by hyperthermia, Science 202(4374) (1978) 1290-1293.

[136] J.N. Weinstein, R.L. Magin, M.B. Yatvin, D.S. Zaharko, Liposomes and local hyperthermia: Selective delivery of methotrexate to heated tumors, Science 204(4389) (1979) 188-191.

[137] G. Kong, G. Anyarambhatla, W.P. Petros, R.D. Braun, O.M. Colvin, D. Needham, M.W. Dewhirst, Efficacy of liposomes and hyperthermia in a human tumor xenograft model: Importance of triggered drug release, Cancer Research 60(24) (2000) 6950-6957.

[138] P.T. Chelvi, S.K. Jain, R. Ralhan, Heat-mediated selective delivery of liposome associated melphalan in murine melanoma, Melanoma Research 5(5) (1995) 321-326.

[139] D. Needham, G. Anyarambhatla, G. Kong, M.W. Dewhirst, A new temperature-sensitive liposome for use with mild hyperthermia: Characterization and testing in a human tumor xenograft model, Cancer Research 60(5) (2000) 1197-1201.

[140] A.M. Ponce, Z. Vujaskovic, F. Yuan, D. Needham, M.W. Dewhirst, Hyperthermia mediated liposomal drug delivery, International Journal of Hyperthermia 22(3) (2006) 205-

213.

[141] P. Pradhan, J. Giri, F. Rieken, C. Koch, O. Mykhaylyk, M. Döblinger, R. Banerjee, D. Bahadur, C. Plank, Targeted temperature sensitive magnetic liposomes for thermo-chemotherapy, Journal of Controlled Release 142(1) (2010) 108-121.

[142] M. Babincová, P. Čičmanec, V. Altanerová, Č. Altaner, P. Babinec, AC-magnetic field controlled drug release from magnetoliposomes: design of a method for site-specific chemotherapy, Bioelectrochemistry 55(1–2) (2002) 17-19.

[143] M. Babincová, V. Altanerová, M. Lampert, C. Altaner, E. Machová, M. Srámka, P. Babinec, Site-specific in vivo targeting of magnetoliposomes using externally applied magnetic field, Zeitschrift fur Naturforschung C 55(3/4) (2000) 278-281.

[144] M. Gonzales, K.M. Krishnan, Synthesis of magnetoliposomes with monodisperse iron oxide nanocrystal cores for hyperthermia, Journal of Magnetism and Magnetic Materials 293(1) (2005) 265-270.

[145] K. Kono, H. Hayashi, T. Takagishi, Temperature-sensitive liposomes: liposomes bearing poly (N-isopropylacrylamide), Journal of Controlled Release 30(1) (1994) 69-75.

[146] K. Ninomiya, T. Yamashita, S. Kawabata, N. Shimizu, Targeted and ultrasound-triggered drug delivery using liposomes co-modified with cancer cell-targeting aptamers and a thermosensitive polymer, Ultrasonics Sonochemistry 21(4) (2014) 1482-1488.

[147] B.M. Dicheva, T.L.M. ten Hagen, D. Schipper, A.L.B. Seynhaeve, G.C. van Rhoon, A.M.M. Eggermont, G.A. Koning, Targeted and heat-triggered doxorubicin delivery to tumors by dual targeted cationic thermosensitive liposomes, Journal of Controlled Release (0) (2014).

[148] R.B. Campbell, D. Fukumura, E.B. Brown, L.M. Mazzola, Y. Izumi, R.K. Jain, V.P. Torchilin, L.L. Munn, Cationic charge determines the distribution of liposomes between the vascular and extravascular compartments of tumors, Cancer Research 62(23) (2002) 6831-6836.

[149] S. Krasnici, A. Werner, M.E. Eichhorn, M. Schmitt-Sody, S.A. Pahernik, B. Sauer, B. Schulze, M. Teifel, U. Michaelis, K. Naujoks, M. Dellian, Effect of the surface charge of liposomes on their uptake by angiogenic tumor vessels, International Journal of Cancer 105(4) (2003) 561-567.

[150] P. Sapra, T.M. Allen, Ligand-targeted liposomal anticancer drugs, Progress in Lipid Research 42(5) (2003) 439-462.

[151] A.H. Negussie, J.L. Miller, G. Reddy, S.K. Drake, B.J. Wood, M.R. Dreher, Synthesis and in vitro evaluation of cyclic NGR peptide targeted thermally sensitive liposome, Journal of Controlled Release 143(2) (2010) 265-273.

[152] B. Smith, I. Lyakhov, K. Loomis, D. Needle, U. Baxa, A. Yavlovich, J. Capala, R.

Blumenthal, A. Puri, Hyperthermia-triggered intracellular delivery of anticancer agent to HER2+ cells by HER2-specific affibody (ZHER2-GS-Cys)-conjugated thermosensitive liposomes (HER2+ affisomes), Journal of Controlled Release 153(2) (2011) 187-194.

[153] S. Dromi, V. Frenkel, A. Luk, B. Traughber, M. Angstadt, M. Bur, J. Poff, J. Xie, S.K. Libutti, K.C.P. Li, B.J. Wood, Pulsed-high intensity focused ultrasound and low temperature–sensitive liposomes for enhanced targeted drug delivery and antitumor effect, Clinical Cancer Research 13(9) (2007) 2722-2727.

[154] P.R. Patel, A. Luk, A. Durrani, S. Dromi, J. Cuesta, M. Angstadt, M.R. Dreher, B.J. Wood, V. Frenkel, In vitro and in vivo evaluations of increased effective beam width for heat deposition using a split focus high intensity ultrasound (HIFU) transducer, International Journal of Hyperthermia 24(7) (2008) 537-549.

[155] B.E. O'Neill, K.C.P. Li, Augmentation of targeted delivery with pulsed high intensity focused ultrasound, International Journal of Hyperthermia 24(6) (2008) 506-520.

[156] T. Ta, E. Bartolak-Suki, E.-J. Park, K. Karrobi, N.J. McDannold, T.M. Porter, Localized delivery of doxorubicin in vivo from polymer-modified thermosensitive liposomes with MR-guided focused ultrasound-mediated heating, Journal of Controlled Release 194(0) (2014) 71-81.

[157] H. Grüll, S. Langereis, Hyperthermia-triggered drug delivery from temperature-sensitive liposomes using MRI-guided high intensity focused ultrasound, Journal of Controlled Release 161(2) (2012) 317-327.

[158] M.R. Dreher, W. Liu, C.R. Michelich, M.W. Dewhirst, A. Chilkoti, Thermal cycling enhances the accumulation of a temperature-sensitive biopolymer in solid tumors, Cancer Research 67(9) (2007) 4418-4424.

[159] G. Kong, R.D. Braun, M.W. Dewhirst, Characterization of the effect of hyperthermia on nanoparticle extravasation from tumor vasculature, Cancer Research 61(7) (2001) 3027-3032.

[160] A. Ranjan, G.C. Jacobs, D.L. Woods, A.H. Negussie, A. Partanen, P.S. Yarmolenko, C.E. Gacchina, K.V. Sharma, V. Frenkel, B.J. Wood, M.R. Dreher, Image-guided drug delivery with magnetic resonance guided high intensity focused ultrasound and temperature sensitive liposomes in a rabbit Vx2 tumor model, Journal of Controlled Release 158(3) (2012) 487-494.

[161] A.A. Manzoor, L.H. Lindner, C.D. Landon, J.-Y. Park, A.J. Simnick, M.R. Dreher, S. Das, G. Hanna, W. Park, A. Chilkoti, G.A. Koning, T.L.M. ten Hagen, D. Needham, M.W. Dewhirst, Overcoming limitations in nanoparticle drug delivery: Triggered, intravascular release to improve drug penetration into tumors, Cancer Research 72(21) (2012) 5566-5575.

[162] L. Li, T.L.M. ten Hagen, M. Bolkestein, A. Gasselhuber, J. Yatvin, G.C. van Rhoon, A.M.M. Eggermont, D. Haemmerich, G.A. Koning, Improved intratumoral nanoparticle

extravasation and penetration by mild hyperthermia, Journal of Controlled Release 167(2) (2013) 130-137.

[163] A. Gasselhuber, M.R. Dreher, F. Rattay, B.J. Wood, D. Haemmerich, Comparison of conventional chemotherapy, stealth liposomes and temperature-sensitive liposomes in a mathematical model, PloS one 7(10) (2012) e47453.

[164] A. Gabizon, R. Catane, B. Uziely, B. Kaufman, T. Safra, R. Cohen, F. Martin, A. Huang, Y. Barenholz, Prolonged circulation time and enhanced accumulation in malignant exudates of doxorubicin encapsulated in polyethylene-glycol coated liposomes, Cancer Research 54(4) (1994) 987-992.

[165] R.T.P. Poon, N. Borys, Lyso-thermosensitive liposomal doxorubicin: a novel approach to enhance efficacy of thermal ablation of liver cancer, Expert Opinion on Pharmacotherapy 10(2) (2009) 333-343.

[166] Celsion, Analysis of 285 patient subgroup shows an impressive statistically significant 59% improvement in overall survival results at two years post treatment continue to support protocol for ongoing phase III OPTIMA trial, 2015.

[167] https://clinicaltrials.gov/ct2/results?term=thermodox, Thermodox clinical trials http://clinicaltrials.gov/ct2/results?term=thermodox. <http://clinicaltrials.gov/ct2/results?term=thermodox>).

[168] Celsion, ThermoDox® continues to demonstrate impressive local response rate in highly refractory patients company to initiate euro-DIGNITY trial this quarter European early access program set to launch this month. <http://investor.celsion.com/releasedetail.cfm?ReleaseID=906654>, 2015).

[169] C.D. Landon, J.-Y. Park, D. Needham, M.W. Dewhirst, Nanoscale drug delivery and hyperthermia: The materials design and preclinical and clinical testing of low Temperature-sensitive liposomes used in combination with mild hyperthermia in the treatment of local cancer, The Open Nanomedicine Journal 3 (2011) 38-64.

[170] H. Wei, S.-X. Cheng, X.-Z. Zhang, R.-X. Zhuo, Thermo-sensitive polymeric micelles based on poly(N-isopropylacrylamide) as drug carriers, Progress in Polymer Science 34(9) (2009) 893-910.

[171] M. Nakayama, T. Okano, T. Miyazaki, F. Kohori, K. Sakai, M. Yokoyama, Molecular design of biodegradable polymeric micelles for temperature-responsive drug release, Journal of Controlled Release 115(1) (2006) 46-56.

[172] H. Wei, X.-Z. Zhang, Y. Zhou, S.-X. Cheng, R.-X. Zhuo, Self-assembled thermoresponsive micelles of poly(N-isopropylacrylamide-b-methyl methacrylate), Biomaterials 27(9) (2006) 2028-2034.

[173] M. Moussa, S.N. Goldberg, G. Kumar, R.R. Sawant, T. Levchenko, V.P. Torchilin, M. Ahmed, Nanodrug-enhanced radiofrequency tumor ablation: Effect of micellar or

liposomal carrier on drug delivery and treatment efficacy, PLoS ONE 9(8) (2014) e102727.

[174] W. Liu, M.R. Dreher, D.Y. Furgeson, K.V. Peixoto, H. Yuan, M.R. Zalutsky, A. Chilkoti, Tumor accumulation, degradation and pharmacokinetics of elastin-like polypeptides in nude mice, Journal of Controlled Release 116(2) (2006) 170-178.

CHAPTER 3

EFFECTS OF HEATING TEMPERATURE AND DURATION BY GOLD NANOROD-MEDIATED PLASMONIC PHOTOTHERMAL THERAPY ON COPOLYMER ACCUMULATION IN TUMOR TISSUE

3.1 Introduction

Increased delivery and accumulation of chemotherapeutics to solid tumors has received much attention in the past decades. Improved delivery of chemotherapeutics to solid tumors can enhance therapy and reduce toxicity. Delivery of conventional drugs lacks significant accumulation and selectivity to the tumor site leading to insufficient elimination of cancer cells as well as side effects that can threaten the life of the patient, restricting further dosing. Poor drug accumulation and penetration within the tumor tissue can be attributed to several factors resulting from tumor anatomy that makes delivery difficult. These include physiological barriers as a result of growth induced solid stresses, dense interstitial structure, elevated interstitial pressures, and abnormal blood vessel networks within many tumor types [1]. The extent to which these characteristics are expressed is also variable within and between tumor types [2]. Additionally, poor water solubility and short circulation half-lives of many chemotherapeutics limit their bioavailability. Recent

---

Reprinted *in part* with permission of ACS. N. Frazier, R. Robinson, A. Ray, H. Ghandehari. Effects of heating temperature and duration by gold nanorod-mediated plasmonic photothermal therapy on copolymer accumulation in tumor tissue. Molecular Pharmaceutics. 12(5):1605-1614. (2015).

developments in nanomedicine have focused on combating these problems by increasing the amount of drug delivered to the target site and reducing harmful side effects from accumulation in healthy vital organs such as the liver, spleen, and kidneys.

One strategy for targeted drug delivery has been to attach different therapeutic agents to the side chains of water-soluble polymers. Polymer-drug conjugates or polymer therapeutics have been used in a variety of applications to aid delivery of hydrophobic drugs to cancers [3-8]. N-(2-hydroxypropyl)methacrylamide (HPMA) copolymers, specifically, have been utilized often due to their hydrophilicity, biocompatibility, and multifunctionality [9, 10]. Conjugation of hydrophobic anticancer agents to these copolymers improves the water solubility of hydrophobic drugs, prolongs blood circulation times (sizes above 45 kDa to avoid renal clearance) [11], allows for passive and active targeting strategies, and alters the mode of cellular internalization from passive diffusion or transporter mediated internalization to endocytosis, overcoming multidrug resistance from drug efflux pumps [9]. Several different drugs have been conjugated to HPMA copolymers including doxorubicin [12, 13], paclitaxel [14], docetaxel [14, 15], cisplatin [16], aminohexylgeldanamycin [17], and camptothecin [18] as well as radiotherapeutics [19, 20] and gene therapies [21]. Although improvements in drug delivery have occurred with polymer-drug conjugation, the potential for clinical translation is still hampered by the relatively low accumulation and tumor mass penetration in solid tumors [1]. Improvements in localization, penetration, and efficacy can advance the clinical applicability of HPMA copolymer-drug conjugates.

Previously, it was shown that gold nanorod (GNR) mediated plasmonic photothermal therapy (PPTT) is capable of increasing the overall accumulation of albumin

and HPMA copolymer conjugates [22, 23], tumor penetration [24], and improve the efficacy of prostate cancer treatment [15, 20]. GNR mediated PPTT is a method of heating tumors selectively through absorption of near infrared (NIR) laser light. In these previous studies, tumors were treated with mild hyperthermia (43°C for 10 min) which was first shown to maintain the temperature within the tumor at 42-43°C and enhance macromolecular delivery through increased accumulation of Evans blue dye (EBD) at 5 h post treatment [22]. PPTT was additionally shown to improve delivery of untargeted and heat shock targeted HPMA copolymers [23]. In these studies, it was shown that untargeted polymer accumulation after PPTT led to a transient increase in accumulation peaking at 4 h and returning to baseline at 8 h post treatment [23]. With the incorporation of heat shock targeting, the enhanced accumulation was retained over longer periods of time [23]. The enhanced accumulation was finally visualized by MRI. These experiments showed that PPTT could also increase the penetration of HPMA copolymers within the tumor tissue [24].

The enhanced accumulation and penetration were finally examined with chemo- and radio-therapeutic copolymer conjugates. Efficacies of heat shock targeted and untargeted HPMA copolymer-docetaxel conjugates were shown to be significantly improved over free drug alone with significant improvements in synergy as well [15]. Additionally, 90Yttrium was conjugated to HPMA copolymers and used in conjunction with PPTT [20]. The efficacy of these conjugates was also greatly improved as radiotherapy is known to have improved effects in combination with hyperthermia.

In each of these experiments, the same heat treatment was used to improve delivery and enhance treatment in preclinical prostate cancer models. However, limited information

is available on the role of varying heating parameters (temperature and duration) of PPTT and the effects on HPMA copolymer accumulation, retention, and consequently efficacy. Work described in this chapter aims to investigate how altering heating parameters of PPTT can change polymer accumulation profiles. In this study, different heating temperatures and durations of heat were used and changes in polymer accumulation within the heated tumors were observed. It was observed that altering the heating duration between 10 or 30 min and temperatures of 40, 43, 46, and 49°C had a significant effect on polymer accumulation. As these temperatures and times vary with different combinations of each, it is then valuable to consider these treatments as thermal doses. Using the equation developed by Sapareto and Dewey the different treatments can be compared on the same scale [25].

3.2 Materials and methods

3.2.1 Materials

Gold(III) chloride solution, hexadecyltrimethylammonium bromide (CTAB), silver nitrate, ascorbic acid, sodium borohydride, methacryloyl chloride, amino-2-propanol, tyrosinamide, 2-cyano-2-propyl dodecyl trithiocarbonate, and Iodogen (1,3,4,6-Tetrachloro-3α,6α-diphenylglycouril), were all purchased from Sigma-Aldrich (St. Louis, MO, USA). Poly(ethylene glycol) (mPEG-SH, MW=5 kDa) was purchased from Creative PEG works (Winston-Salem, NC, USA). Spectra/Por 6 dialysis tubing, (10K MWCO, 45mm flat width, 33-foot length) was purchased from Spectrum Laboratories (Rancho Dominguez, CA, USA). 2,2'-Azobis[2-(2-imidazolin-2-yl)propane] dihydrochloride (VA-044) was purchased from Wako Pure Chemical Industries (Richmond, VA, USA).

^{125}Iodine radionuclide as sodium iodide was purchased from American Radiolabel Chemicals (St. Louis, MO, USA).

3.2.2 Synthesis and characterization of HPMA copolymers

HPMA [26] and N-methacryloyl-tyrosinamide (MA-Tyr) [27] comonomers were synthesized as described previously. Copolymerization of these two monomers was performed by reversible addition-fragmentation chain transfer (RAFT) polymerization using 2-cyano-2-propyl dodecyl trithiocarbonate as the chain transfer agent (CTA) and VA-044 as the initiator in methanol at 50°C for 24 h. The product was then precipitated and washed with diethyl ether followed by dialysis against deionized water to remove unreacted monomers, CTA, and initiator. The copolymers were lyophilized to obtain the final product. Weight average molecular weight (Mw), number average molecular weight (Mn), and polydispersity index (Mw/Mn) were estimated by size-exclusion chromatography (SEC).

MA-Tyr comonomer was included in copolymerization for the ability to attach the radiolabel ^{125}Iodine by the Iodogen method with slight modification [28]. The synthesized copolymer (2 mg) and 0.5 mCi Na-^{125}I were dissolved in 0.5M NaH2PO4 at pH 7.0 and incubated at room temperature in Iodogen tubes for 10 min. Free radiolabel was removed by dialysis against 0.9% saline and verified by SEC for radiolabel attachment and purity of the polymer conjugate using a disposable size exclusion PD10 column. Radiolabeled copolymers were used to track accumulation within tumor tissue and quantify enhancement achieved by specific thermal doses.

3.2.3 Synthesis and characterization of gold nanorods

Poly(ethylene glycol) (PEG) coated GNRs were synthesized according to procedures described previously by seed-mediated growth methods [29]. This method has been optimized for yielding GNRs with an aspect ratio such that the corresponding surface plasmon resonance (SPR) absorbance peak lies between 800 and 810 nm. To remove large amounts of CTAB used during the synthesis, the particles were washed three times with deionized water by centrifugation. Subsequently, the GNRs were PEGylated by addition of methoxy-PEG-thiol to the particle suspension with a final PEG concentration of 100 μM and stirred for 1 h. The suspension was dialyzed against deionized water using a 10 K MWCO dialysis bag to remove excess PEG and remaining CTAB and finally concentrated by centrifugation to 120 optical density (OD) and sterile filtered for later use in animal experiments. Characterization was performed by transmission electron microscopy (TEM) (FEI Tecnai T12 microscope, University of Utah Core Research Facilities, Salt Lake City, UT, USA) to determine the size and shape of the particles and ultraviolet (UV) spectrophotometry to characterize the light absorbance profile of the GNRs.

3.2.4 Tumor model

In vivo experiments were carried out with CD1 mice containing two S-180 subcutaneous sarcoma tumor xenografts, one on each flank. Inoculations were performed by injecting 200 μL containing $10x10^6$ cells subcutaneously and allowing tumors to grow for 7-10 days to reach 7 mm in diameter. Once the tumors reached their desired size, they were then treated with PPTT.

3.2.5 Polymer accumulation

Once the tumors were the appropriate size, 200 μL of PEGylated GNRs in 0.9% saline were injected intravenously via tail vein at an OD ≈ 120 with a total mass of GNRs ≈ 725 μg. The particles were allowed to circulate for 48 h before PPTT. After the particles had accumulated in the tumor tissue, mice were anesthetized (2% isoflurane) and tumor regions were shaved and swabbed with 50% propylene glycol to enhance laser penetration depth [30]. Tumors on the right flank only were then radiated using an 808nm fiber-coupled laser diode (Oclaro Inc., San Jose, CA) with collimating lens with a spot size = 15 mm in diameter (Thorlabs, Newton, NJ) able to cover the entire tumor. The intratumoral temperature was monitored using a 33 gauge needle thermocouple (Omega, Stamford, CT) and tumor temperature was maintained between +/- 0.5°C. For these experiments, the laser power ranged from 1.0 to 1.6 W/cm2 depending on the desired temperature. In order to maintain the heating temperature at the predetermined heat schedule, the laser power was adjusted slightly in real time. The right tumors were heat treated with PPTT with a predetermined heat schedule (10 or 30 min at either 40, 43, 46, or 49°C). The left tumors were untreated to serve as an internal control accounting for possible variances in injected dose of radiolabeled HPMA copolymers from animal to animal and as a reference for calculating thermal enhancement ratio (ratio of accumulation in heated tumor/unheated tumor). Immediately before treatment, ^{125}I radiolabeled HPMA copolymers were injected intravenously, 200 μL with 7.5 mg/ml dissolved in 0.9% saline for a dose of 50 mg/kg and 120,000 counts per minute (CPM). The working solution was prepared by first dissolving unlabeled polymers at the appropriate concentration and then adding a small amount of radiolabeled polymers to achieve a radioactive dose of 120,000 CPM. At 2, 4, 6, and 8 h

post treatment the animals were euthanized by CO2 inhalation, tumors were removed, weighed, and gamma counted. Radioactive polymer accumulation for all combinations of temperatures and durations were measured for radioactivity levels at 4 h while only select groups (tumors treated with 43, 46, or 49°C for 10 min and 46°C for 30 min) were analyzed over an 8 h period. The radioactivity in each tumor correlates to polymer accumulation over time with the ratio of right to left tumor giving the thermal enhancement ratio (TER).

3.2.6 Tumor histology

Histological analysis was performed to observe damage to tumor vasculature after PPTT groups treated with 43, 46, or 49°C for 10 min and 46°C for 30 min. The same procedure was followed for GNR injections and PPTT in Section 2.5 except no injection of radiolabeled copolymers was performed. Ten hours post treatment animals were sacrificed, tumors were removed and fixed in neutral buffered formalin, paraffin-embedded, sectioned, stained with hematoxylin and eosin (H&E), and imaged by light microscopy. Tumor samples were analyzed for signs of vascular damage. Untreated control tumors were also included.

3.2.7 Statistics

Statistical analyses were performed in GraphPad Prism. Comparisons between two groups (left vs. right tumors) were performed by one-way ANOVA for each group. P-values less than 0.05 were considered statistically significant (* $P \leq 0.05$, ** $P \leq 0.01$, *** $P \leq 0.001$). Data was reported as mean ± STD.

3.3 Results

3.3.1 HPMA copolymer synthesis and characterization

The HPMA copolymers were synthesized by RAFT copolymerization to be approximately 60-80 kDa to have a size slightly above the renal threshold and take advantage of the EPR effect as well as being consistent with the size of other polymers used in accumulation studies [23, 24] (Table 3.1). Copolymers included MA-Tyr comonomer for eventual radiolabeling with ^{125}I. The attachment of ^{125}I was confirmed by determining the elution volumes of free and conjugated ^{125}I.

3.3.2 GNR synthesis and characterization

The GNRs were synthesized with an SPR peak at 810 nm (corresponding to a size of 62 × 17 +/- 7 × 2 nm with an aspect ratio equal to 3.6, Figure 3.1) as light at this wavelength is capable of penetrating tissue several centimeters [31]. These GNRs are found to be stable in a wide variety of buffers including saline due to steric protection from aggregation.

3.3.3 HPMA copolymer accumulation 4 h after treatment with PPTT

In this experiment, animals (n=5) were administered with GNRs 48 h prior in order to localize within the tumor tissue and allow for heat treatment with PPTT. The heating parameters were altered between a total of eight combinations using four different temperatures (40, 43, 46, or 49°C) and two different heating durations (10 or 30 min). The radioactive polymer accumulation for each heat treatment combination was observed at 4

Table 3.1: HPMA copolymer characteristics

Sample	Apparent MW (M_w)	Polydispersity Index (PDI)
HPMA-^{125}I	78.0 KDa	1.21

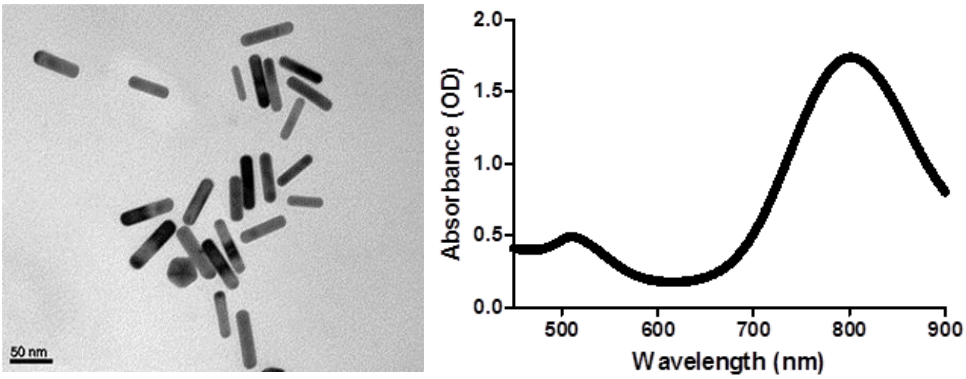

Figure 3.1: Characterization of gold nanorods by transmission electron microscopy (TEM) and UV absorbance of GNRs

h post treatment (Figure 3.2). It was observed that for both 40°C groups there is minimal enhancement of polymer accumulation at 4 h post treatment (TER ≈ 1.2). For both 43°C treatment groups, there is a larger peak of accumulation at 4 h (TER ≈ 1.6) which is consistent with previous experiments [22-24]. There is a slight decrease in average accumulation for the 43°C/30 min group but not statistically significant compared to the 43°C/10 min group. The 46°C group does not have much accumulation when treated for 10 min but increases when applied for 30 min (TER ≈ 1.2 vs 1.6). Both 49°C groups have increased accumulation (TER ≈ 1.5). Polymer accumulation at 4 h had significantly decreased for the 46°C/10 min group but then increased again for the 46°C/30 min as well as for both 49°C groups.

3.3.4 HPMA copolymer accumulation over 8 h with select groups

Select groups were examined for polymer accumulation over 8 h post treatment. These groups included 43, 46, and 49°C for 10 min and 46°C for 30 min with the TER of each group shown in Figure 3.3. First, this data shows that the peak accumulation enhancement for 43°C occurs at 4 h. As the thermal dose is increased to 46°C for 10 min, the same peak in enhancement is shifted to 2 h post treatment. Similar accumulation is observed at 2 h for 49°C which does not return to baseline (TER > 1.2) until 8 h post treatment. The treatment group that observed the highest accumulation enhancement and retained accumulation for at least 8 h was the treatment of 46°C for 30 min.

The area under the curve (AUC) for each of these groups was determined and compared (Figure 3.4). The comparison shows that there is a similar accumulation over the 8 h for both 43°C and 46°C for 10 min (AUC ≈ 2). However, when the dose is increased

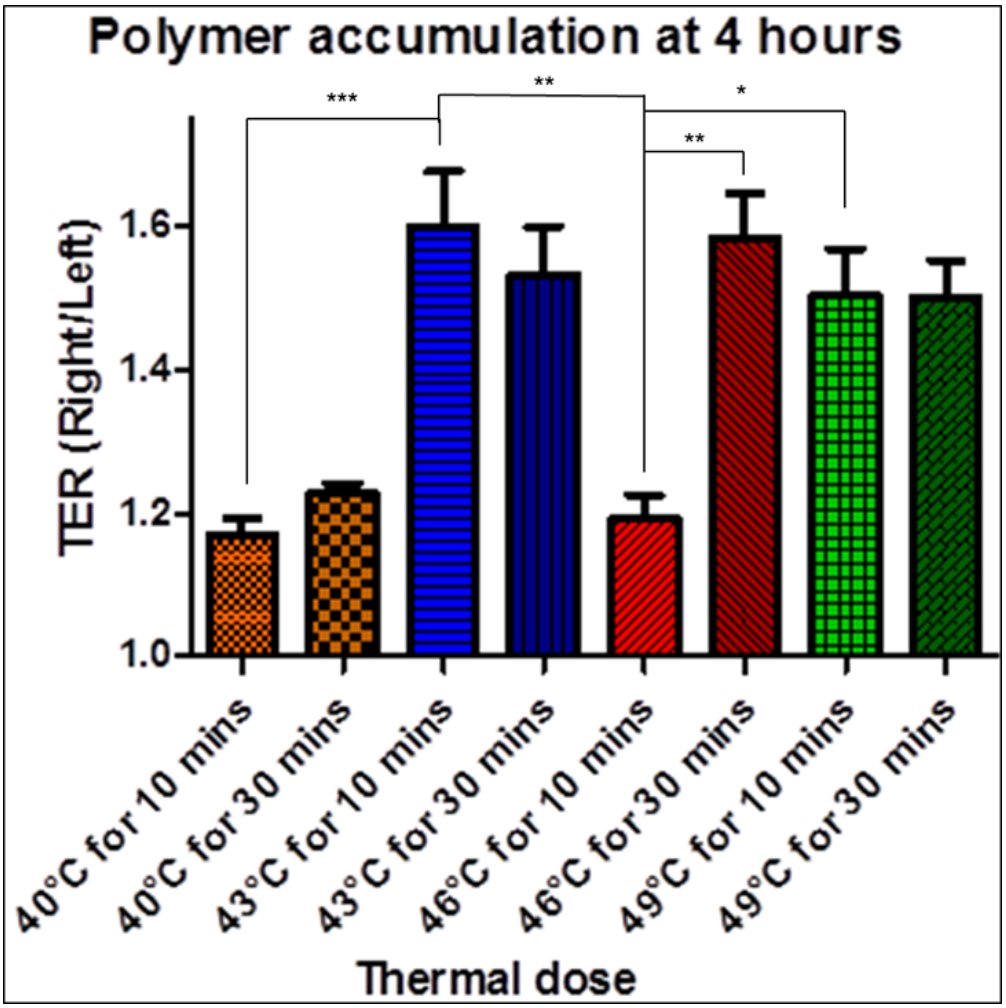

Figure 3.2: Polymer accumulation 4 h post treatment with combinations of different temperatures and durations.

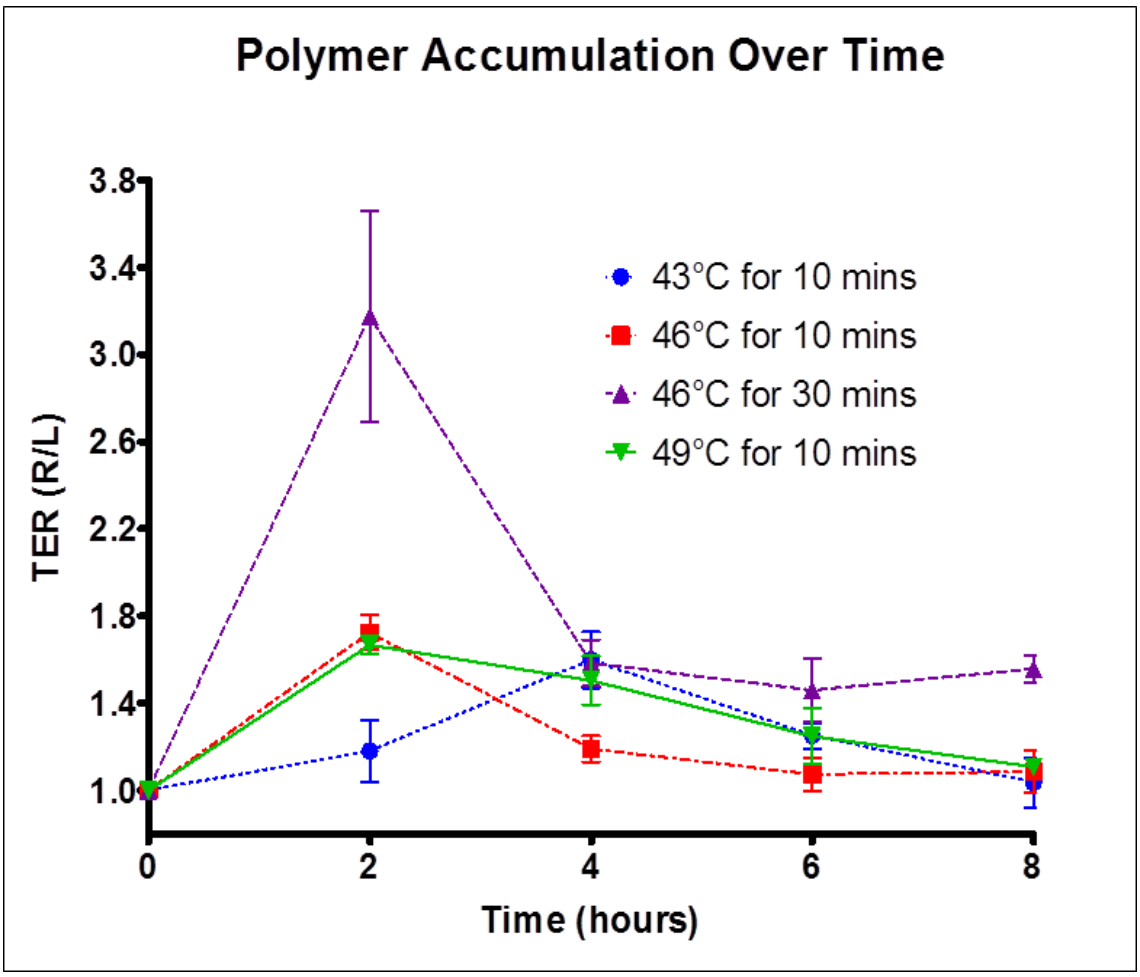

Figure 3.3: Polymer accumulation over 8 h post treatment with selected groups.

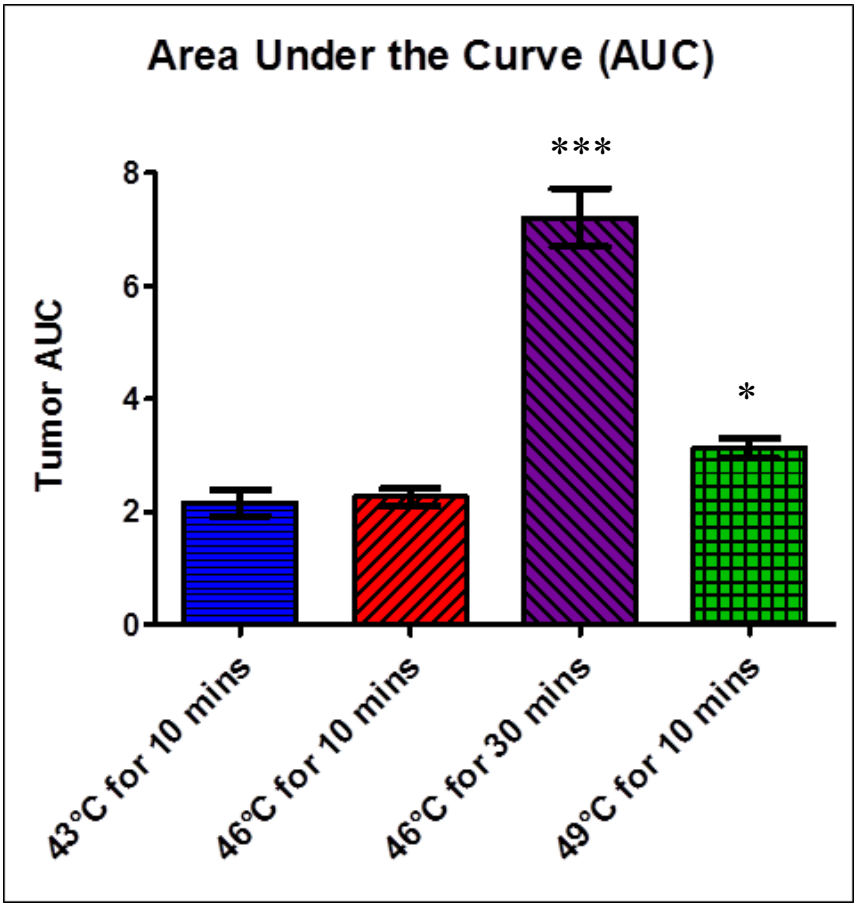

Figure 3.4: Area under the curve for selected groups in Figure 3.3.

further to 46°C for 30 min, the AUC is significantly larger (≈ 7) while it is also interesting to note that the heat treatment with 49°C for 10 min saw the AUC drop back down to 3.

3.3.5 Tumor histological analyses for observations of tumor vascular damage

Tumor histology was used to examine vascular damage caused by PPTT and to help understand the vascular mechanisms involved with polymer accumulation. Histological analyses were performed in the same four groups as the previous section (3.3.4) and also including a nonheated control tumor. Based on the observation made from the image analysis of these tumor sections the damage to the tumor vasculature was observed to progressively increase in groups 46°C for 10 min to 49°C for 10 min with no signs of damage seen in the lower temperature groups (Figure 3.5). There are small signs of red blood cell damage and clot formation in 46°C for 10 min which continues to grow in 46°C for 30 min. Finally, as seen in 49°C for 10 min there are vessels present in the tissue that have been completely occluded with small numbers of red blood cells (RBCs) entrapped. It is important to note that not all vessels exhibit the same vessel damage but the extent of progressive vascular damage is distinct for these groups represented in the images of Figure 3.5 such that only this extent of damage is observed in the specific treatment group. The top image for each group shows a section of tumor tissue with a blood vessel labeled with a blue arrow with the bottom image zoomed in on the labeled blood vessel to better observe RBC damage. In the magnified image at 100x magnification, clot formation within the vessel is labeled with yellow arrows and changes in RBC morphology are labeled with red arrows additionally showing the progression of vessel damage as the thermal dose is

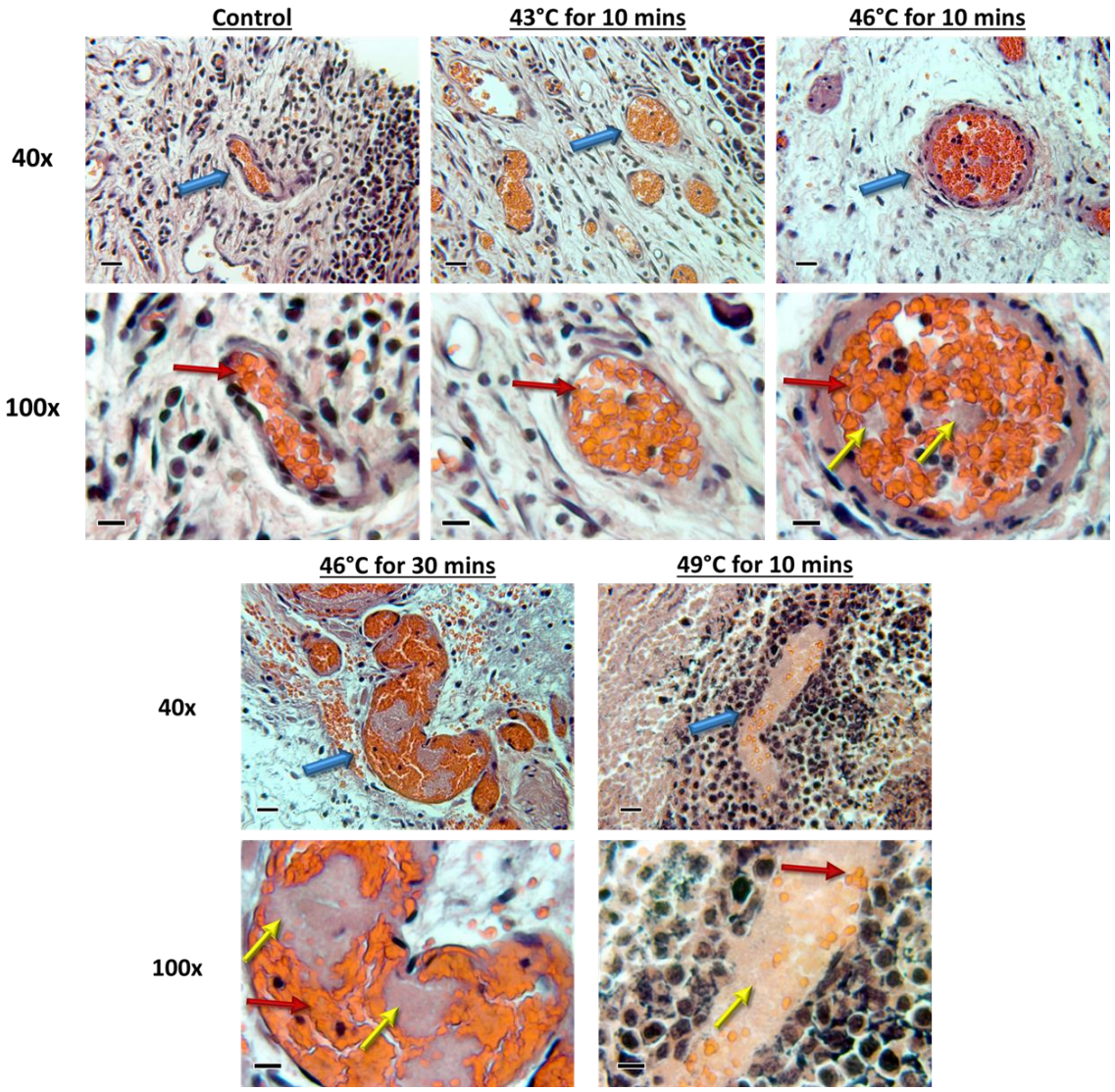

Figure 3.5: Histology sections of untreated and treated tumors. **Arrows** Blue: blood vessels, Red: lymphatic vessels, Red: red blood cell morphology, Yellow: fibrin deposition. Scale bars = 20 µm at 40x and 10 µm at 100x.

increased.

3.6 Thermal dose equivalent

To better present this data based on the arbitrary combination of temperature and time, each thermal dose was converted to time (min) at 43°C for better comparison [25]. This was done using the equation in Figure 3.6A which was previously developed for comparison of heat treatments in clinical applications. Previous data of Figure 3.2 was converted to the thermal dose equivalent to help aid discussion. As the thermal dose (time at 43°C) increases from about 10 s to 10 min, the accumulation at 4 h increases. After this point, the accumulation begins to decrease as thermal dose increases from 10 to 80 min. As thermal dose continues to increase to 240 min the accumulation enhancement increases again. However, as the thermal dose is increased from 240 to 640 min the amount of polymer delivered to the tumor site is reduced.

Next, the AUC of Figure 3.4 was additionally plotted against the thermal dose equivalent to each treatment group to better present the effects of altering the heating regimen (Figure 3.6C). As the dose increases from 10 to 80 min, the AUC does not change. As thermal dose further increases to 240 min, the AUC drastically rises. There is then a drop in AUC for the last group when the dose reaches 640 min.

3.4. Discussion

Previous studies in our lab have shown to significantly enhance the delivery of macromolecular polymer conjugates with PPTT at 43°C for 10 min [22-24]. This heating regimen was able to increase penetration of HPMA copolymers in prostate cancer tumors

A

$$t_{43} = \sum_{t=0}^{t=final} R^{(43-T)}\,\Delta t$$

B

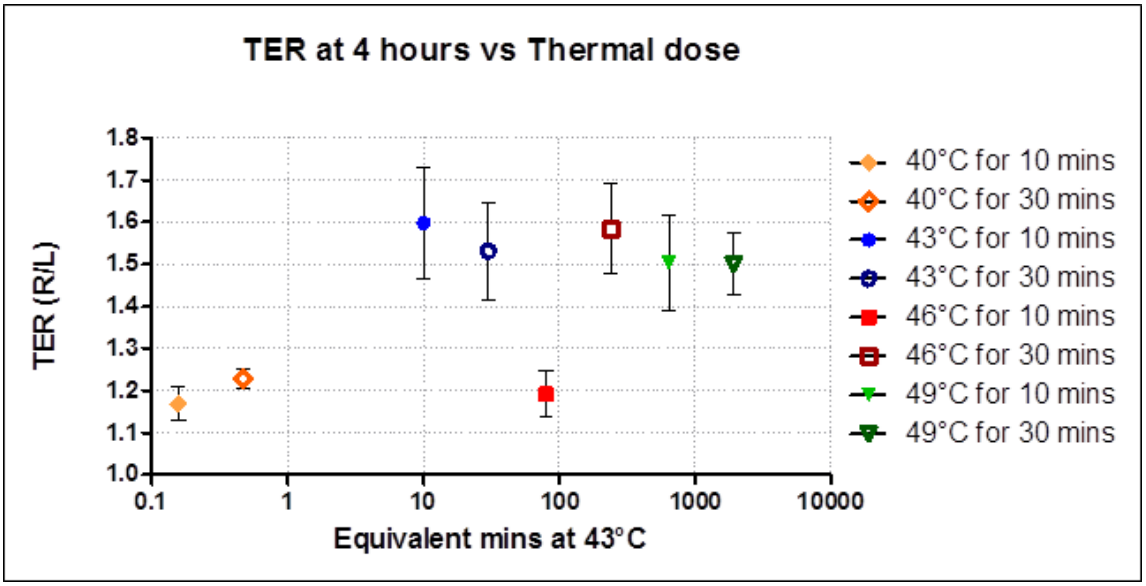

C

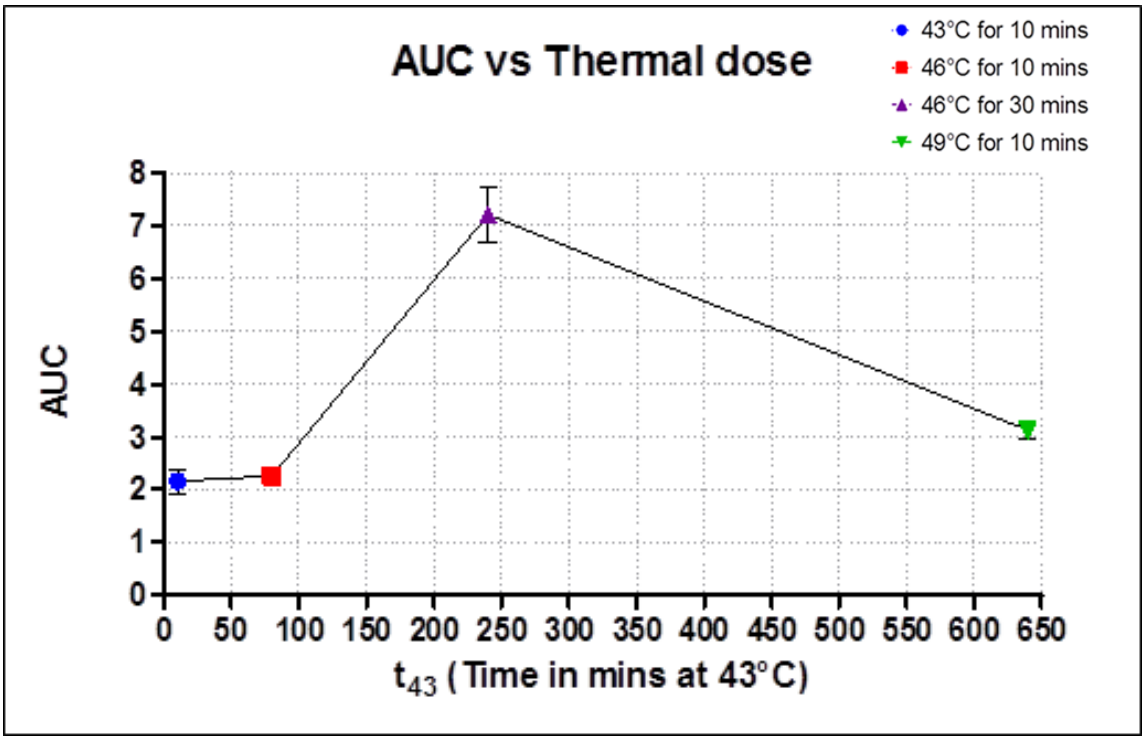

Figure 3.6: A) Equation for thermal dose equivalent for time (min) at 43°C, B) Polymer accumulation at 4 h of all groups plotted against thermal dose equivalent time at 43°C, C) Area under the curve plotted against thermal dose as a function of time at 43°C.

and was further improved through the use of specific heat shock targeting strategies increasing cellular uptake and tumor tissue retention [23]. It was unknown, however, if altering the heating regimen would alter the accumulation profile and therefore it was of interest to investigate if the conjugate accumulation could be further optimized for maximal enhancement with the use of different heating parameters.

In this study, the heating regimen was altered between temperatures of 40, 43, 46, and 49°C and with heating durations of either 10 or 30 min. It was observed that these changes lead to significant differences in polymer accumulation enhancement profiles with different groups. Finally, it was suggested that this study could advance the mechanistic understanding of tumor vascular events that occur in response to heat treatment ultimately leading to improved accumulation of polymer-drug conjugates and greater therapeutic efficacy.

The temperatures for these experiments were chosen in increments of 3°C starting from 43°C as this was used in prior experiments [15, 20, 22-24]. It is widely considered that temperatures above 46°C are thermoablative [32]. Therefore, temperatures at 46°C and one above (49°C) were selected. Finally, one temperature lower than 43°C was selected to observe how longer durations could affect treatments with lower temperatures (40°C) and therefore the duration was extended to 30 min for all groups versus only 10 min used in prior experiments [15, 20, 22-24]. The polymer accumulation was initially chosen to be observed at 4 h post treatment as this is the time where the peak of accumulation was observed in previous experiments [22-24] and was also consistent with our results showing the peak accumulation occurs at 4 h for 43°C for 10 min. It was later realized that 4 h may or may not be the peak accumulation time for all other treatment groups and therefore the

accumulation profile was expanded at 2 h intervals to 6 and 8 h post treatment correlating again back to previous studies showing a return to baseline accumulation 8-12 h later [22-24]. Lastly, an early time point was included at 2 h to have 2 h intervals over the whole 8 h time period.

Some previous studies have used prostate cancer animal models for examining the effects of PPTT on polymer accumulation [23, 24]. S-180 tumors were used here as they are known to exhibit the enhanced permeability and retention effect for passive accumulation of GNRs and ability to observe augmentation of this effect with hyperthermia without the need of an immune compromised mouse strain. Additionally, heat shock targeting would not be used in these experiments where prostate cancer cells are known to express these cell surface receptors. The molecular weight of the HPMA copolymers was also designed to be above the renal threshold for long circulation to additionally take advantage of the EPR effect and observe the ability for PPTT heat treatments to alter this phenomenon.

Initially, the polymer accumulation for all heat treatment groups was observed at 4 h post PPTT as it was shown that the peak accumulation of untargeted polymers occurs at this time in previous studies [23]. With examination of these results (Figure 3.2), the trend of increasing polymer accumulation for 40 and 43°C groups followed by a drop in TER for 46°C/10 min and subsequent increase again for 46°C/30 min and 49°C groups became an area of interest. To better understand the dynamics of the polymer accumulation with altering thermal dose, groups were selected for larger accumulation profiles. Thus, for additional experiments, four groups were selected to be observed over an 8 h period. These included 43°C/10 min to serve as a control, 46°C/10 min since it had an unexpected drop,

46°C/30 min as this is where the accumulation increased again and finally 49°C /10 min as this group also exhibited increased accumulation.

It was initially hypothesized, as accumulation is known to be transient, that for the 46°C/10 min group, the accumulation and washout was accelerated with the increased thermal dose from 43°C groups. However, when the thermal dose is increased further, there is a threshold for damage within the tumor vasculature which has an effect of the washout of these polymers. Thus, for the higher thermal dosed groups (46°C /10 min and both 49°C groups), this damage was probably generated which led to prolonged retention observed. To test this hypothesis, the four groups were selected to be examined for 8 h accumulation profiles and histological analyses (Figures 3.3-3.5).

It was hypothesized that for 46°C/10 min the influx and washout would be accelerated shifting the peak accumulation to an earlier time point. As can be seen in Figure 3.3, the data supports that hypothesis. For 46°C/30 min, the accumulation at 2 h was much greater, likely due to further increased flow within the tissue from increasing the duration of heating and thermal dose. The polymer accumulation is then retained over the 8 h time period and does not return to baseline likely due to vascular damage being initiated. For 49°C/10 min, the polymer accumulation at 2 h is not as high but was retained within the tissue over time as the thermal dose was increased. The residual retention over the 8 h time period observed in both of these treatment groups is likely due to damage of the vasculature at a certain threshold that limits clearance or washout.

When the polymer accumulation of 8 h is examined as AUC, the total exposure of polymers within the tumor, there is no significant difference between 43°C/10 min and 46°C/10 min. The AUC for 46°C/30 min does have a significantly larger increase which

then drops back down when the thermal dose is further increased to 49°C/10 min (Figure 3.4). This decrease in AUC can possibly be explained by the fact that the threshold for generating vascular damage is achieved much sooner for the 49°C/10 min group. For 49°C /10 min, the induction of vascular damage occurs at a faster rate and limits the amount of polymer that can be delivered to the tumor site. Likely the burst accumulation is what is being "trapped" in these treatment groups. Therefore, the polymer accumulation is only slightly enhanced before the flow is obstructed whereas, for 46°C/30 min, the damage is generated at a later point after the polymer accumulation is enhanced.

To summarize, as thermal dose increases, the flow within the tumor vasculature increases leading to more polymer extravasation as does the rate of vascular damage. When this damage is initiated later, the polymers that were accumulated become trapped, but if the damage occurs too soon, the polymers do not have a chance to enter the tumor tissue and so accumulation or tumor AUC is decreased. Thus, there is an optimal window for enhancing delivery of macromolecular polymer conjugates and subsequently trapping them within the tumor tissue. This data shows that, of these groups, 46°C/30 min has the greatest polymer accumulation over the 8 h period and is the optimal thermal dose for this application.

The previous data supports the hypothesis of altered dynamics with changes in thermal dose. However, they do not support whether vascular damage is the cause for prolonged retention and decrease in AUC for the 49°C/10 min group. With the aid of histological analyses it can be concluded that that the prolonged retention seen in 46°C/30 min and 49°C/10 min (Figure 3.3) of HPMA copolymers can be attributed to the vasculature damage due to increased heating dosage as both prolonged retention and

vascular damage are only observed in these groups (Figure 3.5). Vascular damage is indeed a factor in the polymer accumulation profiles observed previously leading to longer retention or slower washout.

When the data for polymer accumulation is displayed on the same scale as a thermal dose equivalent (Figure 3.6B and 3.6C), the trends of increasing temperature and duration can be visualized more easily. In Figure 3.6B, it is observed that there is a trend, although some consecutive points are not statistically significant, for accumulation at 4 h with increasing dose which can be explained by the previously presented findings. As the thermal dose (time at 43°C) increases from about 10 s to 10 min, the accumulation at 4 h increases. After this point, the accumulation begins to decrease as thermal dose increases from 10 to 80 min. This is likely due to the accelerated influx and washout shifting the peak accumulation to earlier times (e.g., 2 h post treatment). As thermal dose continues to increase to 240 min, the accumulation enhancement increases again, most likely due to accelerated flow dynamics but more importantly vascular damage restricting washout of accumulated polymers. However, as the thermal dose is increased from 240 to 640 min the induction of vascular damage occurs at a faster rate and limits the amount of polymer that can be delivered to the tumor site. Likely the burst accumulation is what is being “trapped” in these treatment groups.

Next, the AUC of Figure 3.4 was additionally plotted against the thermal dose equivalent to each treatment group to better present the effects of altering the heating regimen (Figure 3.6C). As the dose increases from 10 to 80 min the AUC does not change, indicating that although the flow may be accelerated shifting peak accumulation to earlier times, the overall polymer exposure within the tumor tissue has not changed. As thermal

dose further increases to 240 min, the AUC drastically rises. This is likely 2-fold from increased vascular dynamics and the subsequent onset of vascular damage. It should also be noted that between 80 and 240 min there exists a threshold at which the thermal dose will induce vascular damage within the tumor. There is then a drop in AUC for the last group when the dose reaches 640 min. This can likely be attributed to the onset of vascular damage where at 240 min the damage occurs more slowly and allows for more polymer accumulation while at 640 min this event occurs faster restricting the amount of polymer influx.

The accumulation data suggests that there are two threshold temperatures: one at which to achieve significantly enhanced delivery and a second to create vascular damage within the tissue. The vascular damage can be correlated with increased retention times within the tumor, or slower washout, with histological analyses supporting that this vasculature damage is seen only in groups exhibiting this characteristic. This data supports the hypothesis that increasing the thermal dose beyond what has been used previously can further enhance the delivery of polymer conjugates along with longer retention times within the tumor tissue. The groups that are shown to achieve this effect are 46°C for 30 min (t_{43} = 240 min), 49°C for 10 min (t_{43} = 640 min), and 49°C for 30 min (t_{43} = 1920 min). Although 46°C for 10 min (t_{43} = 80 min) was increased beyond the previously used t_{43} = 10 min, the ability to further enhance delivery was not observed. This suggests that there is a maximal exposure which can be produced below the vascular damage threshold. Beyond the thermal dose at which this threshold is achieved there can be improvements in polymer exposure within the tumor. However, raising the thermal dose too much beyond 240 min can have negative effects as well, hindering further accumulation. Therefore, there

must be a balance between increasing flow within the heated area and then triggering damage later on. Of the groups that were tested in this study, 46°C for 30 min (t_{43} = 240 min) was able to achieve this goal. Polymer accumulation was significantly enhanced and eventually induced the damage "trapping" the previously accumulated polymers.

The results of these experiments have additionally shown to be consistent with previous work examining the thermal threshold for tissue damage. For thermal damage to be induced with different temperature groups used here, 43°C would need to be applied for around 600-700 min, 46°C for 40-50 min, and 49°C applied for around 9-10 min [33]. Similarly, we found this to also be true where the 43°C groups had no signs of damage as the amount of time spent at this temperature was nowhere near 600-700 min. For 46°C, the 10 and 30 min groups both showed increasing amounts of thermal damage respectively as the thermal dose gets closer to the threshold around 40-50 min. Finally, much larger amounts of damage are observed for 49°C at 10 min, consistent with this being at the thermal threshold for tissue damage. These prior data support our current findings showing that a thermal dose at or just under the thermal threshold is best for enhancing delivery of polymer therapeutics and that the induction of vascular damage does play a role.

Additional mechanistic understanding is desired to visualize and determine the exact effects these different heating regimens have on vascular dynamics. Knowing what to expect in response to different heat treatments can possibly lead to better design of nanomedicines and macromolecular drug conjugates to take advantage of specific events that are taking place. It is unknown exactly if tumor blood flow and vascular damage are the only responsible functions affecting the delivery and accumulation. Thus, experiments with the use of intravital microscopy to observe changes in vascular dynamics and tracking

of fluorescent polymer accumulation *in vivo* would further aid in understanding the mechanisms that determine enhanced drug delivery with hyperthermia.

Distribution of gold nanorods throughout the tumor tissue is another area of interest. The accumulation of GNRs by the EPR effect may not be homogeneous resulting in a nonhomogenous distribution of heat when the laser is applied. Along with tissue attenuation of the laser light, it is likely that there is temperature distribution within the tumor tissue. Here, only a single point measurement was recorded via a needle thermocouple. Additional temperature imaging methods (i.e., magnetic resonance thermometry) should be considered to determine if there is homogenous distribution of heat and heating profile variability from animal to animal based on GNR distribution. Another potential factor that could lead to a greater influx of fluid and enhanced polymer delivery is that areas adjacent to GNRs cause local regions of dehydration and reduced interstitial pressure. It has been previously shown that hyperthermia is able to reduce the interstitial fluid pressure [34] and would, therefore, be of interest to see if this leads to enhanced delivery that is dependent on local GNR distribution throughout the tumor tissue. To study this effect on local tumor accumulation intravital microscopy could be used along with methods to correlate changes in interstitial pressure with polymer accumulation over time.

Finally, it would be worth studying if the same thermal dose from different heating parameters such as 43°C/640 min and 49°C/10 min can achieve the same effects on polymer accumulation. Although this cannot be definitely confirmed by the current studies, the expected results may be extrapolated. If 43°C were extended to longer times, the overall thermal dose would increase, but the time it takes to reach the thermal damage threshold

would be much longer than the time it would take at 49°C to reach the same threshold. With this longer time, the damage would occur at a slower rate and allow for greater amounts of polymer accumulation. For the same thermal dose of 43/640 min vs. 49/10 min, it would be expected that more polymer accumulation would occur for 43/640 min. However, the heat treatment would have to be for 640 min or 10.6 h which is not likely to be logistically possible. There are obviously trade-offs for each heat treatment with the same thermal dose and so a balance must be considered. It is believed that the best treatment would increase the amount of polymers in tumor tissue with increased vascular dynamics but then eventually reach the thermal dose equivalent to induce vascular damage in order to "trap" the polymers for longer periods of time. As such we have shown that 46°C for 30 min is able to achieve such a desired outcome.

Drug delivery applications for the treatment of different solid tumors can potentially benefit from using heating regimens that take advantage of these aspects. Mild hyperthermia is considered to be mild heating varying anywhere between 40-46°C applied for differing lengths of time. This type of heating is only aimed to transiently enhance delivery but also affect cellular mechanisms that can sensitize the cells to an adjuvant therapy. Above 46°C the therapy is considered to be ablative causing direct tissue necrosis and coagulation [35]. Methods have been steadily improved upon to achieve noninvasive, selective, and uniform heating throughout the tumor. With the ability to localize the heating to the target site one can potentially mildly heat the tumor to increase perfusion and permeability. While this is happening, a macromolecular drug conjugate can be administered and be significantly delivered to the heated tumor. After this event has occurred, the power or temperature could be further increased to ablate the tumor tissue.

This would trap the therapeutic agent, be it chemo- or radiotherapy, and reduce significant washout.

In clinical hyperthermia treatments, 43°C or lower is most commonly used for cancer therapies in order to avoid thermal damage. Hyperthermia has shown its benefits for synergistic enhancement of both chemo- [36, 37] and radio-therapies [38, 39] as well as in thermally triggered drug delivery systems [40-43]. If a clinician was to use the strategy we have proposed here with a treatment at 46°C for 30 min, the higher temperatures may possibly damage surrounding tissues. To better assure this does not happen in higher thermal dose or even ablative therapies it would be very helpful to know the precision of PPTT heat treatment. The optimal system would heat only the tumor tissue that contains GNRs while the surrounding tissue would have little to no heating. Using alternative imaging techniques it may be possible to observe this effect and better support the use of higher temperatures for specifically heating tumors and maximally enhancing polymer-dug accumulation while leaving healthy tissues unharmed. Ablative therapies are known to be very effective at eliminating cancerous tissue but are also shown to miss a significant population of cells at the periphery bordering healthy tissue. In order to fully eliminate these cells surviving the heat treatment, an adjuvant therapy can be used to clean up what is left behind, increasing the accumulation and retention of therapeutic agents within the tumor.

3.5 Conclusions

Altering the heating regimen for treatment of tumors with GNR mediated PPTT for enhancing polymeric drug delivery can create different accumulation profiles. Of the

groups that were tested, 46°C for 30 min had a significantly larger amount of accumulation over time. The changes can be attributed to damage of vasculature within the tumor and possibly greater blood flow in the tissue. Altering the heating parameters of PPTT can change the accumulation profiles of untargeted HPMA copolymers in the tumor tissue. This is shown by enhanced damage to tumor vasculature leading to longer retention times.

3.6 References

[1] V.P. Chauhan, T. Stylianopoulos, Y. Boucher, R.K. Jain, Delivery of molecular and nanoscale medicine to tumors: Transport barriers and strategies, Annual Review of Chemical and Biomolecular Engineering 2(1) (2011) 281-298.

[2] U. Prabhakar, H. Maeda, R.K. Jain, E.M. Sevick-Muraca, W. Zamboni, O.C. Farokhzad, S.T. Barry, A. Gabizon, P. Grodzinski, D.C. Blakey, Challenges and key considerations of the enhanced permeability and retention effect for nanomedicine drug delivery in oncology, Cancer Res. 73(8) (2013) 2412-2417.

[3] R. Duncan, The dawning era of polymer therapeutics, Nat Rev Drug Discov 2(5) (2003) 347-360.

[4] R. Haag, F. Kratz, Polymer therapeutics: Concepts and applications, Angewandte Chemie International Edition 45(8) (2006) 1198-1215.

[5] S. Kim, J.-H. Kim, O. Jeon, I.C. Kwon, K. Park, Engineered polymers for advanced drug delivery, European Journal of Pharmaceutics and Biopharmaceutics 71(3) (2009) 420-430.

[6] R. Duncan, Polymer therapeutics as nanomedicines: New perspectives, Current Opinion in Biotechnology 22(4) (2011) 492-501.

[7] F. Canal, J. Sanchis, M.J. Vicent, Polymer–drug conjugates as nano-sized medicines, Current Opinion in Biotechnology 22(6) (2011) 894-900.

[8] J. Kopeček, Polymer–drug conjugates: Origins, progress to date and future directions, Advanced Drug Delivery Reviews 65(1) (2013) 49-59.

[9] J. Kopeček, P. Kopečková, T. Minko, Z.-R. Lu, HPMA copolymer–anticancer drug conjugates: design, activity, and mechanism of action, European Journal of Pharmaceutics and Biopharmaceutics 50(1) (2000) 61-81.

[10] R. Duncan, Development of HPMA copolymer–anticancer conjugates: Clinical experience and lessons learnt, Advanced Drug Delivery Reviews 61(13) (2009) 1131-

1148.

[11] L.W. Seymour, R. Duncan, J. Strohalm, J. Kopeček, Effect of molecular weight (Mw) of N-(2-hydroxypropyl)methacrylamide copolymers on body distribution and rate of excretion after subcutaneous, intraperitoneal, and intravenous administration to rats, Journal of Biomedical Materials Research 21(11) (1987) 1341-1358.

[12] T. Mrkvan, M. Sirova, T. Etrych, P. Chytil, J. Strohalm, D. Plocova, K. Ulbrich, B. Rihova, Chemotherapy based on HPMA copolymer conjugates with pH-controlled release of doxorubicin triggers anti-tumor immunity, Journal of Controlled Release 110(1) (2005) 119-129.

[13] R. Duncan, J.K. Coatsworth, S. Burtles, Preclinical toxicology of a novel polymeric antitumour agent: HPMA copolymerdoxorubicin (PK1), Human & experimental toxicology 17(2) (1998) 93-104.

[14] T. Etrych, M. Šírová, L. Starovoytova, B. Říhová, K. Ulbrich, HPMA copolymer conjugates of paclitaxel and docetaxel with pH-controlled drug release, Molecular Pharmaceutics 7(4) (2010) 1015-1026.

[15] N. Larson, A. Gormley, N. Frazier, H. Ghandehari, Synergistic enhancement of cancer therapy using a combination of heat shock protein targeted HPMA copolymer–drug conjugates and gold nanorod induced hyperthermia, Journal of Controlled Release 170(1) (2013) 41-50.

[16] E. Gianasi, M. Wasil, E.G. Evagorou, A. Keddle, G. Wilson, R. Duncan, HPMA copolymer platinates as novel antitumour agents: In vitro properties, pharmacokinetics and antitumour activity in vivo, European Journal of Cancer 35(6) (1999) 994-1002.

[17] N. Larson, A. Ray, A. Malugin, D. Pike, H. Ghandehari, HPMA copolymer-aminohexylgeldanamycin conjugates targeting cell surface expressed GRP78 in prostate cancer, Pharmaceutical Research 27(12) (2010) 2683-2693.

[18] S. Sakuma, Z.-R. Lu, P. Kopečková, J. Kopeček, Biorecognizable HPMA copolymer–drug conjugates for colon-specific delivery of 9-aminocamptothecin, Journal of Controlled Release 75(3) (2001) 365-379.

[19] A. Mitra, A. Nan, J.C. Papadimitriou, H. Ghandehari, B.R. Line, Polymer-peptide conjugates for angiogenesis targeted tumor radiotherapy, Nuclear Medicine and Biology 33(1) (2006) 43-52.

[20] B. Buckway, N. Frazier, A.J. Gormley, A. Ray, H. Ghandehari, Gold nanorod-mediated hyperthermia enhances the efficacy of HPMA copolymer-90Y conjugates in treatment of prostate tumors, Nuclear Medicine and Biology 41(3) (2014) 282-289.

[21] R.N. Johnson, D.S.H. Chu, J. Shi, J.G. Schellinger, P.M. Carlson, S.H. Pun, HPMA-oligolysine copolymers for gene delivery: Optimization of peptide length and polymer molecular weight, Journal of Controlled Release 155(2) (2011) 303-311.

[22] A.J. Gormley, K. Greish, A. Ray, R. Robinson, J.A. Gustafson, H. Ghandehari, Gold nanorod mediated plasmonic photothermal therapy: A tool to enhance macromolecular delivery, International Journal of Pharmaceutics 415(1–2) (2011) 315-318.

[23] A.J. Gormley, N. Larson, S. Sadekar, R. Robinson, A. Ray, H. Ghandehari, Guided delivery of polymer therapeutics using plasmonic photothermal therapy, Nano Today 7(3) (2012) 158-167.

[24] A.J. Gormley, N. Larson, A. Banisadr, R. Robinson, N. Frazier, A. Ray, H. Ghandehari, Plasmonic photothermal therapy increases the tumor mass penetration of HPMA copolymers, Journal of Controlled Release 166(2) (2013) 130-138.

[25] S.A. Sapareto, W.C. Dewey, Thermal dose determination in cancer therapy, International Journal of Radiation Oncology*Biology*Physics 10(6) (1984) 787-800.

[26] J. Strohalm, J. Kopeček, Poly[N-(2-hydroxypropyl)methacrylamide]. IV. Heterogeneous polymerization, Die Angewandte Makromolekulare Chemie 70(1) (1978) 109-118.

[27] J.H. Lee, P. Kopeckova, J. Kopecek, J.D. Andrade, Surface properties of copolymers of alkyl methacrylates with, methoxy (polyethylene oxide) metiiacrylates and their application as protein-resistant coatings, Biomaterials 11(7) (1990) 455-464.

[28] R.F. Boyer, The protein protocols handbook (2nd ed.): Walker, J. (ed.), Biochemistry and Molecular Biology Education 30(5) (2002) 337-338.

[29] B. Nikoobakht, M.A. El-Sayed, Preparation and growth mechanism of gold nanorods (NRs) using seed-mediated growth method, Chemistry of Materials 15(10) (2003) 1957-1962.

[30] R.K. Wang, V.V. Tuchin, Enhance light penetration in tissue for high resolution optical imaging techniques by the use of biocompatible chemical agents, Journal of X-Ray Science and Technology 10(3) (2002) 167-176.

[31] S. Stolik, J.A. Delgado, A. Pérez, L. Anasagasti, Measurement of the penetration depths of red and near infrared light in human “ex vivo” tissues, Journal of Photochemistry and Photobiology B: Biology 57(2–3) (2000) 90-93.

[32] C.S.S.R. Kumar, F. Mohammad, Magnetic nanomaterials for hyperthermia-based therapy and controlled drug delivery, Advanced Drug Delivery Reviews 63(9) (2011) 789-808.

[33] M.W. Dewhirst, Basic principles of thermal dosimetry and thermal thresholds for tissue damage from hyperthermia, International Journal of Hyperthermia 19(3) (2003) 267.

[34] M. Leunig, A.E. Goetz, M. Dellian, G. Zetterer, F. Gamarra, R.K. Jain, K. Messmer, Interstitial fluid pressure in solid tumors following hyperthermia: Possible correlation with therapeutic response, Cancer Research 52(2) (1992) 487-490.

[35] A. Jordan, R. Scholz, P. Wust, H. Fähling, F. Roland, Magnetic fluid hyperthermia (MFH): Cancer treatment with AC magnetic field induced excitation of biocompatible superparamagnetic nanoparticles, Journal of Magnetism and Magnetic Materials 201(1–3) (1999) 413-419.

[36] H.H. Kampinga, Cell biological effects of hyperthermia alone or combined with radiation or drugs: A short introduction to newcomers in the field, International Journal of Hyperthermia 22(3) (2006) 191-196.

[37] R.D. Issels, Hyperthermia adds to chemotherapy, European Journal of Cancer 44(17) (2008) 2546-2554.

[38] J. van der Zee, D. González, G.C. van Rhoon, J.D.P. van Dijk, W.L.J. van Putten, A.A.M. Hart, Comparison of radiotherapy alone with radiotherapy plus hyperthermia in locally advanced pelvic tumours: a prospective, randomised, multicentre trial, The Lancet 355(9210) (2000) 1119-1125.

[39] E.L. Jones, J.R. Oleson, L.R. Prosnitz, T.V. Samulski, Z. Vujaskovic, D. Yu, L.L. Sanders, M.W. Dewhirst, Randomized trial of hyperthermia and radiation for superficial tumors, Journal of Clinical Oncology 23(13) (2005) 3079-3085.

[40] A.M. Ponce, Hyperthermia mediated liposomal drug delivery, International Journal of Hyperthermia 22(3) (2006) 205-213.

[41] M.S. Yavuz, Y. Cheng, J. Chen, C.M. Cobley, Q. Zhang, M. Rycenga, J. Xie, C. Kim, K.H. Song, A.G. Schwartz, L.V. Wang, Y. Xia, Gold nanocages covered by smart polymers for controlled release with near-infrared light, Nat Mater 8(12) (2009) 935-939.

[42] F. Mohammad, N.A. Yusof, Doxorubicin-loaded magnetic gold nanoshells for a combination therapy of hyperthermia and drug delivery, Journal of Colloid and Interface Science 434(0) (2014) 89-97.

[43] M.B. Yatvin, J.N. Weinstein, W.H. Dennis, R. Blumenthal, Design of liposomes for enhanced local release of drugs by hyperthermia, Science 202(4374) (1978) 1290-1293.

CHAPTER 4

HIGH INTENSITY FOCUSED ULTRASOUND HYPERTHERMIA FOR ENHANCED MACROMOLECULAR DELIVERY

4.1 Introduction

Many conventional chemotherapeutics exhibit less than 1% accumulation of the injected dose (ID) within solid tumors [1]. This can be attributed to poor water-solubility, short circulation half-life, and biological barriers hindering extravasation and penetration [2]. To overcome these issues, nanomedicines have been developed to increase site-specific accumulation through passive targeting by the enhanced permeability and retention (EPR) effect and through active targeting strategies to ultimately improve efficacy. Although improvements have been observed with these systems, the increased accumulation is marginal at best where <5% ID localizes within the tumor [1]. Ways to further enhance the delivery of nanomedicines include augmentation of the EPR effect with the use of vascular mediators or mild hyperthermia to increase blood flow and vascular permeability [3]. Hyperthermia has been used as a combination therapy to further increase the delivery of targeted nanomedicines and enhance the efficacy of chemotherapy [4]. This is

---

Reprinted *in part* with permission of Elsevier. N. Frazier, A. Payne, J. de Bever, C. Dillon, A. Panda, N. Subrahmanyam, H. Ghandehari, High intensity focused ultrasound for enhanced macromolecular delivery, Journal of Controlled Release, Revision Submitted (2016).

accomplished by increasing blood flow in the heated tumor tissue while also dilating the tumor vessels, further expanding the fenestrae and allowing for greater extravasation. Methods to selectively heat the tumor tissue include radiofrequency ablation (RFA), magnetic fluid hyperthermia (MFH), gold nanoparticle mediated laser therapy, and high intensity focused ultrasound (HIFU). Previously, our lab utilized gold nanorod (GNR)-mediated plasmonic photothermal therapy (PPTT) to enhance the delivery of water-soluble HPMA copolymers. This method was shown to be effective in improving delivery [5], tumor penetration [6], and efficacy [7] against prostate cancer xenografts. However, the application of heat through this method is limited by several factors. Delivery of gold nanoparticles to the tumor site mainly depends on the EPR effect which may not be exhibited in all tumors and tumor types [2], and can limit the heating capacity in methods that require nanoparticle accumulation by this route. Systemic administration of gold nanoparticles leads to long-term accumulation in filtration organs, such as the liver and spleen, as a majority of the GNRs accumulate in these tissues (>90%) as opposed to the tumor tissue [8]. The potential adverse effects over time of this off-target accumulation are not fully understood, potentially hampering their translation to the clinic. Additionally, the limited penetration depth of light reduces the utility of GNR-mediated mild hyperthermia to superficial tumors. Alternative methods are needed to generate mild hyperthermia to enhance delivery of nanomedicines.

One such method is high intensity focused ultrasound (HIFU). This method generates heat without the insertion of a probe as with RFA or prior injection of nanoparticles as with MFH or PPTT. HIFU produces heat within the body through focusing ultrasound waves to a focal point creating an intense deposition of energy that can cause

change at the cellular level using both thermal and mechanical effects. This phenomenon can cause heating in tissues resulting in hyperthermic or ablative effects. Using phased-array transducers with multiple transducer elements, the focal point can be electronically phased to compensate for the acoustic properties of different tissues and create subject-specific heating patterns [9]. HIFU additionally allows for heating with a high degree of temporal control, as the rate of heating depends on the magnitude and duration of the ultrasound exposure [10]. While HIFU has been performed under ultrasound and magnetic resonance imaging (MRI) guidance, MRI provides excellent soft tissue contrast as well as the ability to monitor the temperature rise in real time through MRI thermometry. Integration of MR guidance during HIFU exposure allows for simultaneous imaging to guide the treatment and MR thermometry to monitor the temperature and provide real time feedback [11, 12].

One challenge of HIFU in comparison to the other methods of heating is that the focal zone does not preferentially heat the tumor tissue and needs to be guided to the tumor site through MR or ultrasound imaging prior to treatment. The HIFU focal spot also has a relatively small, ellipsoidal focal zone, on the scale of a few millimeters (e.g., 1-3 x 3-8 mm), and needs to be moved throughout a larger tumor to achieve uniform heating [13]. Electronic beam steering or physically steering the transducer can be used in combination with real time temperature mapping by MR thermometry to heat the pathological tissues at a predefined temperature over a certain length of time [14]. This MR-guided HIFU (MRgHIFU) technology platform is currently Food and Drug Administration (FDA) approved for thermal ablation of uterine fibroids, treatment of bone metastases, and for treatment of prostate cancer [15], but has potential applications in temperature-induced

local drug delivery with hyperthermia [16] and other ablative therapies in oncology (i.e. breast, prostate, liver, brain) [17]. Because of these attributes, HIFU has emerged as an effective modality for drug delivery applications.

The aim of this work was to create an MRgHIFU controller system to uniformly heat tumor tissue in a subcutaneous mouse tumor model at approximately 43°C and further enhance the delivery of macromolecules. *Ex vivo* techniques were first used to evaluate the MRgHIFU controller system and determine treatment parameters that would achieve uniform hyperthermia. These parameters were then translated to the *in vivo* model. The ability to enhance delivery of macromolecules including Evans blue dye (EBD) bound to albumin and HPMA copolymers was evaluated.

4.2 Materials and methods

4.2.1 Synthesis and characterization of HPMA copolymers

HPMA was synthesized and confirmed by NMR [18] and aminopropylmethacrylamide-1,4,7,10-tetraazacyclododecane-1,4,7,10-tetraacetic acid (APMA-DOTA) was synthesized and confirmed by mass spectroscopy [19]. Free radical precipitation copolymerization with a feed ratio of 90 mol% HPMA and 10 mol% APMA-DOTA using azobisisobutyronitrile (AIBN) as the initiator in methanol at 50°C for 24 h was used to prepare the copolymers. The product was then precipitated and washed with diethyl ether followed by dialysis against deionized water to remove unreacted comonomers and initiator. The copolymers were lyophilized to obtain the final product. Weight average molecular weight (Mw), number average molecular weight (Mn), and polydispersity index (Mw/Mn) were estimated by size-exclusion chromatography (SEC).

APMA-DOTA comonomer was included in copolymerization for the ability to chelate Gadolinium (Gd).

The resulting copolymer was then dissolved in deionized (DI) water with Gd (III) acetate hydrate (1.2 mol equivalent to APMA-DOTA) and the pH was raised between 5.0 and 5.5. The solution was stirred overnight for 16 h followed by addition of ethylenediaminetetraacetic acid (EDTA) to remove excess Gd (EDTA:GD, 1:1). The product was then dialyzed against 0.9% saline and lyophilized. M_w, M_n, and M_w/M_n were estimated by SEC. The amount of chelated Gd and free Gd was determined by inductively coupled plasma mass spectrometry (ICP-MS). Chelated Gd and free Gd were separated using a disposable size exclusion PD10 column and the different fractions were analyzed by ICP-MS to determine purity.

The longitudinal relaxivity (T1) of the copolymers was characterized and compared to previously synthesized Gd-chelated copolymers [6, 19, 20]. Four different concentrations of Gd (0.1 to 0.015 mM Gd) were prepared in DI water and placed in a Bruker BioSpec 7.1 T horizontal bore MRI. T1 values were measured by an inversion recovery fast spin-echo imaging sequence using inversion times of 50, 100, 300, 500, 800, 1000, 2000, 4000, 7000, and 8000 ms, echo time (TE) of 4.2 ms, and repetition time (TR) of 12000 ms. T1 for each vial was calculated using Bruker software and the relaxation rate (R1 = 1/T1) was plotted against Gd equivalent concentration. The relaxivity was measured as the slope of this plot.

4.2.2 Stability of HPMA copolymer-Gd conjugates

HPMA copolymer-Gd conjugates were dissolved in mouse serum and incubated at 43°C for 10 min followed by incubation at 37°C for a total of 72 h. Samples were analyzed at 10 min, 24, 36, and 72 h and run on a PD10 column to separate free Gd from HPMA copolymer-Gd conjugates. The fractions were then analyzed by ICP-MS for Gd content. The amount of free Gd was compared to that of the chelated HPMA copolymer-Gd fraction to determine the percent of free Gd over time.

4.2.3 MRgHIFU controller system and *ex vivo* evaluation

All heating was performed using an MRgHIFU small animal system (Image Guided Therapy, Inc., Bordeaux, France. 16-element annular transducer, f=3MHz, 1x1x3 mm full-width-half-maximum focal spot size, +/- 1.5 cm steering along beam direction) placed in a Siemens 3T Trio MRI scanner. Because the phased-array transducer has an annular design, in plane focal spot motion was achieved by physically moving the transducer through the use of piezoelectric motors. The experimental setup is shown in Figure 4.1A. To determine MRgHIFU heating parameters that would produce stable hyperthermic conditions, different combinations of ultrasound power, heating trajectory shape, and speed were evaluated in an *ex vivo* chicken breast model. To best mimic the conditions required for the *in vivo* model, uniformity of heating over a 10 x 10 mm region of interest (ROI) was evaluated for each parameter set and the combination of parameters that produced a spatially uniform and stable temperature rise of 43°C over a 10-min period were identified. Temperatures were assessed in real time using the proton resonance frequency shift MR thermometry method [21] using a 2D segmented-echo planar imaging (Seg-EPI)

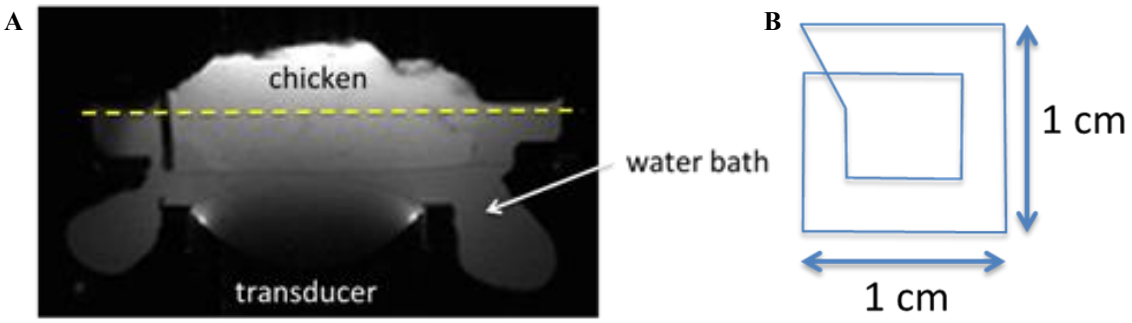

Figure 4.1: (A) *Ex vivo* experimental setup using chicken breast as a tumor phantom model. (B) Heating pattern for producing uniform heating.

sequence (TR/TE = 150/13 ms, echo-train length (ETL)=9, 1.2 s acquisition, 2x2x3 mm resolution, 3 slices). Susceptibility effects due to ultrasound transducer motion were mitigated using an atlas-based reconstruction [22] where approximately 50 baseline library images were acquired with the transducer moving along the defined trajectory (Figure 4.1B) multiple times without firing the ultrasound. During sonication, the current MR phase measurement was subtracted from the baseline library phase image that was most similar in a least squared difference sense. An ROI was defined which excluded the heated region in the computation of least squared difference. With the best-matched reference image determined, the phase difference, $\Delta\phi$, was computed and converted to a temperature change, ΔT, using Equation 1:

$$\Delta T = -\frac{\Delta\phi}{\gamma B_0 \alpha TE} \quad (1)$$

where γ is the gyromagnetic ratio of hydrogen, B_0 is the static magnetic field strength, TE is the echo time parameter, and α is a tissue proportionality constant which is approximately 0.009 ppm/°C for most soft tissues.

During sonication, the maximum and mean temperature in the heated region was monitored. The technician was able to adjust the ultrasound power output trajectory in real time using a user interface written in Matlab. A target maximum temperature rise of 43°C was selected to induce mild hyperthermia but not ablation.

4.2.4 *In vivo* tumor model

In vivo experiments were carried out using CD1 mice containing two S-180 subcutaneous tumor xenografts, one on each flank. Inoculations were performed by injecting 200 μL of phosphate buffered solution (PBS) containing $10x10^6$ cells

subcutaneously and allowing tumors to grow for 10-14 days to reach 7-10 mm in diameter. Once the tumors reached their desired size, they were then treated with HIFU hyperthermia.

4.2.5 *In vivo* MRgHIFU heating

Prior to HIFU treatment, the mice were anesthetized (2% isoflurane), and tumor regions were shaved and swabbed with a depilatory cream to remove all hair surrounding the tumor region. Immediately before heating, a needle thermocouple was inserted into the center of the tumor and 2 min of temperature data were obtained to determine a baseline tumor temperature. The mouse was placed in the same MRgHIFU small animal system as described above. The setup is shown in Figure 4.2 with an axial and coronal image. The mouse was placed on an agar mold with the tumor placed in an access hole. The agar mold provided a large region to obtain MRI phase measurements to improve the temperature measurement with atlas-based reconstruction. A custom two-channel radiofrequency coil was placed on top of the animal, and a small animal monitoring system was used to monitor the animal (respiration and temperature, SA instruments, Inc.). Similar to the *ex vivo* studies, MR temperatures were monitored using the 2D seg-EPI sequence (parameters above).

During sonication, the maximum and mean temperature in the tumor was monitored. Using the MRgHIFU controller, a power range between 3.3 and 5.6 W was implemented (approximately 3.5 to 4.6 MPa in water) to achieve a maximum temperature rise of 43°C. Temperatures were temporally filtered for respiratory artifact using a low pass digital filter.

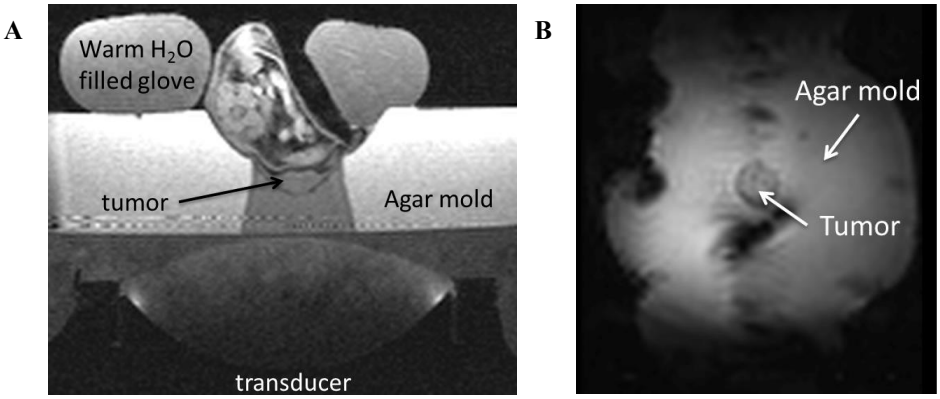

Figure 4.2: (A) Axial image of small animal MRgHIFU system used to heat tumor tissue *in vivo*. (B) Coronal image of *in vivo* setup with the treated tumor surrounded by the agar mold.

4.2.6 Evans blue dye accumulation

MRgHIFU was used to treat one S-180 tumor for each of the five CD1 mice. The second S-180 tumor was left untreated and used as an internal control. EBD was injected intravenously through the tail vein at a dose of 10 mg/kg dissolved in 0.9% sterile saline. Immediately after injection, one subcutaneous tumor was treated with MRgHIFU to achieve uniform heating of approximately 43°C for 10 min. Five hours after treatment, the animals were sacrificed and the tumors removed and weighed. The tumors were then placed in 1.5 mL of formamide for 48 h at 60°C to extract the EBD from the tissue. The EBD leaches into the surrounding media and is analyzed by measuring the absorbance of the solution at 620 nm. Absorption was normalized by tumor mass and the ratio of treated to untreated tumor accumulation was calculated to determine the thermal enhancement ratio (TER) which corresponds to increase in macromolecular delivery. To investigate the ultrasound's mechanical effect on tumor accumulation of EBD separately from the thermal effects, 5 CD1 mice with S-180 tumors were treated with MRgHIFU, but only to a target temperature of approximately 37 °C (normothermia).

4.2.7 Gadolinium polymer accumulation

MRgHIFU was again used to treat one of two S-180 tumors in three CD1 mice. Immediately after heat treatment, an axial image slice including both tumors was recorded as a baseline. Quantitative T1(spin-lattice relaxation time) data maps were acquired using a Modified Look-Locker Inversion Recovery imaging (MOLLI) [23] sequence (TR/TE = 912/1.58 ms, 0.8x0.7x3.5 mm resolution, 35° flip angle, nonselective inversion recovery with inversion times of 169/249/329 ms). The animal was then injected intravenously with

HPMA copolymer-Gd conjugates (0.03 mmol Gd/kg) in 0.9% sterile saline and imaged every 15 min for 5 h post heating. This was done to collect accumulation data of the HPMA-Gd copolymer conjugates over time. HPMA-Gd copolymers were injected after the heating as opposed to immediately prior since heating was measured by MR thermometry. Injecting HPMA copolymer-Gd would dynamically change the T1 signal adversely influencing the MR temperature images. The images collected from MR imaging were then analyzed to determine the change in signal over the 5-h time period.

4.2.8 Image analysis

T1 images were analyzed using Matlab software to determine the mean T1 values within the tumor ROI. A Matlab code was generated to select the ROI for both heated and control tumors within the MOLLI images and separate ROIs were created for each slice and time point. Mean T1 and R1 (1/T1) values were determined over each ROI at each time point. Heated and control tumor $\Delta R1$ values were plotted individually and averaged with standard deviation (STD) reported.

4.2.9 Statistical analysis

Statistical analyses were performed in GraphPad Prism. Comparisons between two groups (treated and control tumors), were performed by t-test for each group, $P < 0.05$ were considered statistically significant (* $P \leq 0.05$, ** $P \leq 0.01$, *** $P \leq 0.001$). Data was reported as mean ± STD.

4.3 Results

4.3.1 HPMA copolymer synthesis and characterization

The HPMA copolymers were synthesized by free radical precipitation copolymerization to be greater than 45 kDa to have a size slightly above the renal threshold and take advantage of the EPR effect as well as to be consistent with the size of polymers used in previous accumulation studies [6, 24, 25]. Copolymers included DOTA in the side chains for chelation of Gd. The attached amount and purity of HPMA copolymer-Gd was confirmed by determining the elution volumes of free and chelated Gd and measured by ICP-MS. The M_w was estimated to be approximately 51 kDa with a polydispersity of 1.67 characterized by SEC. The relaxivity was calculated to be 46.8 s^{-1} mM Gd^{-1} and a Gd content of 0.139 mmol/g of polymer. The percent of free Gd was determined over time after first incubating the copolymer conjugates at 43°C for 10 min and then 37°C for the remainder of the 72 h. At 10 min, 24, 48, and 72 h, the solution was sampled and free Gd was separated from HPMA copolymer-Gd by PD10 column and each fraction analyzed by ICP-MS. Approximately 1% of free Gd was detected over the 72-h period with no significant changes over time.

4.3.2 MRgHIFU controller *ex vivo* evaluation

The combination of ultrasound parameters which met the standards required for maintaining hyperthermia at 43°C for several minutes in an excised chicken breast model was a concentric square spiral pattern (Figure 4.1B) executed at a speed of 2 mm/s and an acoustic power of 3 acoustic W. The distribution was approximately uniform throughout the ROI over time (Figure 4.3A) and the temperature increase maintained a quasi-steady

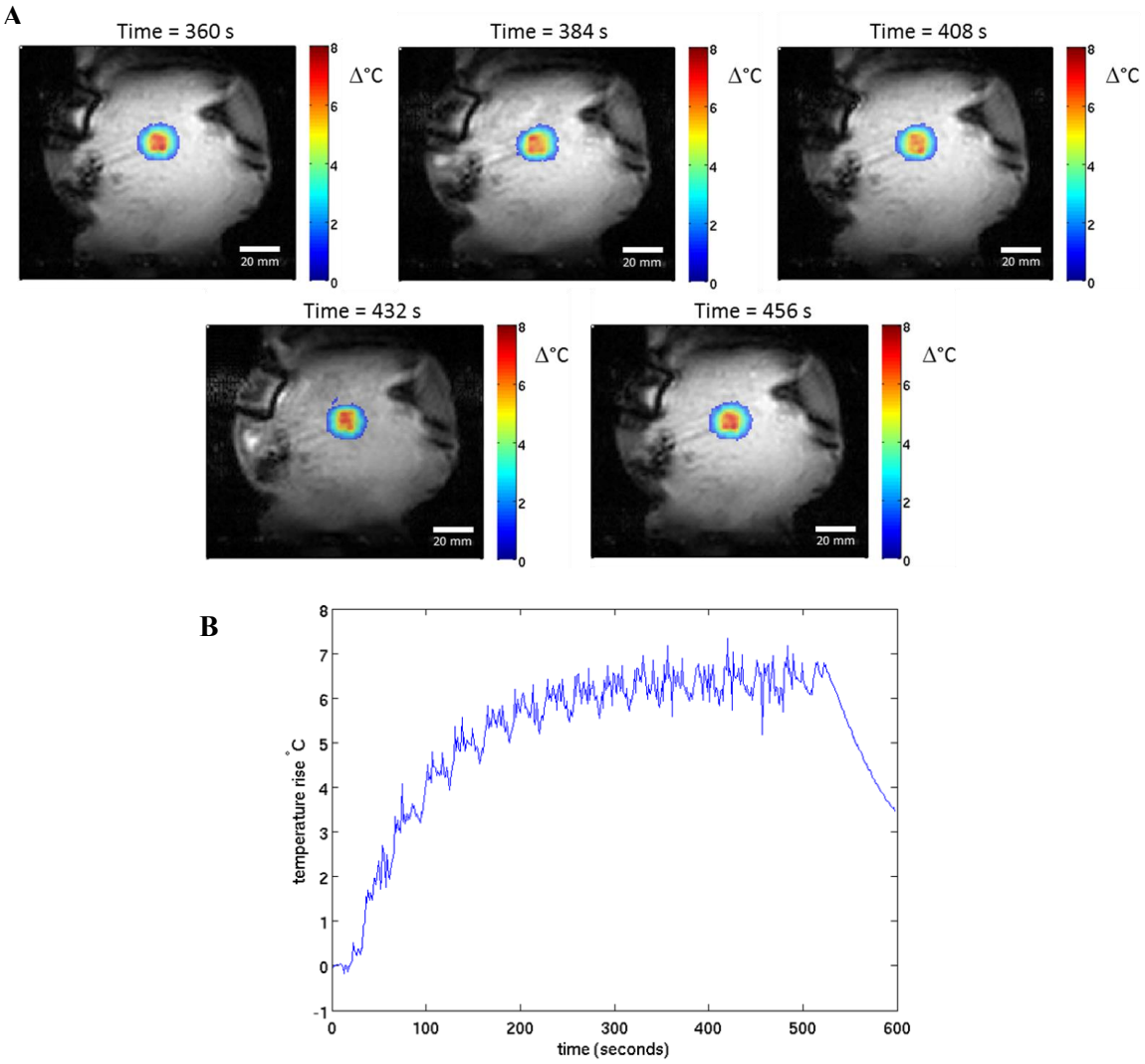

Figure 4.3: MRgHIFU controller evaluation in *ex vivo* chicken breast: (A) Coronal temperature maps over time during heating. (B) Mean temperature rise over time within the heated region of interest.

state of approximately 6°C for about 5 min (Figure 4.3B). The same pattern was used for all tumors *in vivo* adjusted for tumor size with a speed of 2 mm/s and an initial power output of 3 W.

4.3.3 *In vivo* MRgHIFU heating

As expected, the translation of the *ex vivo* results to the *in vivo* model required some modifications to the MRgHIFU protocol. Specifically, as these tumors are subcutaneous and the mice are anesthetized, the tumor temperature is not well-regulated and therefore the tumor baseline temperature is closer to 30°C when assessed via thermocouple before HIFU heating. In order to reach hyperthermia, a rise of approximately 13°C was required. With the use of the real time atlas-based MR temperature feedback and variable control over transducer power, tumor temperature was controlled to hyperthermic conditions in a reproducible fashion (Figure 4.4). Figure 4.4 shows the temperature response achieved in the five treated animals. The mean temperature response was maintained between 42-44°C in the treated tumors meeting the hyperthermia requirements.

4.3.4 Evans blue dye accumulation

When tumors are treated with MRgHIFU hyperthermia, changes occur in the heated tumor when compared to the nonheated tumor. These changes can include an increase in blood flow and vascular permeability leading to greater macromolecular accumulation and increased extravasation through the blood vessels. As seen in Figure 4.5, the tumors that were heated with MRgHIFU hyperthermia had a significant increase in EBD accumulation with an almost 2-fold increase versus that of tumors treated with

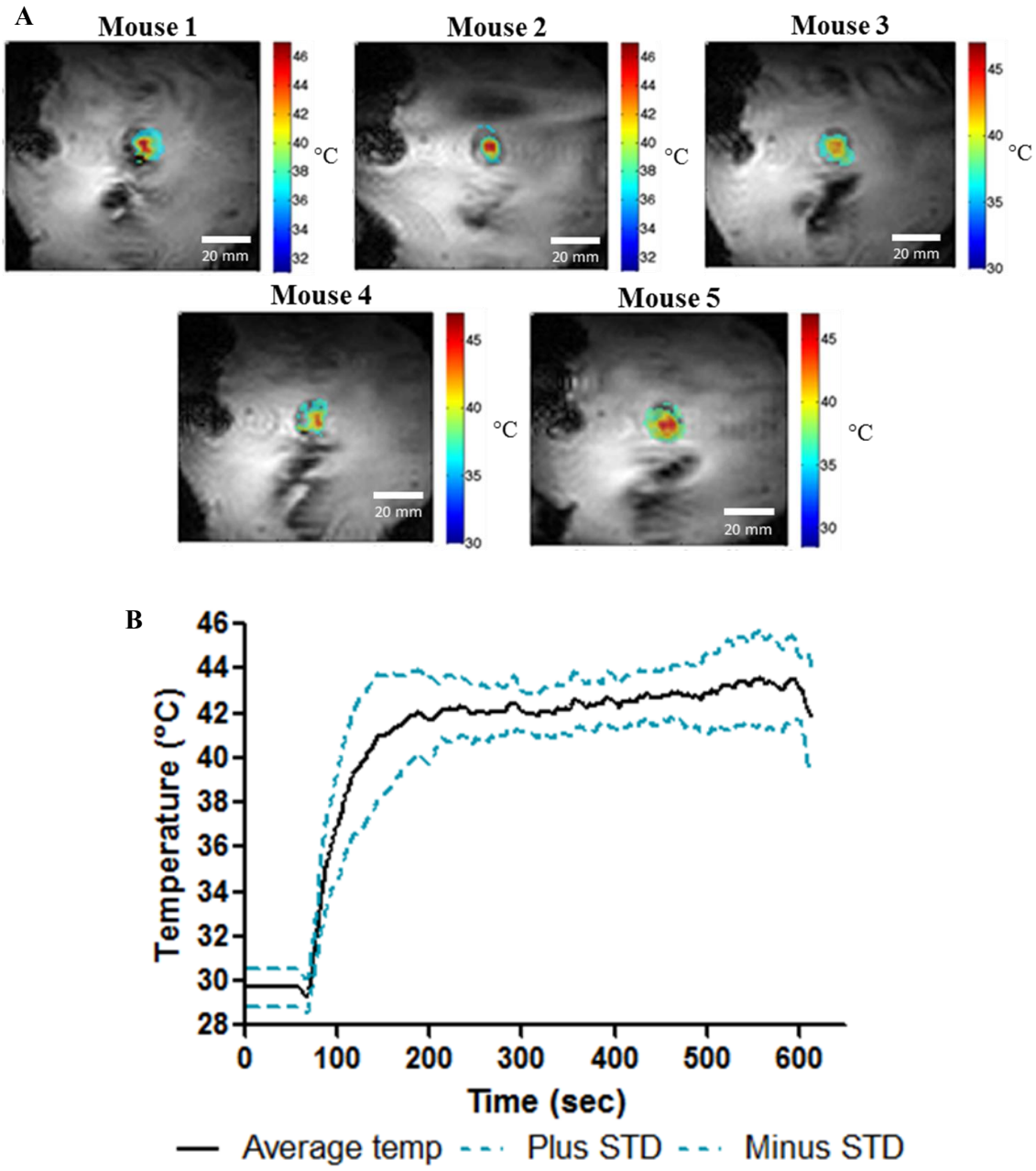

Figure 4.4: *In vivo* MRgHIFU hyperthermia heating. (A) Five animals are shown that achieved uniform heating in the tumor region (Coronal MRI temperature maps). (B) Average temperature data from animals treated with HIFU hyperthermia (n=5 +/-STD).

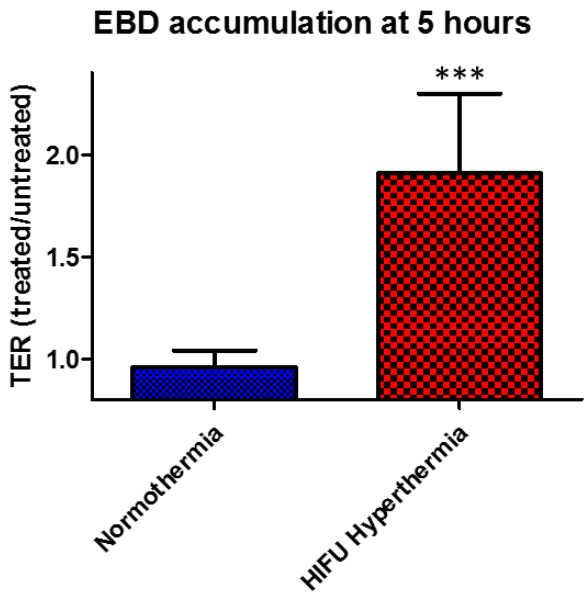

Figure 4.5: Thermal enhancement ratio of EBD with HIFU hyperthermia versus HIFU that does not achieve heating (normothermia) 5 h post treatment.

normothermia. This result shows that ultrasound exposure alone did not enhance the delivery of EBD and that the increased accumulation was due to the thermal contribution of hyperthermia generated by HIFU. It also demonstrates that MRgHIFU hyperthermia possesses the capability to additionally enhance the delivery of other nanomedicines through the same mechanisms of action.

4.3.5 HPMA copolymer-Gd accumulation

Gd-chelated HPMA copolymers were administered to CD1 mice bearing two tumors to evaluate their accumulation. Figure 4.6A shows a representative result obtained from one mouse over the 5-h imaging period. The bottom tumor ROI is the heated tumor and the left ROI is the control tumor. As observed in these images, the T1 values of the heated tumor decreased over time. The shift from higher to lower T1 values is indicative of HPMA copolymer-Gd accumulation as the presence of Gd shortens the T1 relaxation times and leads to a lower T1 value. Therefore, the more Gd present in the tumor, the lower the T1 value. This can also be visualized in the histograms of Figure 4.6A. The heated tumor is represented by the red bars and the control tumor is represented by the blue bars. As time progressed, the T1 values for the control tumor did not shift as much to lower T1 values as did those for the heated tumor. This correlates with larger amounts of HPMA copolymer-Gd accumulating in the heated tumor compared to control. This difference is presented as $\Delta R1$ in Figures 4.6B and 4.6C. Figure 4.6B shows the individual changes for each tumor. Figure 4.6C plots these heated and control tumors as an average and standard deviation of the three tumors treated. The same was done for the control tumors. There was a significant difference between the heated and control tumors at 260 min post

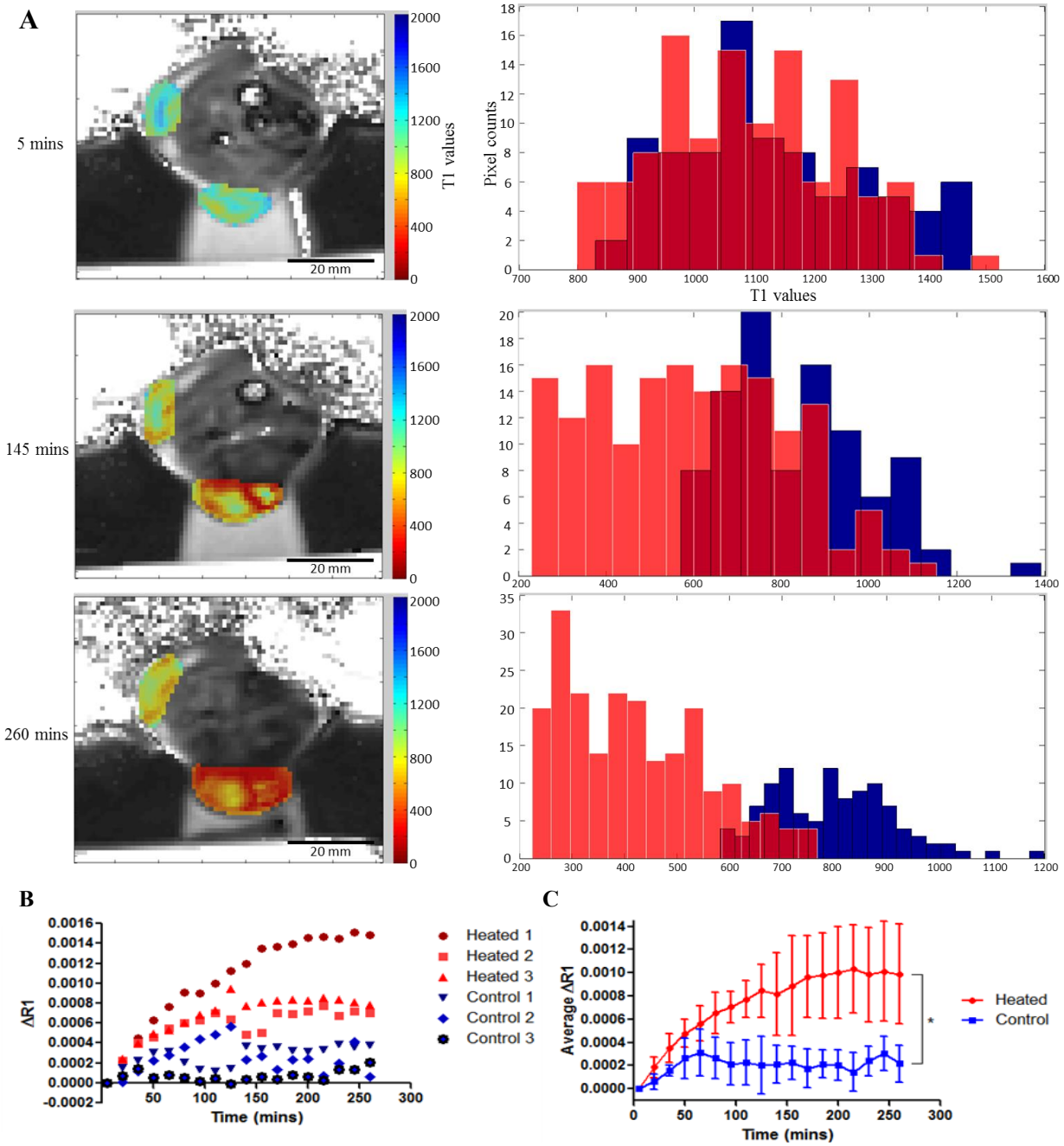

Figure 4.6: A) Representative montage of three time points of one slice over the 5-h time period with histograms of the control T1 values (blue) and heated T1 values (red). B) Individual change in R1 values for each heated and control tumor. C) Average change in R1 values with standard deviation of both heated and control groups.

hyperthermia treatment.

4.4 Discussion

This work clearly demonstrates that mild hyperthermia produced by HIFU can result in the same increase of accumulation of macromolecules within solid tumors as previously demonstrated by using PPTT [5, 6]. In both experiments, the same animal model and macromolecules were used to demonstrate this concept. HIFU hyperthermia, like other methods of hyperthermia, enhances the delivery of nanomedicines through increased blood flow and vascular permeability in the heated tissue leading to increased accumulation of macromolecules [3].

A noninvasive MRgHIFU controller and protocol that heats the tumors evenly and maintains hyperthermia for 10 min was developed and the ability for this method to enhance macromolecular delivery was evaluated. A controller that can adjust the ultrasound power based on the resulting heating profile is critical in achieving the required hyperthermic conditions in an *in vivo* model. Differences in tumor size, morphology, and perfusion result in varied acoustic and thermal properties that result in variable thermal responses that must be accounted for in real time.

For proof of concept, EBD was used as a macromolecular marker to track accumulation within the heated and control tumor. EBD has been shown to form a colloid, about 240 nm in diameter, to which albumin can bind, representing a macromolecular system [26]. EBD-albumin accumulates in the tumor tissue due to the EPR effect with an additional increase in the heated tissues due to increased flow dynamics and vasodilation expanding vascular fenestrae. In previous work using PPTT, EBD was used to determine

enhancement of macromolecular delivery in tumors treated with hyperthermia [5]. In this work, HIFU hyperthermia demonstrated accumulation of EBD at 5 h post HIFU at approximately 1.91 times that of normothermia. These results are similar to our previous observation with PPTT that showed thermal enhancement ratio of 1.68 at similar hyperthermia conditions [5].

HIFU hyperthermia was also evaluated to determine the ability to enhance accumulation of HPMA copolymers over a 5-h period. It was observed that after 5 h post hyperthermia treatment, there was a significant increase in accumulation when the tumor was treated with HIFU versus the tumor left untreated. This is shown by the changes in T1 signal in Figure 4.6A and in the plots of R1 values in Figures 4.6B and 4.6C. The changes in R1 values for the three control tumors and three heated tumors were determined and averaged resulting in a mean change of approximately 0.0002 s^{-1} and 0.001 s^{-1}, respectively, at 260 min. This result indicates significantly more polymer accumulated in the heated tumors versus the untreated tumors. Previous work with PPTT has also shown that Gd-chelated polymers had increased accumulation over 5 h. The results shown here with HIFU are additionally consistent with those of PPTT showing that similar effects can be achieved. In the previous experiments using PPTT, the control tumors had a mean R1 value of 1.02 s^{-1} versus the heated tumors with a mean R1 value of 2.31 s^{-1} [6]. For both experiments, the standard deviations were much higher in the heated groups (either HIFU or PPTT) than that of the control groups. If we represent the data as TER, HIFU has approximately 5 times the accumulation in the heated tumors than that of the control tumors whereas PPTT is approximately 2.3 times higher by this method of visualization using MRI. These results indicate the promising ability of HIFU hyperthermia to enhance

accumulation of targeted polymer therapeutics. Although the number of animals treated for the MRI accumulation study was small (n=3), there is still a significant difference between accumulation in the heated tumors versus the control tumors demonstrating the capability of HIFU hyperthermia to enhance the delivery of HPMA copolymers.

This work suggests that HIFU can elicit the same vascular mechanisms that are able to enhance accumulation of macromolecules in tumor tissue. Hyperthermia can be effective in improving flow throughout these tumors that can overcome some of the biological barriers to delivery when significant localized heating is achieved [3]. For small molecule drugs with short blood circulation half-lives and low accumulation and residence in the tumor tissues, hyperthermia does not significantly improve delivery as the drugs are easily cleared from the tissues [27]. With macromolecules, such as albumin or HPMA copolymers used in this study, prolonged retention is achieved via the EPR effect as the larger sized molecules do not easily escape [28] the vasculature. When hyperthermia is used in conjunction with macromolecules that have longer blood circulation times, more accumulation over time is observed as the vessels dilate expanding the pores leading to greater extravasation, retention, and delivery.

Although heating via HIFU hyperthermia was performed for only 10 minutes, the peak accumulation was observed 4-5 h later. Heat is a physical entity and has damaging effects on tumor tissue depending on the temperature of heating and the duration of application [25, 29]. Since heat can represent an injurious physical insult, it is likely that inflammatory reaction will be involved in the response following tumor heating [30, 31]. While the vascular response of mild hyperthermia within the tumor tissue resolves soon after heating, mild hyperthermia also creates stress within the tissue that can initiate an

acute inflammation and additionally aid in enhanced accumulation of macromolecules for several hours. The time frame and nature of the results presented here are consistent with protein disaggregation and reassembly. Microtubules of the cytoskeleton have been shown to disaggregate during hyperthermia and re-aggregate during subsequent incubation at 37°C [32]. Endothelial cells have been shown to cause a reversible loss of actin filaments that may contribute to increased leakage of tumor microvasculature with recovery after hyperthermia occurring over several hours [32]. Thus, the accumulation over the 5 h is likely not only due to increased blood flow but also due to the longer lasting inflammatory response and recovery of the endothelial cells as the pore sizes return to their original size.

Besides the vascular mechanisms which have been observed here, mild hyperthermia has additionally been shown to induce effects at the cellular level including up-regulation of cell surface heat shock protein GRP78 receptor which can be targeted and additionally supplement this system to further increase retention of targeted copolymers [24]. It is anticipated that our MRgHIFU hyperthermia system can produce these same effects as observed before with PPTT. Hyperthermia by MRgHIFU is likely to induce heat shock protein expression, enhance the delivery of both targeted and untargeted conjugates, and the combination treatment will ultimately result in increased efficacy due to anticipated synergism.

This combination system can likely be applied to any solid tumor that can be ablated but in which the tumor margins are sensitive. It is also worth noting that the application of both the localized heat treatment and the systemic administration of HPMA copolymer-drug conjugates may also have the ability to treat a localized and metastatic disease simultaneously. Furthermore, attaching imaging agents to the copolymer

conjugates can provide a theranostic system to see and treat the disease.

4.5 Conclusions

An MRgHIFU controller and protocol was developed to heat subcutaneous S-180 tumors *in vivo* at 43° for 10 min reproducibly. This method of hyperthermia was then tested to observe an enhancement in macromolecular delivery to heated tumors versus unheated control tumors. It was observed that HIFU hyperthermia increases the amount of EBD accumulation by almost 2-fold at 5 h post heat treatment. Delivery of HPMA-Gd copolymer conjugates was also enhanced to a significant degree and visualized by MRI.

4.6 References

[1] Y.H. Bae, R.J. Mrsny, K. Park, Cancer targeted drug delivery: An elusive dream, Springer Science & Business Media, 2013.

[2] V.P. Chauhan, T. Stylianopoulos, Y. Boucher, R.K. Jain, Delivery of molecular and nanoscale medicine to tumors: Transport barriers and strategies, Annual Review of Chemical and Biomolecular Engineering 2(1) (2011) 281-298.

[3] C.W. Song, Effect of local hyperthermia on blood flow and microenvironment: A review, Cancer Research 44(10 Supplement) (1984) 4721s-4730s.

[4] N. Frazier, H. Ghandehari, Hyperthermia approaches for enhanced delivery of nanomedicines to solid tumors, Biotechnology and Bioengineering 112(10) (2015) 1967-1983.

[5] A.J. Gormley, K. Greish, A. Ray, R. Robinson, J.A. Gustafson, H. Ghandehari, Gold nanorod mediated plasmonic photothermal therapy: A tool to enhance macromolecular delivery, International Journal of Pharmaceutics 415(1–2) (2011) 315-318.

[6] A.J. Gormley, N. Larson, A. Banisadr, R. Robinson, N. Frazier, A. Ray, H. Ghandehari, Plasmonic photothermal therapy increases the tumor mass penetration of HPMA copolymers, Journal of Controlled Release 166(2) (2013) 130-138.

[7] N. Larson, A. Gormley, N. Frazier, H. Ghandehari, Synergistic enhancement of cancer therapy using a combination of heat shock protein targeted HPMA copolymer–drug conjugates and gold nanorod induced hyperthermia, Journal of Controlled Release 170(1)

(2013) 41-50.

[8] A.J. Gormley, A. Malugin, A. Ray, R. Robinson, H. Ghandehari, Biological evaluation of RGDfK-gold nanorod conjugates for prostate cancer treatment, Journal of Drug Targeting 19(10) (2011) 915-924.

[9] J.-L. Thomas, M.A. Fink, Ultrasonic beam focusing through tissue inhomogeneities with a time reversal mirror: Application to transskull therapy, Ultrasonics, Ferroelectrics, and Frequency Control, IEEE Transactions on 43(6) (1996) 1122-1129.

[10] F.J. Fry, Precision high intensity focusing ultrasonic machines for surgery, American Journal of Physical Medicine & Rehabilitation 37(3) (1958).

[11] K. Hynynen, W.R. Freund, H.E. Cline, A.H. Chung, R.D. Watkins, J.P. Vetro, F.A. Jolesz, A clinical, noninvasive, MR imaging-monitored ultrasound surgery method, RadioGraphics 16(1) (1996) 185-195.

[12] K. Hynynen, MRIgHIFU: A tool for image-guided therapeutics, Journal of Magnetic Resonance Imaging 34(3) (2011) 482-493.

[13] D.A. Christensen, Ultrasonic Bioinstrumentation, Wiley, New York, 1988.

[14] M. Pernot, J.F. Aubry, M. Tanter, J.L. Thomas, M. Fink, High power transcranial beam steering for ultrasonic brain therapy, Physics in Medicine and Biology 48(16) (2003) 2577-2589.

[15] FDA Clears focused ultrasound system for prostate cancer treatment, Oncology Times 37(22) (2015) 37.

[16] M. de Smet, E. Heijman, S. Langereis, N.M. Hijnen, H. Grüll, Magnetic resonance imaging of high intensity focused ultrasound mediated drug delivery from temperature-sensitive liposomes: An in vivo proof-of-concept study, Journal of Controlled Release 150(1) (2011) 102-110.

[17] Y.-F. Zhou, High intensity focused ultrasound in clinical tumor ablation, World Journal of Clinical Oncology 2(1) (2011) 8-27.

[18] J. Strohalm, J. Kopeček, Poly[N-(2-hydroxypropyl)methacrylamide]. IV. Heterogeneous polymerization, Die Angewandte Makromolekulare Chemie 70(1) (1978) 109-118.

[19] B. Zarabi, M.P. Borgman, J. Zhuo, R. Gullapalli, H. Ghandehari, Noninvasive monitoring of HPMA copolymer–RGDfK conjugates by magnetic resonance imaging, Pharmaceutical Research 26(5) (2009) 1121-1129.

[20] B. Zarabi, A. Nan, J. Zhuo, R. Gullapalli, H. Ghandehari, HPMA copolymer–doxorubicin–gadolinium conjugates: Synthesis, characterization, and in vitro evaluation, Macromolecular Bioscience 8(8) (2008) 741-748.

[21] J.D. Poorter, C.D. Wagter, Y.D. Deene, C. Thomsen, F. Ståhlberg, E. Achten, Noninvasive MRI thermometry with the proton resonance frequency (PRF) method: In vivo results in human muscle, Magnetic Resonance in Medicine 33(1) (1995) 74-81.

[22] R. Deckers, B. Denis de Senneville, L. Merckel, G. Schubert, F. Knuttel, M. Kohler, W. Mali, C. Moonen, M. van den Bosch, and L.W. Bartels, Performance analysis of a dedicated breast MR-HIFU system for tumor ablation in breast cancer patients, Physics in Medicine and Biology 60(14) (2015) 5527.

[23] D.R. Messroghli, A. Radjenovic, S. Kozerke, D.M. Higgins, M.U. Sivananthan, J.P. Ridgway, Modified look-locker inversion recovery (MOLLI) for high-resolution T1 mapping of the heart, Magnetic Resonance in Medicine 52(1) (2004) 141-146.

[24] A.J. Gormley, N. Larson, S. Sadekar, R. Robinson, A. Ray, H. Ghandehari, Guided delivery of polymer therapeutics using plasmonic photothermal therapy, Nano Today 7(3) (2012) 158-167.

[25] N. Frazier, R. Robinson, A. Ray, H. Ghandehari, Effects of heating temperature and duration by gold nanorod mediated plasmonic photothermal therapy on copolymer accumulation in tumor tissue, Molecular Pharmaceutics 12(5) (2015) 1605-1614.

[26] S.C. Owen, A.K. Doak, P. Wassam, M.S. Shoichet, B.K. Shoichet, Colloidal aggregation affects the efficacy of anticancer drugs in cell culture, ACS Chemical Biology 7(8) (2012) 1429-1435.

[27] D. Needham, M.W. Dewhirst, The development and testing of a new temperature-sensitive drug delivery system for the treatment of solid tumors, Advanced Drug Delivery Reviews 53(3) (2001) 285-305.

[28] H. Maeda, J. Wu, T. Sawa, Y. Matsumura, K. Hori, Tumor vascular permeability and the EPR effect in macromolecular therapeutics: A review, Journal of Controlled Release 65(1–2) (2000) 271-284.

[29] J.A. Dickson, S.K. Calderwood, Temperature range and selective sensitivity of tumors to hyperthermia: A critical review, Annals of the New York Academy of Sciences 335(1) (1980) 180-205.

[30] G. Grile, The Effects of heat and radiation on cancers implanted on the feet of mice, Cancer Research 23(3) (1963) 372-380.

[31] G. Moricca, R. Cavaliere, A. Caputo, A. Bigotti, F. Colistro, Hyperthermic treatment of tumours: Experimental and clinical applications, in: A. Rossi-Fanelli, R. Cavaliere, B. Mondovì, G. Moricca (Eds.), Selective Heat Sensitivity of Cancer Cells, Springer Berlin Heidelberg, Berlin, Heidelberg, 1977, pp. 112-152.

[32] P.S. Lin, K.C. Ho, S.J. Sung, J. Gladding, Effect of tumour necrosis factor, heat, and radiation on the viability and microfilament organization in cultured endothelial cells, International Journal of Hyperthermia 8(5) (1992) 667-677.

CHAPTER 5

ENHANCED EFFICACY OF COMBINATION HEAT SHOCK TARGETED POLYMER THERAPEUTICS WITH HIGH INTENSITY FOCUSED ULTRASOUND

5.1 Introduction

The ultimate goal of drug delivery is to selectively deliver therapeutics to the disease site and allow for increased dosages to be administered to the patient as off-target effects are reduced. Polymer therapeutics have been developed in an attempt to accomplish this goal for delivery of anticancer drugs to solid tumors [1]. Such constructs can extend blood circulation times of conventional drugs and increase accumulation within cancerous tissues through passive delivery by the enhanced permeability and retention (EPR) effect [2]. The use of these and other nanomedicines has led to improved therapeutic outcomes with altered biodistribution in certain cases minimizing side effects (e.g., Doxil reducing the cardiotoxicity of doxorubicin) [3]. Still, in the majority of cases only, moderately enhanced localization to the tumor tissue is observed, increasing from approximately 1% to 5% of injected dose (ID) [4]. The impact of nanoscale delivery systems for treatment of

---

Reprinted in part with permission of Elsevier. N. Frazier, A. Payne, C. Dillon, N. Subrahmanyam, H. Ghandehari, Enhanced efficacy of heat shock targeted polymer therapeutics with high intensity focused ultrasound, Nanomedicine: Nanotechnology, Biology, and Medicine, In Press (2016).

solid tumors can be limited due to the variability of EPR effect depending on tumor type, size, location, and preclinical to clinical correlation [5]. Therefore, combination approaches must be considered including augmentation of the EPR effect [6].

Methods to further enhance the delivery of nanomedicines through augmentation of the enhanced permeability and retention (EPR) effect include mild hyperthermia. At the tissue level, this mechanism can both increase blood flow and improve vascular permeability by vasodilation [7] leading to improvements in local delivery. Mild hyperthermia has been shown to enhance the delivery of nanomedicines to solid tumors [8]. At the cellular level, mild hyperthermia has the ability to up-regulate cell surface HS receptor glucose regulated protein 78 (GRP78) [9]. Specific peptide sequences have been developed by phage display which show a strong binding affinity towards the GRP78 receptors [10]. These peptides include WDLAWMFRLPVG which have been conjugated to polymeric carriers [11]. Methods such as plasmonic photothermal therapy (PPTT), magnetic fluid hyperthermia (MFH), and radiofrequency ablation (RFA) can induce hyperthermic conditions [8]. We have previously demonstrated that mild hyperthermia by gold nanorod (GNR)-mediated PPTT enhances the delivery of *N*-(2-hydroxypropyl)methacrylamide (HPMA) copolymer-drug conjugates containing GRP78 targeting moieties in the side chains to solid tumors [9]. HS-targeted copolymer-docetaxel (DOC) conjugates showed enhanced efficacy when hyperthermia was applied in combination [11]. While results of this research are promising, PPTT in combination with polymer therapeutics requires a prior injection of nanoparticles delivered intravenously which then accumulate in tumor tissue by the EPR effect [12]. The accumulation of these particles in tumor tissue allows for laser energy to be locally absorbed [13]. However, after

this injection, only a small fraction of the gold nanoparticles reach the tumor site leading to a large amount (>90%) of off-target accumulation in other organs such as the liver and spleen [12]. In addition in order to heat deep-seeded tumors, a fiber optic needs to be inserted in the body. These drawbacks can limit the applications of this promising combination strategy. Alternative methods which are noninvasive and provide a higher depth of tissue penetration are needed to improve the clinical application of the combination of mild hyperthermia and polymer therapeutics to treat solid tumors.

High intensity focused ultrasound (HIFU) is a noninvasive technique that can locally heat tissues and achieve a large penetration depth of up to approximately 20 cm through the tissue [14]. We have previously shown that HIFU can be used to generate and maintain uniform hyperthermia in tumor tissue and that the resulting thermal effects can lead to enhanced delivery of HPMA copolymer-gadolinium conjugates in solid tumors [15]. The accumulation of these nontargeted systems enabled a transient increase in copolymer concentration in a mouse sarcoma model peaking at approximately 4-5 h post HIFU heating [15]. To further build on the utility of HIFU mild hyperthermia in enhancing the delivery of macromolecular constructs, in this manuscript, we have used a combination of noninvasive HIFU hyperthermia with HPMA copolymer-WDLAWMFRLPVG conjugates containing docetaxel (DOC) in the side chains to improve the efficacy of the conjugates in a murine model of human prostate xenografts.

5.2 Materials and methods

5.2.1 Synthesis and characterization of HPMA copolymer conjugates

HPMA comonomer was synthesized and confirmed by NMR [16], *N*-methacryloylglycylglycyl-2-thiazolidine-2-thione (MA-GG-TT) comonomer was synthesized and characterized by NMR, and *N*-methacryloyl-glycylphenylalanylleucylglycine-docetaxel (MA-GFLG-DOC) comonomer was synthesized and characterized by mass spectroscopy [17]. DOC was provided by AK Scientific (Mountain View, CA). Free radical precipitation copolymerization was performed using a feed ratio of 82.5 mol% HPMA, 15 mol% MA-GG-TT, and 2.5 mol% MA-GFLG-DOC using azobisisobutyronitrile (AIBN) as the initiator in methanol at 50°C for 24 h was used to prepare the copolymers. The product was then precipitated and washed with diethyl ether three times to removed unreacted monomers. The resulting polymer was dried by vacuum desiccation for later use in peptide conjugation.

The GRP78 targeting peptide WDLAWWMFRLPVG and corresponding scrambled peptide RWLWVADPFLMG were synthesized via Fmoc chemistry using a Protein Technologies (Tuscon, AZ) PS3 solid phase peptide synthesizer verified electrospray ionization mass spectroscopy (ESI/MS). Peptides were then attached to DOC containing polymers via activated ester conjugation. The peptide was added to the polymer with a molar ratio of 1:1 of peptide to TT content. The peptide and polymer were dissolved in minimal amount of dimethyl formamide (DMF) and diisopropylethylamine (DIPEA) was then added to make a 10% v/v solution. The mixture was stirred for 24 h under nitrogen atmosphere. The polymer-peptide conjugates were precipitated in diethyl ether and washed three times by centrifugation to remove DMF. The resulting pellet was dried under vacuum

desiccation, dissolved in sodium citrate buffer to prevent hydrolysis of the DOC, and dialyzed against sodium citrate buffer to remove free peptides. Weight average molecular weight (Mw), number average molecular weight (Mn), and polydispersity index (Mw/Mn) were estimated by size-exclusion chromatography (SEC). Peptide content was determined by amino acid analysis (AAA).

Drug release and drug content was determined by high pressure liquid chromatography (HPLC) by dissolving 5.0 mg of the conjugate in 200 µl DMSO. 10 µl of this solution was incubated in 20 µl buffer A consisting of 0.1 M citrate phosphate buffer containing 2 mM EDTA at pH 6.0, 0.6 mM papain and 100 µl of buffer B consisting of 0.1 M citrate phosphate buffer containing 2 mM EDTA at pH 6.0 and 10 mM of glutathione. The mixture was incubated at 37°C for 24 h. An aliquot (50 µl) of the reaction mixture was removed and diluted in 450 µl water: acetonitrile (65:35) and evaluated for DOC content by HPLC and compared to calibration standards prepared using serial dilutions of DOC in the mobile phase. Mobile phase consisted of deionized water (Milli-Q system, Millipore, Billerica, MA, USA) and HPLC grade acetonitrile (ACN) using the following gradient: 0 min, 35% ACN; 15 min, 65% ACN; 25 min, 75% ACN; 30 min 95% ACN; 39 min, 100% ACN; 40 min 65% ACN. HPLC analyses were performed with an Agilent Series 1100 HPLC (Agilent Technologies, Wilmington, DE, USA) equipped with an Alltima C18 5 µm 150 × 4.6 mm column and a photo diode array detector scanning at 200 – 500 nm. A flow rate of 1.0 mL/min was maintained and the sample injection volume was 20 µl. A post time of 5 min was used to allow column equilibration between samples. UV absorbance at 230 nm was used for quantification of DOC.

5.2.2 Cell culture

The DU145 human prostate cancer cell line was obtained from ATCC (Manassas, VA) and cultured at 37 °C in a humidified atmosphere of 5% CO2 in Eagle's Minimum Essential Medium supplemented with 10% fetal bovine serum (FBS). Cells were maintained in a logarithmic growth phase during all studies.

5.2.3 *In vitro* efficacy of heat shock targeted copolymer-drug conjugates

DU145 cells (3000 per well) were plated in 96-well plates for 24 h. Media was then removed and replaced with media containing treatments. Cells were exposed to either heat shock targeted copolymers or untargeted copolymers for 12 h at varying concentrations between 0 and 1200 nM DOC concentration. One group was incubated at 37°C while a second group was exposed to HS (43°C for 30 min) and then incubated at 37°C for the remainder of the 12 h. This thermal dose profile was chosen to be consistent with previous experiments [11] and as this thermal treatment showed a 4-fold increase in cell receptors *in vitro* [9]. For each treatment case, drug concentrations were varied to include data points ranging from approximately 100% to 0% cell viability. Following drug treatment, media was removed, cells washed with PBS, growth media replaced, and cells were allowed to grow for an additional 60 h (72 h of total experiment duration). Media was then removed and cell viability quantified by CCK-8 assay using a SpectraMax M2 microplate ultraviolet (UV) spectrophotometer (Molecular Devices, Sunnyvale, CA). Each experiment was performed in triplicate, comprising assessment of viability at 10 different drug concentrations with 4 samples analyzed per concentration. Relative viability was calculated by normalization of UV absorbance against untreated cells. Relative viability as

a function of log drug concentration was plotted and nonlinear least-squares regression analysis and calculation of IC_{50} values were performed using GraphPad Prism.

5.2.4 *In vivo* tumor model

In vivo experiments were carried out using nu/nu mice containing two DU145 human prostate cancer subcutaneous tumor xenografts, one on each flank. Inoculations were performed by injecting 200 μL of phosphate buffered solution (PBS) containing 10x106 cells subcutaneously and allowing tumors to grow for 28-30 days to reach a size of 7-11 mm in diameter. Tumor sizes were measured every 3 days using calipers. Once the tumors reached their desired size, they were then treated with HIFU hyperthermia.

5.2.5 *In vivo* MRgHIFU heating

Prior to HIFU treatment, the mice were anesthetized (2% isoflurane), a needle thermocouple was inserted into the center of the tumor and 2 min of temperature data were obtained to determine a baseline tumor temperature. The mouse was then placed in a magnetic resonance imaging (MRI)-guided HIFU (MRgHIFU) small animal system (Image Guided Therapy, Inc.) in a Siemens 3T Trio MRI. The animal was placed on an agar mold with the tumor placed in an access hole. The agar mold provided a large region to obtain MRI phase measurements to improve the MRI temperature measurement with atlas-based reconstruction. A custom two-channel radiofrequency coil was placed on top of the animal, and a small animal monitoring system was used to monitor the animal (respiration and temperature, SA instruments, Inc.). MR temperatures were monitored with the proton resonance frequency (PRF) method using a 2D seg-EPI sequence (TR/TE =

150/13 ms, echo-train length (ETL)=9, 1.2 s acquisition, 2x2x3 mm resolution, 3 slices). All heating was performed using an MRgHIFU small animal system (Image Guided Therapy, Inc., Bordeaux, France. 16-element annular transducer, f=3MHz, 1x1x3 mm full-width-half-maximum focal spot size, +/- 1.5 cm steering along beam direction) placed in a Siemens 3T Trio MRI scanner. Because the phased-array transducer has an annular design, in plane focal spot motion was achieved by physically moving the transducer through the use of piezoelectric motors. The experimental setup is shown in Figure 5.1 with an axial (Figure 5.1A) and coronal (Figure 5.1B) image. Susceptibility effects due to ultrasound transducer motion were mitigated using an atlas-based reconstruction [18] where approximately 50 baseline library images were acquired with the transducer moving along the defined trajectory (Figure 5.1C) multiple times without firing the ultrasound. During sonication, the current MR phase measurement was subtracted from the baseline library phase image that was most similar in a least squared difference sense. Using a previously described MRgHIFU controller [15], the maximum and mean temperatures in the tumor were monitored and a power range between 3.3 and 5.6 W was implemented (approximately 3.5 to 4.6 MPa in water) to achieve and maintain a maximum temperature rise of 43°C. The technician was able to adjust the ultrasound power output trajectory in real time using a user interface written in Matlab. A target maximum temperature rise of 43°C was selected to induce mild hyperthermia but not ablation. During post processing, temperatures were temporally filtered for respiratory artifact using a low pass digital filter.

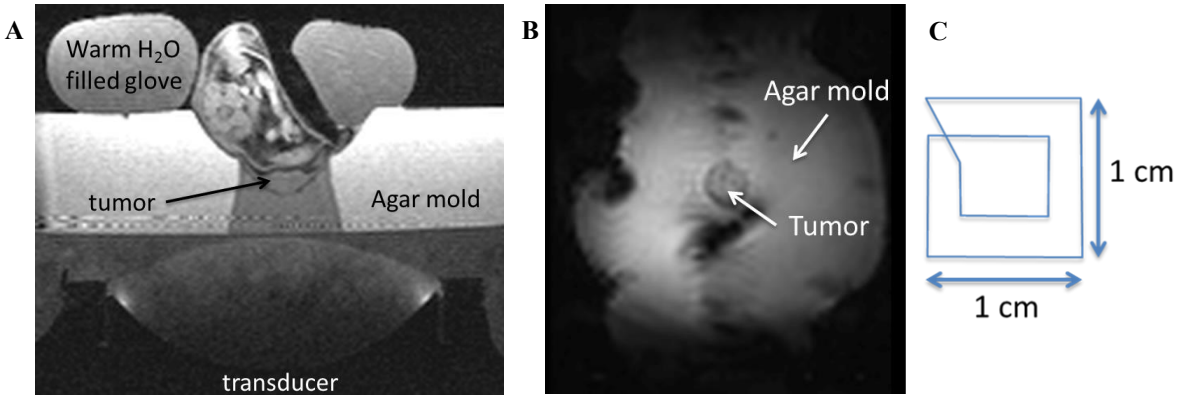

Figure 5.1: Schematic of *in vivo* heating setup. A) Axial image of small animal MRgHIFU system used to heat tumor tissue *in vivo*. B) Coronal image of *in vivo* setup with the treated tumor surrounded by the agar mold. C) Heating pattern for producing uniform heating.

5.2.6 *In vivo* expression of GRP78 with MRgHIFU hyperthermia

MRgHIFU was used to treat one tumor for each of the nu/nu mice (n=3) bearing two subcutaneous DU145 tumors. The second tumor was left untreated and used as an internal control. Hyperthermia by MRgHIFU was used to induce HS and determine the up-regulation of GRP78 receptors in the heated tumor versus the control tumor. Eight hours following induction of heat shock, the mice were sacrificed and both tumors were removed and fixed in 10% buffered formalin. Immunohistochemical analysis of GRP78 expression was then performed on paraffin embedded tumor tissue sliced into 4-micron thick sections and stained using a goat polyclonal anti-GRP78 antibody (Santa Cruz Biotechnology, Santa Cruz, CA).

5.2.7 *In vivo* efficacy of heat shock targeted HPMA-DOC copolymer conjugates with MRgHIFU

The combination of HS-targeted copolymer-drug conjugates and MRgHIFU were evaluated *in vivo* using nu/nu mice bearing two subcutaneous DU145 human prostate cancer tumors. Prior to treatment with MRgHIFU hyperthermia to one tumor, either saline, free DOC (formulated in polysorbate 80:ethanol:saline [20:13:67, v/v/v]), untargeted (scrambled peptide) polymer-DOC, or HS-targeted polymer-DOC was injected intravenously at 10 mg/kg equivalent of DOC. Each treatment group was comprised of six mice. The mice in each treatment group were monitored over 30 days, twice a week for changes in tumor volume and animal weight. Tumor dimensions (length and width) were measured and tumor volume estimated as length × width × $\pi/6$. Normalized tumor volume presented as mean ± standard error of the mean (SEM) and changes in animal weight

presented as mean ± standard deviation (STD) as a function of time. After the 30-day study was completed, tumors and organs were removed, fixed in 10% buffered Formalin, paraffin embedded, sectioned into 4-micron thick slices, and stained with H&E, Ki-67, TUNEL, and Caspace-3 to observe tissue morphology, cell proliferation, and apoptosis.

5.2.8 Statistical analysis

Statistical analyses were performed in GraphPad Prism. Differences in normalized tumor volumes and changes in animal weight were determined by one-way ANOVA. Where differences were detected, Tukey's post test was used to test for significance between groups. The default significance level was set at $\alpha = 0.05$ for all statistical tests. $P < 0.05$ were considered statistically significant (* $P \leq 0.05$, ** $P \leq 0.01$, *** $P \leq 0.001$).

5.3 Results

5.3.1 HPMA copolymer synthesis and characterization

The HPMA copolymers were synthesized by free radical precipitation copolymerization to be greater than 45 kDa to have a size slightly above the renal threshold in order to take advantage of the EPR effect as well as to be consistent with the size of polymers used in previous accumulation studies [9, 19, 20]. The characteristics of the copolymers are summarized in Table 5.1 and size-exclusion chromatographs are shown in the appendix. Drug content was confirmed by HPLC using the calibration curve shown in the appendix.

Table 5.1: HPMA copolymer-drug conjugate characteristics.

Sample	M_W (kDa)	PDI	Drug content (wt%)	Targeting peptide content (wt%)
Targeted copolymer-DOC	97	1.9	4.6 +/- 0.46	14.5 +/- 0.39
Untargeted copolymer-DOC	94	1.9	4.7 +/- 0.37	13.9 +/- 1.16

5.3.2 *In vitro* efficacy of heat shock targeted and untargeted polymer-docetaxel conjugates with human prostate cancer cells

The ability of the HS-targeted and untargeted HPMA copolymer-DOC conjugates to inhibit the growth of DU145 human prostate cancer cells was first evaluated *in vitro*. In Figure 5.2, both targeted and untargeted conjugates were incubated with and without hyperthermia at varying concentrations of DOC. The IC_{50} for the HS-targeted copolymer conjugates and untargeted conjugates under normothermia were 14.9 +/- 3.5 and 16.2 +/- 4.6 nM, respectively. When the copolymer conjugates were incubated with hyperthermia, the IC_{50} for targeted and untargeted copolymer conjugates shifted to 7.4 +/- 2.3 and 11.0 +/- 4.6 nM, respectively. It was expected that HS-targeting and hyperthermia would shift the IC_{50} to a lower concentration.

5.3.3 *In vivo* MRgHIFU heating

Tumor temperatures were recorded during HIFU hyperthermia treatments and mean temperature was plotted as an average of the six mice treated in each group +/- one STD (Figure 5.3). Most groups were largely able to heat and maintain at a temperature of approximately 43°C during the 10-min period. However, a large amount of variability is observed for the tumors heated in the group treated with free DOC and may contribute to variability with tumor growth. Saline injected mice were heated and maintained at approximately 42°C +/- 2°C (Figure 5.3A), free DOC injected mice were heated at approximately 41°C +/- 5°C (Figure 5.3B), untargeted polymer-DOC heated to approximately 42°C +/- 2°C (Figure 5.3C), and HS-targeted polymer-DOC heated to approximately 44°C +/- 1°C (Figure 5.3D).

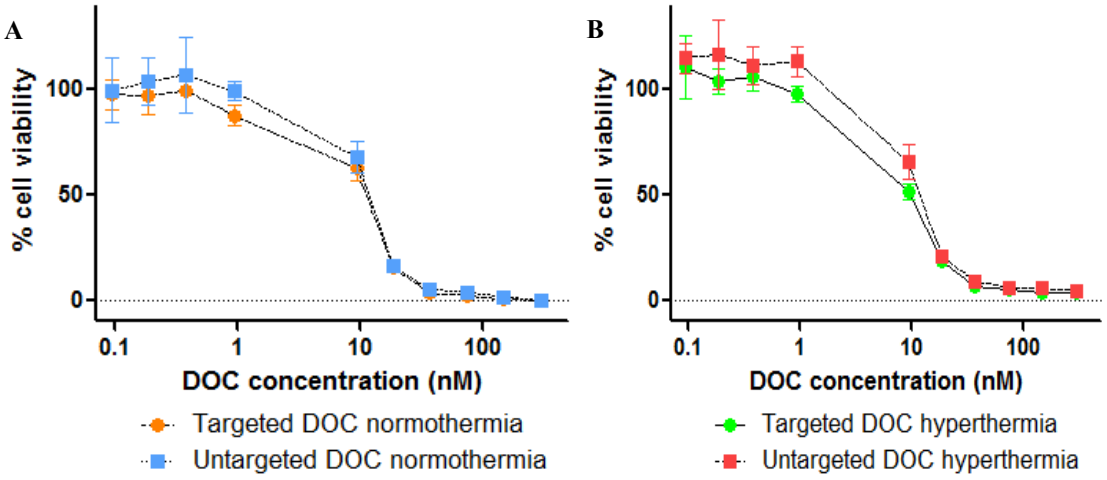

Figure 5.2: *In vitro* efficacy of heat shock targeted and untargeted polymer-docetaxel conjugates incubated in combination with A) normothermia (37°C for 72 h) or with B) hyperthermia (43°C for 30 min followed by 37°C for 71.5 h). Data is expressed as mean +/- STD with n=4 for each sample and concentration.

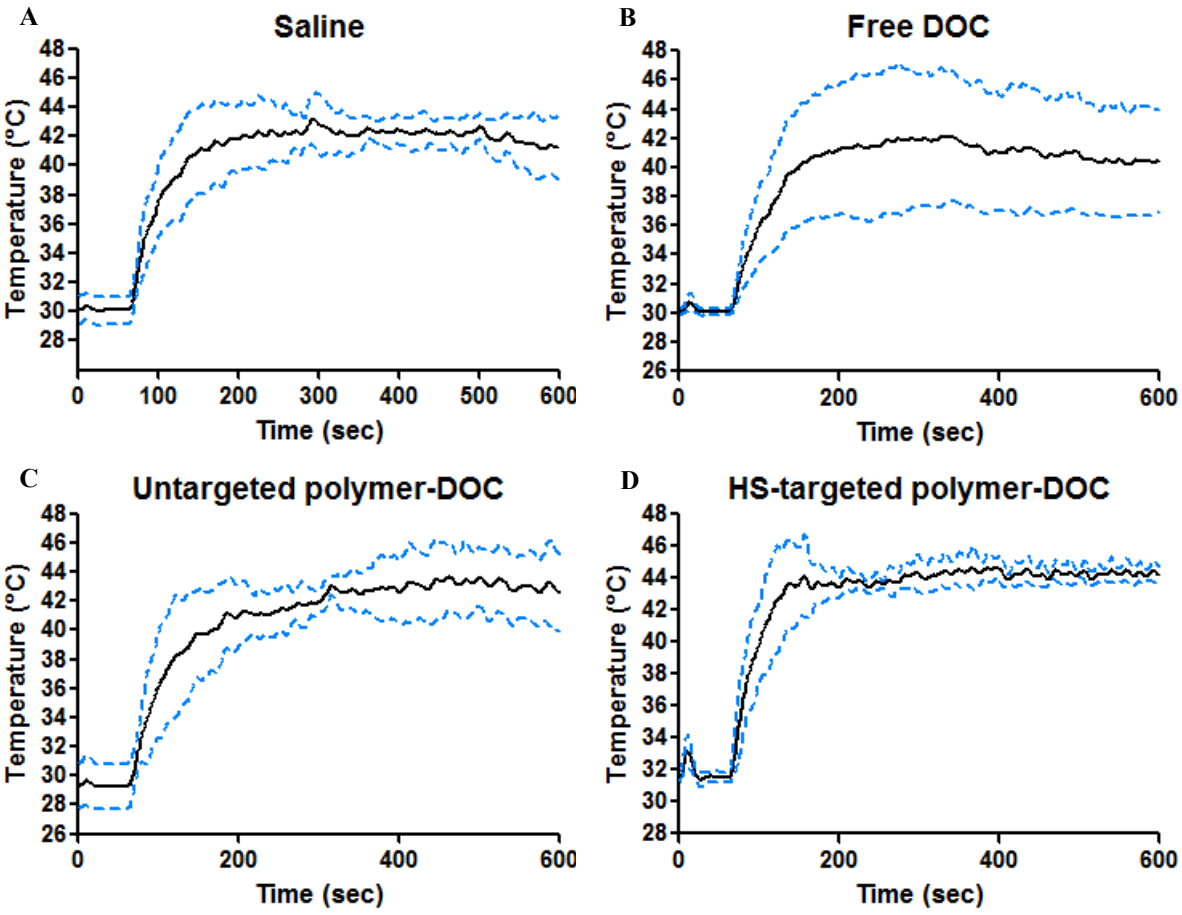

Figure 5.3: *In vivo* MRgHIFU heating temperature profiles of treatment groups A) saline, B) free docetaxel, C) untargeted polymer-docetaxel, and D) heat shock-targeted polymer-docetaxel. For each treatment group n=6.

5.3.4 *In vivo* heat shock expression with and without HIFU hyperthermia

HIFU hyperthermia was used to up-regulate the cell surface expression of GRP78 *in vivo* using DU145 human prostate cancer xenografts. After heat treatment to approximately 43°C for 10 min, the expression was observed 8 h later by immunohistochemical analyses. As seen in Figure 5.4, tumors that were treated with HIFU hyperthermia for 10 min (Figure 5.4B) showed much higher amounts of staining for GRP78 than did the tumors that were left untreated (Figure 5.4A). This result indicates that HIFU hyperthermia by this method has the capability to up-regulate GRP78 receptors *in vivo*.

5.3.5 Tumor growth after combination therapy with HIFU

In previous work, it was shown that the combination of HS-targeted copolymer-DOC and mild hyperthermia via GNR-mediated PPTT led to significant tumor reduction versus controls [11]. Here we examined if the same could be via HIFU (Figure 5.5). Treatment groups of saline, free DOC, and untargeted polymer-DOC were used as controls and compared to HS-targeted polymer-DOC. In combination with hyperthermia, the tumor growth in each group was slightly more reduced. As expected, saline alone had the largest growth (243% of the original tumor size) followed by hyperthermia alone (204%), free DOC alone (201%), free DOC with hyperthermia (159%), untargeted polymer-DOC (136%), HS-targeted polymer-DOC (119%), and untargeted polymer-DOC with hyperthermia (114%). The group with the most tumor size reduction was the combination of HS-targeted polymer-DOC with HIFU hyperthermia at 96% the original tumor volume 30 days after treatment. Additionally, there were no significant changes in animal weight

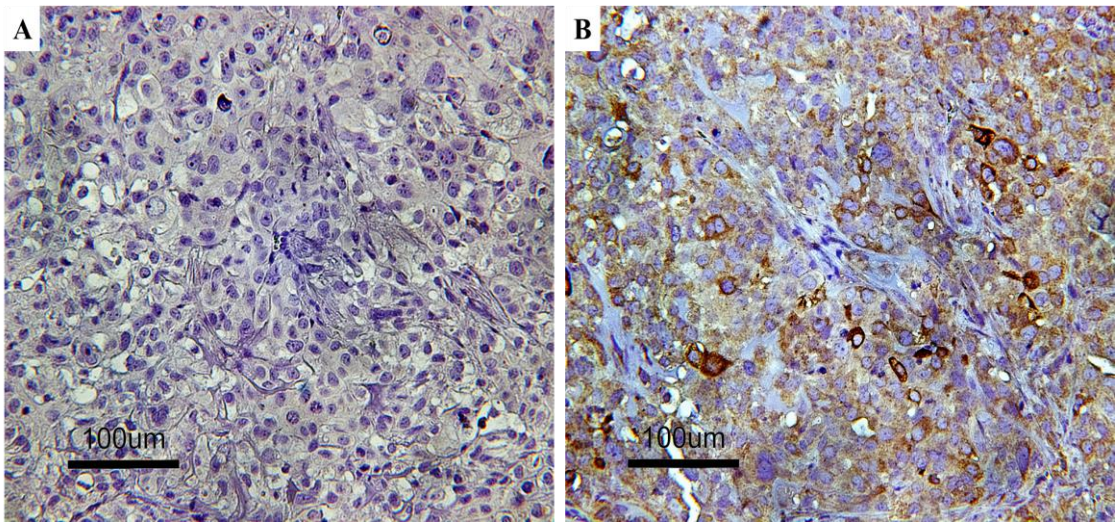

Figure 5.4: (A) Control tumor tissue stained for expression of GRP78 cell receptors. (B) HIFU hyperthermia treated tumor tissue stained for GRP78 cell receptors shown by the red-brown color.

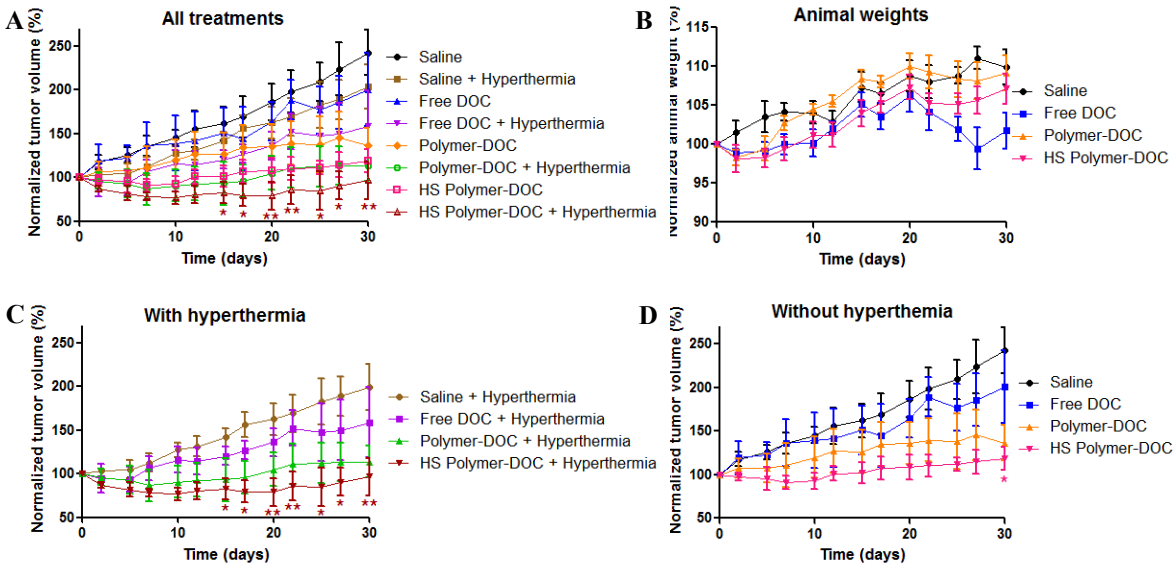

Figure 5.5: *In vivo* efficacy of HIFU hyperthermia and heat shock-targeted polymer-docetaxel. A) Tumor volume over 30 days when injected with saline, free docetaxel (free DOC), untargeted polymer-docetaxel (polymer-DOC), or heat shock-targeted polymer-docetaxel (HS polymer-DOC) with and without HIFU hyperthermia. B) Animal weights when injected with saline, free DOC, polymer-DOC, or HS polymer-DOC. C) Treatment groups with hyperthermia. D) Treatment groups without hyperthermia. For each treatment group n=6. * And ** indicate statistical significance compared to saline control.

over the 30-day experiment although the weights of the free DOC group began to drop from day 20 to day 30.

5.3.6 Histological analyses of *in vivo* tumor efficacy

At the culmination of the 30-day monitoring period, each animal was sacrificed and the tumors were removed, collected, and analyzed by histology. Tissues were stained with H&E to observe tissue morphology, Caspase-3 to observe apoptosis, and Ki-67 to observe cell proliferation. In Figure 5.6, control groups stained with H&E show a higher density of cells indicated by the darker color. Additionally, this shows that the HS-targeted polymers with hyperthermia had the largest amount of necrotic regions (Fig 5.6). Tissues stained with Caspase-3 show cells that have synthesized Caspase-3 in cells undergoing apoptosis. This production is indicated by the brown coloration and is most prevalent in tumor tissues treated with combination of HS-targeted polymer-DOC and HIFU hyperthermia as compared to controls (Fig 5.6). Lastly, tissues stained with Ki-67 show the nuclear protein that is present at low levels in quiescent cells but is increased in proliferating cells. Positively stained cells are stained brown as well. Again, combination of HS-targeted polymer-DOC conjugated and HIFU hyperthermia had the least amount of staining when compared to control groups (Figure 5.6). These results additionally show that this combination therapy leads to the greatest therapeutic outcome against human prostate cancer.

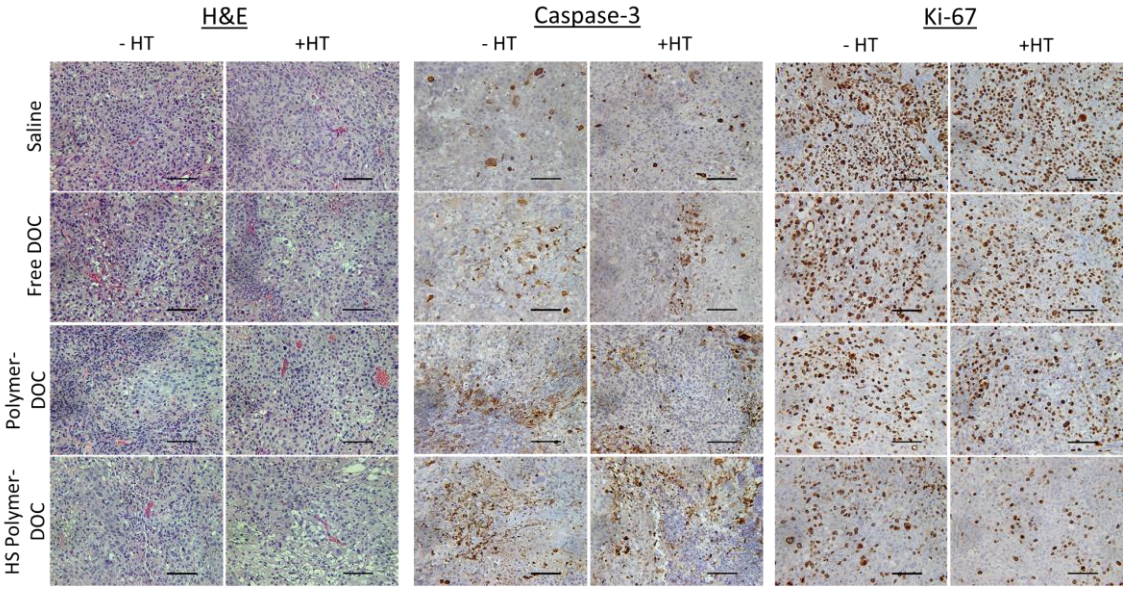

Figure 5.6: Histological analyses of tumor tissue treated with saline, free docetaxel (free DOC), untargeted polymer-docetaxel (polymer-DOC), or heat shock-targeted polymer-docetaxel (HS polymer-DOC) with and without HIFU hyperthermia (HT). Tissues were stained with H&E (tissue morphology), Caspase-3 (apoptosis), and Ki-67 (cell proliferation).

5.4 Discussion

Previously the Ghandehari lab has utilized GNR-mediated PPTT as a method to produce localized hyperthermia selectively in tumor tissue and enhance the delivery and efficacy of HS-targeted HPMA copolymer-drug conjugates [9, 11]. Compared to PPTT, HIFU has a greater penetration depth (20 cm vs. 2 cm) and is noninvasive where PPTT requires a prior injection of nanoparticles delivered intravenously which then accumulates in tumor tissue by the EPR effect. After this injection, only a small fraction of the particles reach the tumor site leading to a large amount of off-target accumulation in other organs such as the liver and spleen [12], and potential long-term effects of this accumulation are unknown. Additionally, not all tumors exhibit the EPR effect and those that do can be variable [5]. PPTT is still in the early developmental stages whereas HIFU has recently been approved by the Food and Drug Administration (FDA) for the ablation of prostate cancer tissue [21].

Mild hyperthermia has been applied to enhance the delivery of other nanomedicines including temperature-sensitive liposomal drug carriers [22-25]. However, when these liposomal systems are triggered for payload release, the extracellular release of drugs at the tumor site occurs. In this case, the free drug can be subject to efflux pumps and hence reduced efficacy. Use of polymer-drug conjugates can be more advantageous since the mechanism of cellular uptake is endocytosis, prohibiting efflux pumps removal of the drug in resistant cancer cases [26]. In addition, covalent attachment of the drug to the polymeric side chains reduces nonspecific leakage in the blood stream. Together our results demonstrate that the combination therapy of HS-targeted conjugates and HIFU hyperthermia has potential for treating prostate cancer and other malignancies.

In this work, it is shown that the combination of HIFU hyperthermia with HS-targeted HPMA copolymer-DOC conjugates leads to improved therapeutic outcome against human prostate cancer xenografts in immune compromised nu/nu mice. Here, we used HS-targeted HPMA copolymer-DOC conjugates as they have shown a high potential for improved therapeutics efficacy in combination with mild hyperthermia [11]. The same HS-targeting peptides were also used for comparison keeping all things similar except using HIFU instead of PPTT to generate hyperthermia [11]. When comparing the HPMA copolymer conjugate characteristics of those synthesized here to those previously used with PPTT [11], the Mw was slightly larger here being closer to 100 kDa than those used before having an Mw closer to 80 kDa [11]. The drug loading here was slightly less, approximately 4.5 wt% compared to 6.5 wt%, and peptide targeting was also slightly less, having approximately 14.5 wt% compared to 16 wt% used previously [11]. The conjugates were again tested *in vitro* to determine the IC_{50} and observe the effects of HS-targeting with and without hyperthermia. Without hyperthermia, the IC_{50} for untargeted and HS-targeted conjugates were similar but slightly improved for the HS-targeted group. When the conjugates were incubated with hyperthermia for 30 min, their IC_{50}s shifted slightly to lower concentrations. Hyperthermia is known to sensitize the cells to chemotherapy and so it is expected that even the untargeted polymers would be able to see a slight shift in IC_{50}.

In vivo, it was expected that the use of hyperthermia via HIFU would up-regulate the expression of GRP78 receptors on the cell surface. For the HS-targeting strategy to be effective, it was important to determine if HIFU hyperthermia had this capability. We previously established that this up-regulation occurs between 8-12 h after heating [9]. Therefore, tumor sections were analyzed 8 h after treatment with HIFU hyperthermia. The

results here show that HIFU hyperthermia does have this capability and is a viable method for use to enhance the efficacy of copolymer-DOC conjugates targeted toward these receptors. This is expected as HIFU has been shown to increase tumor temperature to hyperthermic temperatures and the up-regulation of these receptors is largely due to the increased stress on the cells from the increased heat accumulation in the tissues.

To demonstrate the improved efficacy of the HS-targeted conjugates in combination with HIFU hyperthermia, animals were treated with saline, free DOC, untargeted polymer-DOC, and HS-targeted polymer-DOC. HS-targeted polymer-DOC conjugates showed the greatest reduction in tumor growth versus the saline control without hyperthermia. A large amount of variability was seen with the free DOC treated mice. This variability may be due to a number of factors including varying tumor size, tumor perfusion, and capacity possibly due to the properties of the injected formulation. All of these may contribute to improper heating in 2-3 mice leading to large standard deviations. The tumor growth plots, however, are again similar to those that used PPTT to generate hyperthermia *in vivo* [11]. However, the extent of tumor reduction was not as great as seen with PPTT [11]. This could possibly be due to the slightly lower amounts of drug loading and targeting peptide content, or potential ablative effect of GNR to the cells surrounding the particles even at mild hyperthermia conditions.

It must be noted that under the right conditions GNR-mediated PPTT has some advantages for inducing mild hyperthermia as well. The selective accumulation in the tumor tissue allows for easier application compared with other methods that require expensive imaging techniques (e.g., MRI) in conjunction. Simply irradiating the tumor region along with healthy tissues will only create heating in the tumor tissue as this is where

the GNRs reside. Although the depth of penetration is not as high as other methods of hyperthermia such as HIFU, it can be applied to superficial or easily accessible tumors. The administration of laser irradiation can easily be altered by adjusting the laser power and in turn, tune the temperature without much difficulty. With other methods, obtaining uniform heating at the desired temperature may require several adjustments at once. However, a distinct advantage of HIFU for inducing mild hyperthermia is the ability for deeper penetration of energy and its clinical applicability.

In clinical applications that use HIFU ablation or surgical resection to treat prostate cancer, it may become difficult to ablate or remove the cancerous tissues if they reside near important healthy structures including the urethra. The cancer may have begun to invade the surrounding tissues becoming difficult to ablate or surgically remove because of proximity to these important structures. Therefore, the combination therapy performed here may have the capability to completely destroy those areas which are difficult to treat otherwise by HIFU ablation alone. Incomplete resection or ablation procedures may result in continued cancer growth that may lead to the development of metastatic prostate cancer. If this development occurs, the 5-year survival dramatically drops from near 100% to about 28% with a median survival of about 4 years [27]. Therefore, treatment modalities must ensure that these advanced localized cancers are completely eliminated and not allowed to further progress. In addition to the survival benefit, the use of this proposed combination therapy will decrease complications of incontinence and erectile dysfunction as more precaution can be taken leading to a higher quality of life after the cancer is gone.

As HIFU begins to increasingly be used in the clinic for the treatment of other cancers (breast [18, 28], liver [29, 30], pancreas [31, 32]) as solid tumors, so does the

capability of this combination therapy shown here. HS-targeting can be used in cancers of the liver and breast where the same HS receptors can be targeted [33, 34]. Therefore, this treatment option can potentially be applied to a broad range of malignancies.

5.5 Conclusions

In this study, it was demonstrated that HIFU hyperthermia can be utilized as a tool to selectively heat human prostate cancer xenografts and increase the efficacy of HS-targeted HPMA copolymer-DOC conjugates. The combination of HIFU hyperthermia with these targeted copolymers demonstrates the potential for HIFU to be used as a tool to enhance delivery and efficacy of targeted macromolecules.

5.6 References

[1] R. Duncan, M.J. Vicent, Polymer therapeutics-prospects for 21st century: The end of the beginning, Advanced Drug Delivery Reviews 65(1) (2013) 60-70.

[2] H. Maeda, Macromolecular therapeutics in cancer treatment: The EPR effect and beyond, Journal of Controlled Release 164(2) (2012) 138-144.

[3] P.K. Working, M.S. Newman, S.K. Huang, E. Mayhew, J. Vaage, D.D. Lasic, Pharmacokinetics, biodistribution and therapeutic efficacy of doxorubicin encapsulated in stealth® liposomes (Doxil®), Journal of Liposome Research 4(1) (1994) 667-687.

[4] Y.H. Bae, R.J. Mrsny, K. Park, Cancer targeted drug delivery: An elusive dream, Springer Science & Business Media2013.

[5] V.P. Chauhan, T. Stylianopoulos, Y. Boucher, R.K. Jain, Delivery of molecular and nanoscale medicine to tumors: Transport barriers and strategies, Annual Review of Chemical and Biomolecular Engineering 2(1) (2011) 281-298.

[6] H. Maeda, H. Nakamura, J. Fang, The EPR effect for macromolecular drug delivery to solid tumors: Improvement of tumor uptake, lowering of systemic toxicity, and distinct tumor imaging in vivo, Advanced Drug Delivery Reviews 65(1) (2013) 71-79.

[7] C.W. Song, Effect of local hyperthermia on blood flow and microenvironment: A review, Cancer Research 44(10 Supplement) (1984) 4721s-4730s.

[8] N. Frazier, H. Ghandehari, Hyperthermia approaches for enhanced delivery of nanomedicines to solid tumors, Biotechnology and Bioengineering 112(10) (2015) 1967-1983.

[9] A.J. Gormley, N. Larson, S. Sadekar, R. Robinson, A. Ray, H. Ghandehari, Guided delivery of polymer therapeutics using plasmonic photothermal therapy, Nano Today 7(3) (2012) 158-167.

[10] M. Sato, V.J. Yao, W. Arap, R. Pasqualini, 5 - GRP78 Signaling Hub: A receptor for targeted tumor therapy, in: P. Renata (Ed.), Advances in Genetics, Academic Press2010, pp. 97-114.

[11] N. Larson, A. Gormley, N. Frazier, H. Ghandehari, Synergistic enhancement of cancer therapy using a combination of heat shock protein targeted HPMA copolymer–drug conjugates and gold nanorod induced hyperthermia, Journal of Controlled Release 170(1) (2013) 41-50.

[12] A.J. Gormley, A. Malugin, A. Ray, R. Robinson, H. Ghandehari, Biological evaluation of RGDfK-gold nanorod conjugates for prostate cancer treatment, Journal of Drug Targeting 19(10) (2011) 915-924.

[13] A.J. Gormley, K. Greish, A. Ray, R. Robinson, J.A. Gustafson, H. Ghandehari, Gold nanorod mediated plasmonic photothermal therapy: A tool to enhance macromolecular delivery, International Journal of Pharmaceutics 415(1–2) (2011) 315-318.

[14] D.A. Christensen, Ultrasonic Bioinstrumentation, Wiley, New York, 1988.

[15] N. Frazier, A. Payne, J. de Bever, C. Dillon, A. Panda, N. Subrahmanyam, H. Ghandehari, High intensity focused ultrasound for enhanced macromolecular delivery, Journal of Controlled Release. Submitted. (2016).

[16] J. Strohalm, J. Kopeček, Poly[N-(2-hydroxypropyl)methacrylamide]. IV. Heterogeneous polymerization, Die Angewandte Makromolekulare Chemie 70(1) (1978) 109-118.

[17] A. Ray, N. Larson, D.B. Pike, M. Grüner, S. Naik, H. Bauer, A. Malugin, K. Greish, H. Ghandehari, Comparison of active and passive targeting of docetaxel for prostate cancer therapy by HPMA Copolymer–RGDfK Conjugates, Molecular Pharmaceutics 8(4) (2011) 1090-1099.

[18] R. Deckers, B.D. de Senneville, L. Merckel, G. Schubert, F. Knuttel, M. Kohler, W. Mali, C. Moonen, M. van den Bosch, and L.W. Bartels, Performance analysis of a dedicated breast MR-HIFU system for tumor ablation in breast cancer patients, Physics in Medicine and Biology 60(14) (2015) 5527.

[19] A.J. Gormley, N. Larson, A. Banisadr, R. Robinson, N. Frazier, A. Ray, H. Ghandehari, Plasmonic photothermal therapy increases the tumor mass penetration of HPMA copolymers, Journal of Controlled Release 166(2) (2013) 130-138.

[20] N. Frazier, R. Robinson, A. Ray, H. Ghandehari, Effects of heating temperature and duration by gold nanorod mediated plasmonic photothermal therapy on copolymer accumulation in tumor tissue, Molecular Pharmaceutics 12(5) (2015) 1605-1614.

[21] FDA Clears focused ultrasound system for prostate cancer treatment, Oncology Times 37(22) (2015) 37.

[22] B.M. Dicheva, T.L.M. ten Hagen, D. Schipper, A.L.B. Seynhaeve, G.C. van Rhoon, A.M.M. Eggermont, G.A. Koning, Targeted and heat-triggered doxorubicin delivery to tumors by dual targeted cationic thermosensitive liposomes, Journal of Controlled Release (0) (2014).

[23] L. Li, T.L.M. ten Hagen, A. Haeri, T. Soullié, C. Scholten, A.L.B. Seynhaeve, A.M.M. Eggermont, G.A. Koning, A novel two-step mild hyperthermia for advanced liposomal chemotherapy, Journal of Controlled Release 174(0) (2014) 202-208.

[24] T. Ta, E. Bartolak-Suki, E.-J. Park, K. Karrobi, N.J. McDannold, T.M. Porter, Localized delivery of doxorubicin in vivo from polymer-modified thermosensitive liposomes with MR-guided focused ultrasound-mediated heating, Journal of Controlled Release 194(0) (2014) 71-81.

[25] A.M. Ponce, Hyperthermia mediated liposomal drug delivery, International Journal of Hyperthermia 22(3) (2006) 205-213.

[26] T. Minko, P. Kopečková, J. Kopeček, Efficacy of the chemotherapeutic action of HPMA copolymer-bound doxorubicin in a solid tumor model of ovarian carcinoma, International Journal of Cancer 86(1) (2000) 108-117.

[27] Cancer Facts and Figures 2016, American Cancer Society, Atlanta, Ga, 2016.

[28] F. Wu, G. ter Haar, W.R. Chen, High-intensity focused ultrasound ablation of breast cancer, Expert Review of Anticancer Therapy 7(6) (2007) 823-831.

[29] J.W. Wijlemans, M. de Greef, G. Schubert, L.W. Bartels, C.T. Moonen, M.A. van den Bosch, M. Ries, A clinically feasible treatment protocol for magnetic resonance-guided high-intensity focused ultrasound ablation in the liver, Investigative Radiology (2014).

[30] C. Zavaglia, A. Mancuso, A. Foschi, A. Rampoldi, High-intensity focused ultrasound (HIFU) for the treatment of hepatocellular carcinoma: Is it time to abandon standard ablative percutaneous treatments?, Hepatobiliary Surgery and Nutrition 2(4) (2013) 184-187.

[31] T.D. Khokhlova, J.H. Hwang, HIFU for palliative treatment of pancreatic cancer, Journal of Gastrointestinal Oncology; Vol 2, No 3 (September 2011): Journal of Gastrointestinal Oncology (2011).

[32] H.J. Jang, J.-Y. Lee, D.-H. Lee, W.-H. Kim, J.H. Hwang, Current and future clinical applications of high-intensity focused ultrasound (HIFU) for pancreatic cancer, Gut and

Liver 4(Suppl 1) (2010) S57-S61.

[33] K.L. Cook, P.A.G. Clarke, R. Clarke, Targeting GRP78 and antiestrogen resistance in breast cancer, Future Medicinal Chemistry 5(9) (2013) 1047-1057.

[34] A.S. Lee, Glucose regulated proteins in cancer: Molecular mechanisms and therapeutic potential, Nature reviews. Cancer 14(4) (2014) 263-276.

CHAPTER 6

CONCLUSION AND FUTURE DIRECTIONS

6.1 Conclusions

In this dissertation, the use of localized hyperthermia via gold nanorod (GNR)-mediated plasmonic photothermal (PPTT) and high intensity focused ultrasound (HIFU) was examined for their ultimate use in enhancing the delivery of targeted water-soluble polymer-drug conjugates to solid tumors. When detected at an early stage, prostate cancer poses limited risk and treatment of stages I-II have a 5-year survival rate near 100% [1] as the disease remains localized and surgical resection can provide a cure [2]. However, when detected at later stages (stages III-IV), the survival rates begin to drop where stage III has a high probability of developing metastases (approximately 50%) [3] leading to a dramatic drop in survival to 28% for stage IV where the disease has progressed, spread beyond the prostate gland, and metastasized [1].

The strategy used in this work is aimed to increase the localization of therapeutics to the advanced, localized prostate cancer (stage III) in order to eliminate the disease entirely and prevent further progression and development of metastases. Ablative therapies alone (e.g., noninvasive HIFU) have been shown to be effective in treating localized disease [4, 5] but have the potential to leave residual cancerous cells in efforts to minimize healthy tissue damage. Chemotherapeutics delivered systemically can provide the strategic

benefit of treating and eliminating those cancers that may have been missed but lead to severe side-effects and low tumor accumulation. In order to utilize aspects of both treatments and improve drug delivery, the combination of localized hyperthermia with polymer therapeutics have shown to enhance delivery to prostate tumors through increased blood flow, vascular permeability, and with the incorporation of heat shock (HS)-targeting. PPTT as a method for local heating was previously shown to achieve this goal enhancing delivery [6], penetration [7], and efficacy [8] of HS-targeted *N*-(2-hydroxypropyl)methacrylamide (HPMA) copolymers in human prostate cancer tumor xenografts. This work has shown promise for treatment of advanced localized prostate cancer; however, unresolved issues remain. The first question was whether the use of mild hyperthermia at the previously used parameters of 43° for 10 min was optimal for maximal polymer accumulation as no other combination of temperature and duration was examined. Second was whether PPTT was the best method of heating and if a noninvasive alternative could be used to produce similar results of enhanced accumulation. Last was whether this alternative method could also enhance the efficacy of HS-targeted polymer-drug conjugates toward prostate cancer tumor *in vivo*.

In Chapter 3, it was investigated how altering the parameters of GNR-mediated PPTT heat treatment could create different accumulation profiles of water-soluble HPMA copolymers [9]. Eight different combinations of temperature and duration were tested ranging from 40-49°C at durations of 10 or 30 min. Of the groups that were tested, 46°C for 30 min had a significantly larger amount of accumulation over an 8-h period. This increase was likely due to finding a heating zone where blood flow was increased to a greater extent than with a lower thermal dose (43°C for 10 min) and where damage of

vasculature occurred at a slower rate within the tumor than with a larger thermal dose (49°C for 10 min). This region gives the largest increase in accumulation as it increases the amount delivered via vascular mechanisms and then limits the outflow of polymers from the tumor tissue due to vascular damage occurring at a slower rate. When the thermal dose was increased beyond this "sweet spot", the vascular damage occurred at a faster rate and limited the amount of polymer accumulation.

In Chapter 4, an alternate method of selective heating of tumor tissue was investigated. The most clinically relevant noninvasive heating method in HIFU was selected for this work. To heat tumor tissue both uniformly and reproducibly *in vivo* at 43°C for 10 min, the HIFU system parameters needed to be altered. This temperature and duration was selected to be consistent with previous experiments and ultimately compare to results obtained using PPTT. Differences in tumor size, morphology, and perfusion results in varied acoustic and thermal properties that lead to variable thermal responses accounted for in real time. In this work, a magnetic resonance imaging-guided HIFU (MRgHIFU) controller and protocol were developed to produce heating in a controlled fashion. The MRgHIFU controller was used to adjust the ultrasound power based on the resulting heating profile in coordination with improved real time temperature imaging. Once this system was shown to reproducibly produce hyperthermia in tumor tissue, it was then used to enhance the delivery of macromolecules and compared to results achieved with PPTT. Here it was shown that HIFU hyperthermia can produce similar results with enhanced accumulation of Evans blue dye (EBD) nearly doubling that of an unheated tumor at 5 h post heating. Accumulation of Gadolinium (Gd)-chelated HPMA copolymers was also imaged over a 5-h period leading to a significant increase in accumulation over

time. The use of HS-targeting to heated prostate cancer tissues has also been shown to further improve accumulation with PPTT. Therefore, HIFU hyperthermia was additionally evaluated to show its potential to provide a noninvasive means of heating in this combination therapy.

Finally, in Chapter 5, the use of HIFU hyperthermia was further developed to create a more clinically relevant combination therapy with HS-targeted HPMA copolymer-drug conjugates. In this work, it was demonstrated that HIFU hyperthermia could be utilized as a tool to selectively heat human prostate cancer xenografts and increase the efficacy of HS-targeted HPMA copolymer-DOC conjugates as compared to controls. When this work is compared to that in combination with PPTT, again, a similar result is observed. The combination of HIFU hyperthermia with these targeted copolymer-drug conjugates demonstrates the potential for HIFU to be used as a tool to enhance delivery and efficacy of targeted macromolecules. The combination therapy shows greater promise today as HIFU has also been approved by the Food and Drug Administration (FDA) for the treatment of prostate cancer [10].

6.2 Challenges and future directions

The completion of this work indicates that the combination of HIFU and HS-targeted water-soluble polymer-drug conjugates can be used to treat prostate cancer. This combination therapy can potentially be used for the treatment of clinical advanced localized prostate cancer (stage III) that resides close to important tissues which need to be avoided by ablative therapies. However, before application in the clinic, critical issues need to be addressed.

To begin, the HIFU temperature controller used in this work is still not ideal. Although a tremendous amount of hard work was done, improvements to the system can be achieved. Here, only the ultrasound power parameter was altered during heat treatments to achieve mild hyperthermia (43°C). Additional parameters, such as focal spot pattern and focal spot speed in different sections within the pattern, can be adjusted during pre-planning or in real time during the procedure to achieve uniform heating of unusually shaped heterogeneous tumors. Tumors are not always perfectly spherical and will require different patterns in order to heat uniformly. Irregularly shaped tumors necessitate the adaptation of unique patterns. Figure 6.1 gives a few examples of alternative patterns that can be used for different shaped tumors by adapting the reduced square spiral pattern. A repertoire of patterns as such can be a valuable tool for clinicians and scientists when preparing to treat with HIFU hyperthermia. With heterogeneous perfusion and varying tissue densities, heat capacity will change in the tissue leading to variability in spatial distribution. More specifically, temperatures will be higher in regions that absorb the ultrasound energy more readily. In those regions, it may be useful to speed up the focal spot movement. In spots that do not absorb well, the focal spot could be slowed down to heat at the proper temperature. Lastly, a detailed planning procedure should be developed based on pre-imaging. With tumor location (prostate, breast, liver, kidney), shape, overall tissue density, and heterogeneity, the parameters mentioned previously can be pre-planned to heat and maintain a precise desired temperature uniformly throughout the tumor.

The work done here was performed in subcutaneous animal models. These models provide important insight for investigational treatments but do not accurately depict the tumor anatomy and microenvironment observed in humans. Tumors grown in mice in a

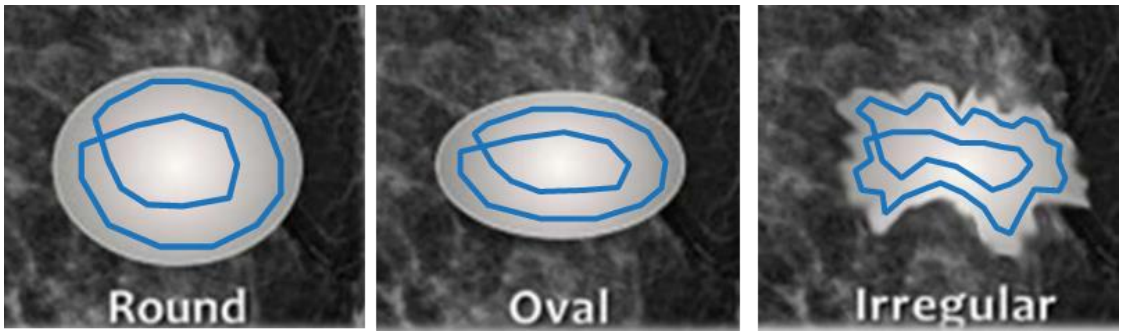

Figure 6.1: Examples of different patterns that can be used in future experiments for different shaped tumors. The previously used reduced square spiral pattern can be adapted to varying shapes and sizes.

matter of a few weeks do not accurately represent the same rates at which tumors grow spontaneously in human prostate glands. Therefore, it is difficult to conclude that success in a murine model will equal success in humans. The next logical step for this work would then be to attempt this therapy in a situation more resembling of a human cancer. To do this, an orthotopic model should be used to show that tumors grown within an actual prostate gland of a large animal can be treated in a fashion similar to how one in a human has been proposed to be treated and have the same effects as shown in subcutaneous models.

Additionally, it is important to determine if human diseased tissues respond in the same fashion as those in our representative animal models. As HIFU is now FDA approved for ablation of prostate cancer, in cases where the physician is attempting to avoid ablation of vital surrounding structures, noting the tissue responses in those areas would be beneficial for eventual translation of this combination therapy. Knowing that blood flow and vascular permeability are increased and that up-regulation of HS receptors occurs could provide greater rationale for use of this combination therapy in clinical scenarios. If these effects do not occur, then this combination therapy would likely not achieve its desired effect.

Finally, staging of the treatment should be investigated as it may have additional benefits for improving accumulation in heated tumor tissues. It has been shown that through vascular effects, the peak accumulation of untargeted water-soluble polymers occurs around 5 h post heat treatment [6, 7, 9]. After treatment with hyperthermia for HS-targeting, the maximal expression of glucose-regulated protein 78 (GRP78) cell surface receptors occurs between and 8 and 12 h post heat treatment. Thus, it may be possible to

coordinate the maximal accumulation of HS-targeted copolymers with the maximal expression of the GRP78 receptors. This, however, would require two heat treatments: one to upregulate the receptors and then a second to increase accumulation of polymers. Other factors including sensitivity to multiple heat treatments may play a role in the success of this delayed injection and dual heat treatment as tumor tissues may respond differently to a second heat dose as they become thermotolerant.

It has been suggested that the use of HPMA-copolymers with covalently attached drugs may have better repeated treatments for drug-resistant cancers in comparison to delivered drugs with liposomes due to their mechanisms of internalization. The comparison of these two delivery vehicles would be useful in a side-by-side study to determine the efficacy of multiple treatments in drug-resistant and nonresistant cancers.

Since this work developed a HIFU system to heat at hyperthermic conditions, this system could be leveraged for other scenarios where noninvasive heating would augment or improve another therapeutic strategy. For example, HIFU hyperthermia can be used to improve the viral translational efficiency of locally delivered adenoviruses.

Additionally, chemotherapies are considered a last resort therapy when all other treatments have been considered. Other therapeutics must be considered instead of chemotherapeutics which have harmful side-effects. These therapies could also have enhanced effectiveness towards cancerous tissues which has been exposed to hyperthermia.

The work shown in this dissertation has further expanded on previously promising research. This research represents progress that will move forward to one day providing clinicians with an additional tool for the treatment of advanced localized prostate cancer.

With further development suggested here, it may one day be possible to provide this treatment to many patients in the effort to eliminate cancers which have begun to invade healthy vital tissues before they metastasize. While treatment of prostate cancer was the intended motivation of this work, the tools and knowledge developed here can also be applied in other scenarios and diseases.

6.3 References

[1] Cancer Facts and Figures 2016, American Cancer Society, Atlanta, Ga, 2016.

[2] A. Bill-Axelson, L. Holmberg, M. Ruutu, M. Häggman, S.-O. Andersson, S. Bratell, A. Spångberg, C. Busch, S. Nordling, H. Garmo, J. Palmgren, H.-O. Adami, B.J. Norlén, J.-E. Johansson, Radical prostatectomy versus watchful waiting in early prostate cancer, New England Journal of Medicine 352(19) (2005) 1977-1984.

[3] J.-E. Damber, G. Aus, Prostate cancer, The Lancet 371(9625) 1710-1721.

[4] L. Poissonnier, J.-Y. Chapelon, O. Rouvière, L. Curiel, R. Bouvier, X. Martin, J.M. Dubernard, A. Gelet, control of prostate cancer by transrectal HIFU in 227 patients, European Urology 51(2) (2007) 381-387.

[5] E.R. Cordeiro, X. Cathelineau, S. Thüroff, M. Marberger, S. Crouzet, J.J.M.C.H. de la Rosette, High-intensity focused ultrasound (HIFU) for definitive treatment of prostate cancer, BJU International 110(9) (2012) 1228-1242.

[6] A.J. Gormley, N. Larson, S. Sadekar, R. Robinson, A. Ray, H. Ghandehari, Guided delivery of polymer therapeutics using plasmonic photothermal therapy, Nano Today 7(3) (2012) 158-167.

[7] A.J. Gormley, N. Larson, A. Banisadr, R. Robinson, N. Frazier, A. Ray, H. Ghandehari, Plasmonic photothermal therapy increases the tumor mass penetration of HPMA copolymers, Journal of Controlled Release 166(2) (2013) 130-138.

[8] N. Larson, A. Gormley, N. Frazier, H. Ghandehari, Synergistic enhancement of cancer therapy using a combination of heat shock protein targeted HPMA copolymer–drug conjugates and gold nanorod induced hyperthermia, Journal of Controlled Release 170(1) (2013) 41-50.

[9] N. Frazier, R. Robinson, A. Ray, H. Ghandehari, Effects of heating temperature and duration by gold nanorod mediated plasmonic photothermal therapy on copolymer accumulation in tumor tissue, Molecular Pharmaceutics 12(5) (2015) 1605-1614.

[10] FDA clears focused ultrasound system for prostate cancer treatment, Oncology Times 37(22) (2015) 37.

APPENDIX

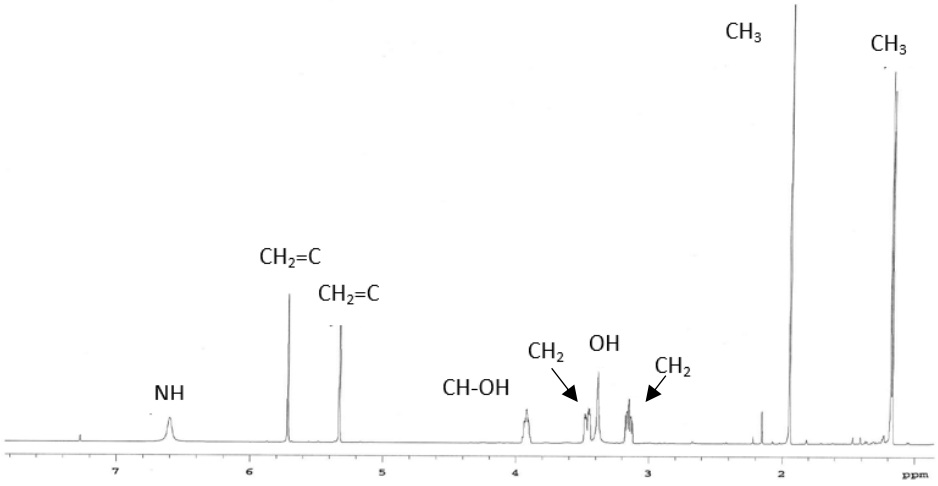

Figure A.1: NMR confirmation of HPMA monomer.

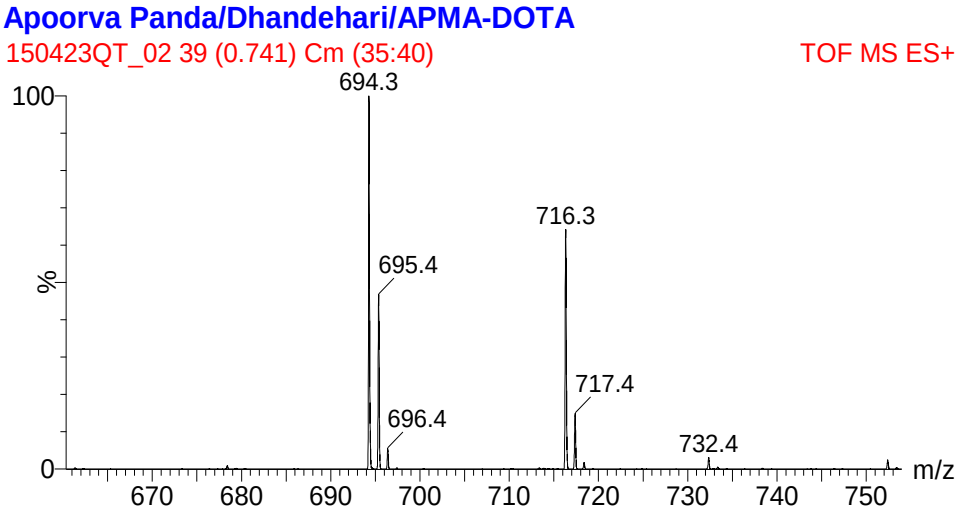

Figure A.2: Mass spectroscopy confirmation of APMA-DOTA monomer. Expected molecular weight is 693 daltons. Peaks show expected plus one hydrogen atom (694 daltons) and plus one sodium atom (716 daltons).

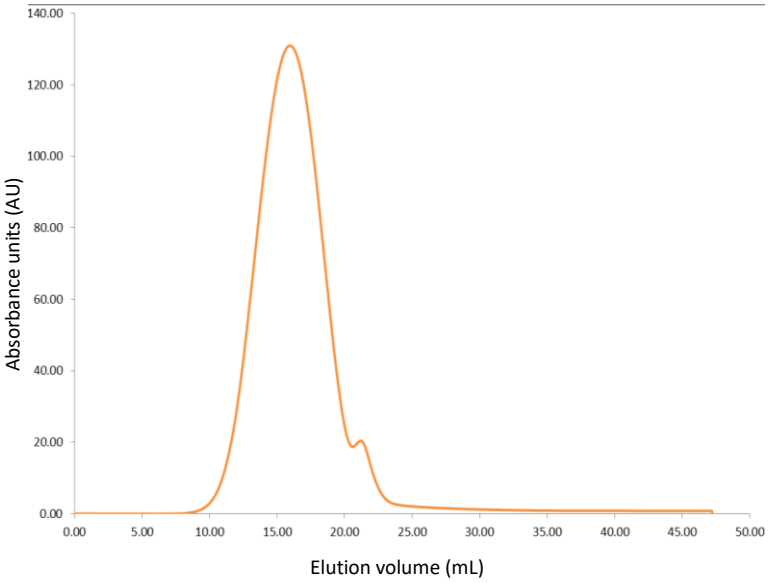

Figure A.3: Size-exclusion chromatograph of HPMA-DOTA copolymer after chelation of gadolinium and dialysis. M_w = 51 kDa. PDI = 1.67.

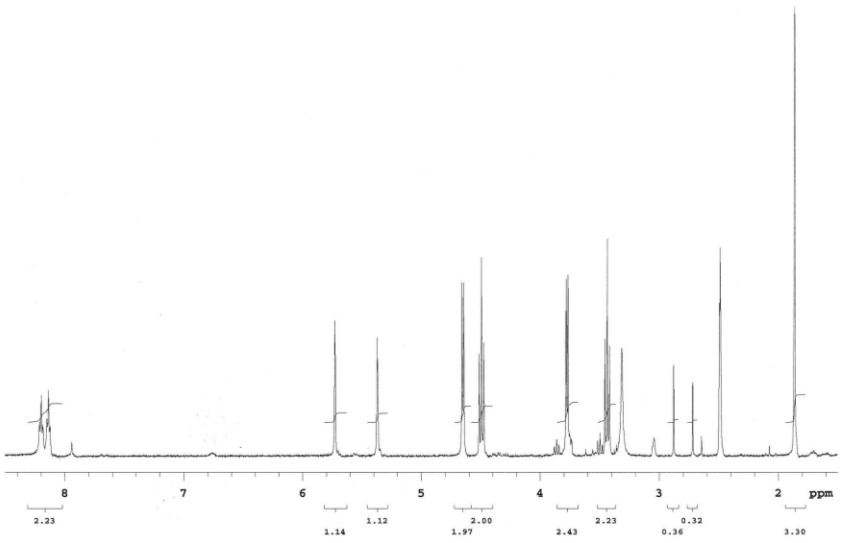

Figure A.4: NMR characterization of MA-GG-TT monomer.

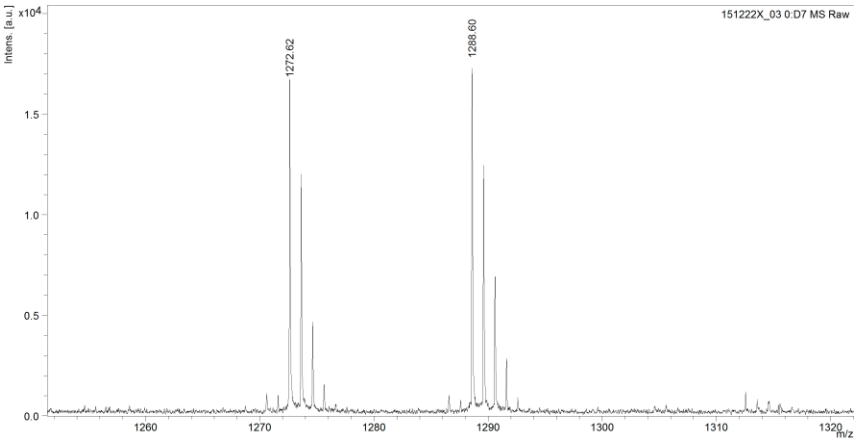

Figure A.5: Mass spectroscopy of MA-GFLG-DOC monomer. Expected molecular weight is 1272 daltons. Second peak is expected plus one oxygen atom. (1288 daltons).

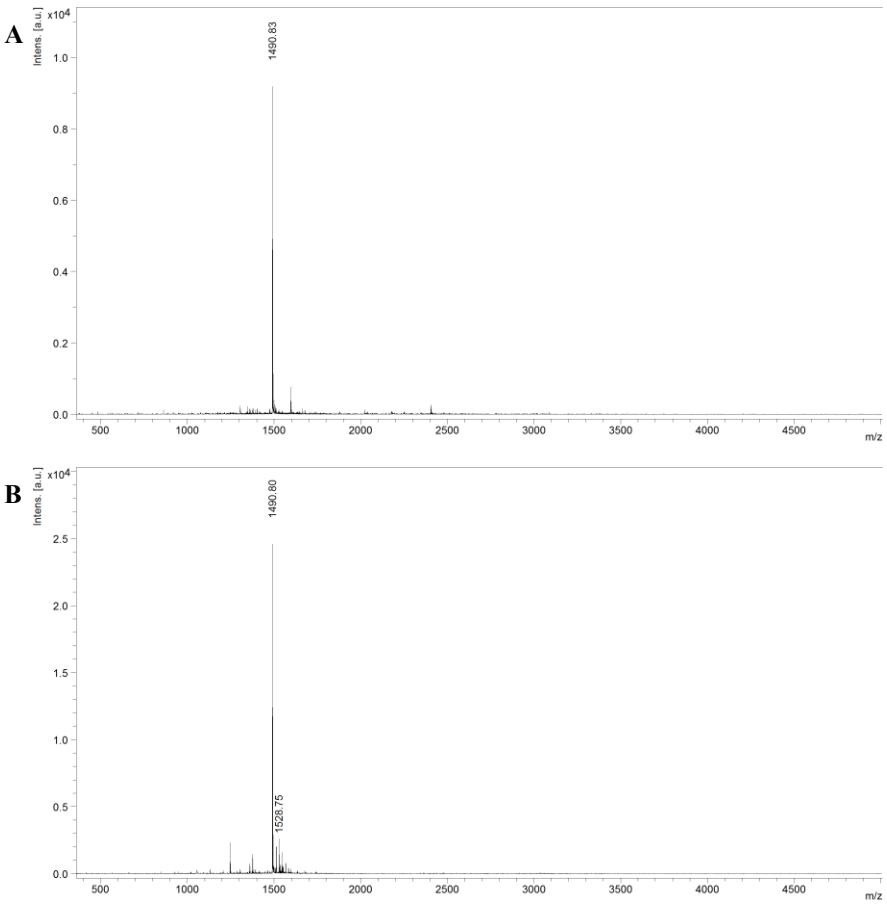

Figure A.6: Mass spectroscopy of A) heat shock-targeting and B) scrambled peptides. Expected molecular weight is 1490 daltons.

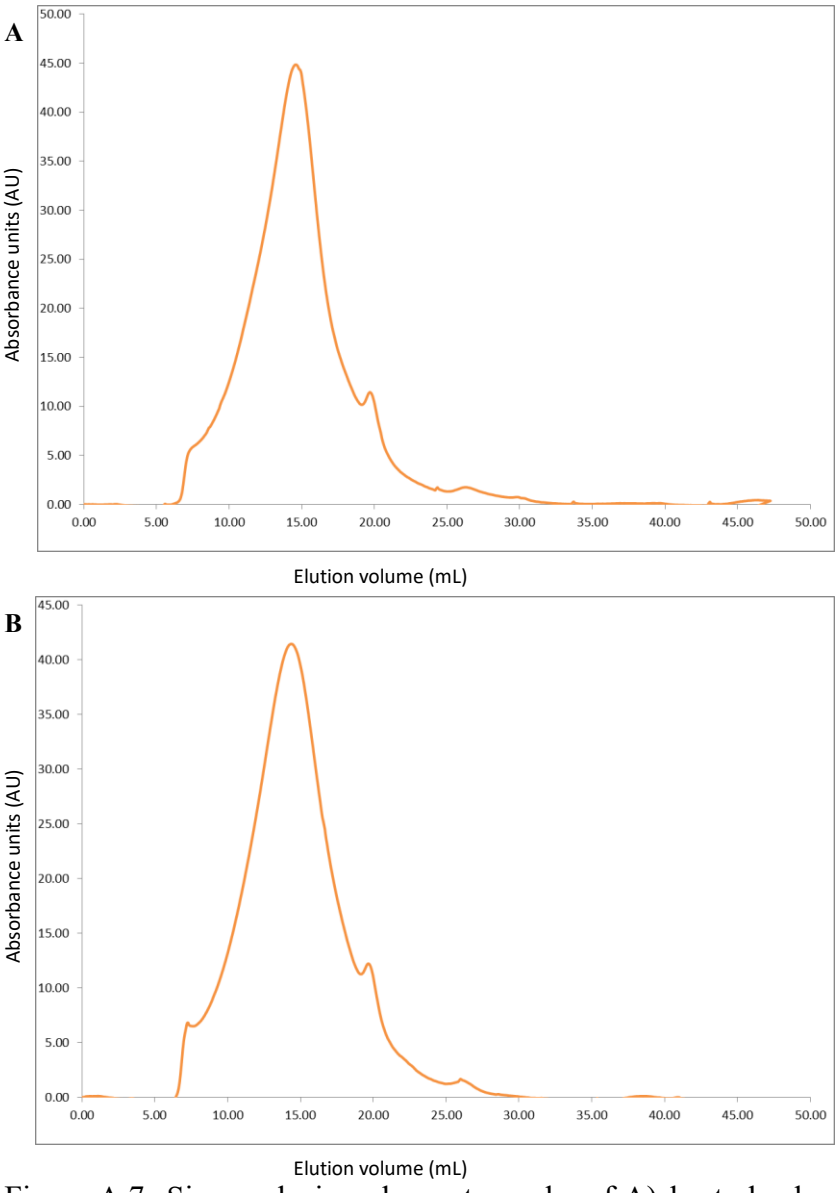

Figure A.7: Size-exclusion chromatographs of A) heat shock-targeted polymer-DOC conjugates and B) untargeted polymer-DOC conjugates. Polymer characteristics (M_w and PDI) are summarized in Table 5.1.

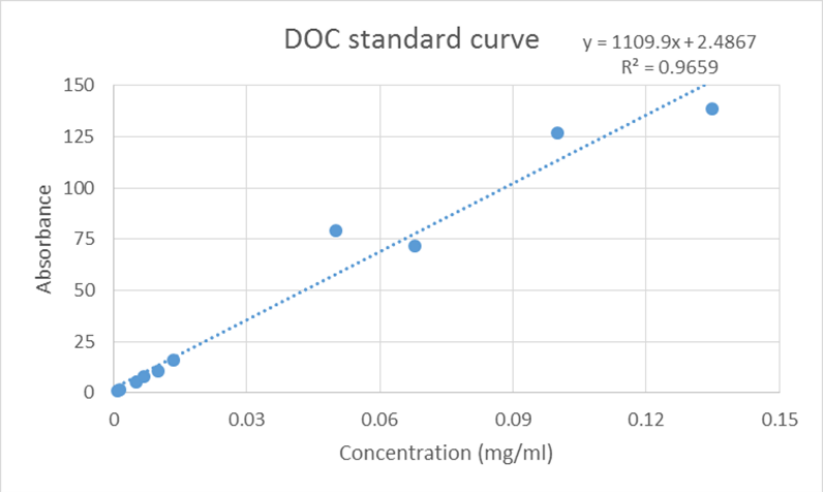

Figure A.8: Standard curve of DOC concentrations used to determine the amount of drug release from the polymer-drug conjugates. Drug content was determined by peak height on HPLC and back calculated based on concentration to determine DOC wt %.